UNIVERSITY OF OKLAHOMA

GRADUATE COLLEGE

CHARACTERIZATION OF MILDEW RESISTANCE LOCUS O MEDIATED POLLEN TUBE RECEPTION

A DISSERTATION

SUBMITTED TO THE GRADUATE FACULTY

in partial fulfillment of the requirements for the

Degree of

DOCTOR OF PHILOSOPHY

By

DANIEL SCOTT JONES
Norman, Oklahoma
2017

CHARACTERIZATION OF MILDEW RESISTANCE LOCUS O MEDIATED POLLEN TUBE RECEPTION

A DISSERTATION APPROVED FOR THE
DEPARTMENT OF MICROBIOLOGY AND PLANT BIOLOGY

BY

_____
Dr. Sharon Kessler, Co-Chair

_____
Dr. Ben Holt III, Co-Chair

_____
Dr. Scott Russell

_____
Dr. Laura Bartley

_____
Dr. John P. Masly

© Copyright by DANIEL SCOTT JONES 2017
All Rights Reserved.

This dissertation is dedicated to my wonderful wife Aimee Jones who always supports and encourages me in everything I do. I would not be where I am today without her love.

Also to my family: my mother Ralene Jones, my father Kent Jones, and my brother David Jones. Thank you all for your continuous support throughout my life and for always allowing me to question and think for myself.

Acknowledgements

Many people have helped me throughout my time at OU. I would like to thank my advisor Dr. Sharon Kessler for giving me the opportunity to work in her lab and for her continual support and counsel. I would also like to thank Dr. Ben Holt for taking me in during the final part of my PhD and for treating me as one of his own in the lab. Advice and training from both Dr. Kessler and Dr. Holt have been essential to my development as a scientist. I would like to thank my committee members, both current and past, for their feedback and advice during my program: Dr. Scott Russell, Dr. JP Masly, Dr. Ben Smith, and Dr. Laura Bartley.

I could not have made it through all of the ups and downs without my fellow lab mates, past and present, from the Kessler and Holt Labs. Many taught me how to function in a molecular lab, many helped with experiments and basic lab support, and everyone made it a fun environment to work in! Big thanks to Zach Myers, Andrew Willoughby, Jing Yuan, Cole Davis, Dr. Rod Kumimoto, Dr. Swadhin Swain, Dr. Chami Siriwardana, Emily Kumimoto and Arianna Dino for experimental support/training and helping me to maintain my sanity. I'd also like to thank Henry Lee, Nic Cejda, and Patrick Day for day-to-day help around the lab throughout the years! I would like to give a special shout out to everyone in the Sam Roberts Noble Microscopy Lab for their help and guidance with imaging. Dr. Ben Smith, Greg Strout, Preston Larson and Dr. Scott Russell have all taught me everything I know about microscopy, which has become a major reason I love what I do!

Table of Contents

Acknowledgements iv

List of Tables viii

List of Figures ix

Abstract xii

Chapter 1: Introduction 1

Reproduction in flowering plants 2

Pollen tube attraction and reception 3

MLO-mediated cell-to-cell communication 4

NORTIA is an integral part of the pollen tube reception pathway 5

Examining MLO-mediated pollen tube reception 7

Figures 8

Chapter 2: MILDEW RESISTANCE LOCUS O Function in Pollen Tube Reception Is Linked to Its Oligomerization and Subcellular Distribution 10

Summary 12

Introduction 13

Results 15

Discussion 26

Methods and Materials 32

Figures and Tables 39

Chapter 3: Cell Type-Dependent Localization of MLO Proteins 59

Summary 60

Introduction 61

Results and Discussion 62
Figures 66
Chapter 4: Analysis of the secretory pathway in the haploid synergid cells of *Arabidopsis thaliana* 69
Summary 71
Introduction 72
Results 75
Discussion 80
Conclusion 85
Methods and Materials 85
Figures and Tables 89
Chapter 5: Interaction with calmodulin influences MLO function during pollen tube reception 100
Summary 101
Introduction 102
Results 106
Discussion 110
Methods and Materials 113
Figures 120
Chapter 6: Clade III MLO expression in ovules: regulatory elements in intragenic regions of NTA and the initial characterization of MLO overexpression lines 125
Summary 127

Results and Discussion 128
Methods and Materials 135
Figures 138
Chapter 7: Conclusions and Future Directions 153
References 160
Appendix A: List of Constructs 168

List of Tables

Supplemental Table 2.1. Primers Used for Cloning. 58

Supplemental Table 4.1 – Secretory markers analyzed in the Col-0 background 96

Supplemental Table 4.2 – Number of synergids expressing TGN markers with FA-localizaiton vs. no FA-localization 97

Supplemental Table 4.3 – Secretory markers co-expressed and imaged with LRE and NTA 98

Supplemental Table 4.4 – List of primers used for cloning secretory markers. 99

List of Figures

Figure 1.1 - Retention of male and female gametophytes in the flower of *Arabidopsis thaliana*.v 8

Figure 1.2 - Pollination, PT Reception and PT Overgrowth – Secretory markers analyzed in the Col-0 background 9

Figure 2.1 - Native MLO expression patterns in *Arabidopsis* ovules. 39

Figure 2.2 - Analysis of MLO proteins expressed in synergids of *nta-1.* 40

Figure 2.3 - NTA co-localization with secretory markers in synergids. 41

Figure 2.4. MLO co-localization with a Golgi marker in synergids. 42

Figure 2.5. NTA, MLO10, and MLO8 co-localization with a trans-Golgi network (TGN) marker in synergids. 43

Figure 2.6. Analysis of domain swaps between MLO8 and NTA. 44

Figure 2.7. Co-localization of NEL1 and CTerm swaps with a Golgi marker in synergids 46

Figure 2.8. Detection of oligomerization of MLO constructs via FRET analysis. 47

Supplemental Fig. 2.1 Protein alignment of the *Arabidopsis thaliana* MLO family 48

Supplemental Fig. 2.2 MLO8pro::MLO8-GFP expression pattern in mature ovules. 49

Supplemental Fig. 2.3 Comparison of NTApro::NTA-GFP and MYB98pro::NTA-GFP expression in *nta-1*. 50

Supplemental Fig 2.4. Analysis of full length MLO distribution in synergid cells. 51

Supplemental Fig 2.5. SignalP 4.0 Prediction results and N-terminal peptide alignment for all 15 MLO proteins in *Arabidopsis thaliana.* 52

Supplemental Fig. 2.6 Analysis of NTA without its predicted signal peptide (sp). 53

Supplemental Fig. 2.7 MLO-GFP distributions of domain swaps and truncations within synergids. 54

Supplemental Fig 2.8. Analysis of NEL1 and CTerm domain swap distribution in synergid cells. 55

Supplemental Fig 2.9. Analysis of IL1 and IL2 domain swaps between MLO8 and NTA. 56

Supplemental Fig 2.10. FRET detection via acceptor photobleaching. 57

Figure 3.1 Transient co-expression of 35Spro:NTA-GFP with mCherry-labeled secretory markers in tobacco epidermal cells 66

Figure 3.2 MLO co-localization with a Golgi marker in tobacco epidermal cells. 67

Figure 3.3 Distribution of ectopically expressed MLO1 and NTA in the epidermal cells of *Arabidopsis thaliana.* 68

Figure 4.1 – LORELEI and NORTIA expression in the synergid cell. 89

Figure 4.2 – Secretory marker distribution in Col-0 synergids. 90

Figure 4.3 – LRE-cYFP co-localization with secretory markers in synergids. 91

Figure 4.4 – NTA-GFP co-localization with secretory markers in synergids. . 93

Supplemental Figure 4.1 – LRE-cYFP co-localization with EXPO in the FA of mature synergids. 95

Figure 5.1 - Analysis of NTA variants expressed in synergids of *nta-1* 120

Figure 5.2 - NTA W458A co-localization with Golgi and TGN makers in synergid cells 121

Figure 5.3 – NORTIA and NTA W458A distribution in the synergid at PT arrival 122

Supplemental Figure 5.1 – Transient expression of MLOs and AtCaM1 in *N. benthamiana* epidermal cells for FRET interaction assay. 123

Supplemental Figure 5.2 – Co-IP assay to detect interaction between NTA and AtCaM1. 124

Figure 6.1 – Expression patterns of native promoter NTA genomic GUS constructs in flowers. 138

Figure 6.2 – Alternative NTA-GUS expression pattern in flowers. 139

Figure 6.3 – NTA cDNA expression patterns under native and ectopic promoters. 140

Figure 6.4 – Expression patterns of MLO10-GUS and MLO8-GUS under their native promoters throughout ovule development. 141

Figure 6.5 – MLO10-GFP expression in tissue surrounding megaspore mother cell. 142

Figure 6.6 – MLO8-GFP expression in developing ovules. 143

Figure 6.7 – MLO8-GFP expression in following PT reception. 144

Figure 6.8 – MLO8-GFP accumulation at the filiform apparatus in mature ovules. 145

Figure 6.9 – *35Spro::MLO-YFP* localization in epidermal cells of *A. thaliana*. 146

Figure 6.10 – MLO overexpression lines in *A. thaliana*. 147

Figure 6.11 – Overexpression of NORTIA in Col-0. 148

Figure 6.12 – Overexpression of MLO10 in Col-0. 149

Figure 6.13 – Overexpression of MLO8 in Col-0. 150

Figure 6.14 – Aniline blue staining reveals successful self-pollination in MLO10 and MLO8 overexpression lines. 151

Figure 6.15 – Ectopic callose accumulation in flowers of MLO10 and MLO8 overexpression lines. 152

Abstract

Beyond its importance for the subsistence of all plant species, and thus life on earth, plant reproduction is fundamental to all human agricultural exploits. Understanding the mechanisms regulating reproduction is central to improving current agricultural practices in order to keep pace with a rapidly changing global environment. In flowering plants, intercellular communication controls every aspect of reproduction from pollination to double fertilization. In *Arabidopsis thaliana*, the MILDEW RESISTANCE LOCUS O (MLO) family protein NORTIA (NTA) is a critical component of reproductive communication regulating the final phase of sperm cell delivery, pollen tube (PT) reception. NTA is a seven-transmembrane protein that localizes to the endomembrane system of the synergid cell, a specialized cell in the embryo sac that controls the delivery of sperm cells through the processes of PT attraction and reception. MLO proteins regulate cell-cell communication in a number of physiological responses, including interactions with the biotrophic fungal pathogen powdery mildew and responses to mechanical stimuli during root growth. In this dissertation, I investigated the function of NTA within the process of PT reception through a structure-function analysis to determine the molecular and cellular requirements for MLO-mediated communication in this pathway. During these analyses, I generated a suite of markers expressed in the synergid cell that enables reproductive and cell biologists to study the secretory pathway of this specialized cell type. Additionally, I determined the expression patterns of two closely related MLO proteins (MLO10 and MLO8) in female reproductive tissues and generated lines to study the developmental effects of overexpressing MLO proteins. This dissertation contributes to our overall understanding of MLO-mediated communication, providing evidence of the molecular requirements for MLO function as well as identifying additional roles that MLOs may

play during reproductive development and signaling. MLO proteins directly regulate many agronomically important developmental and environmental intercellular communication pathways. Thus, determining the molecular role of MLO proteins during reproductive communication can provide critical insight into how plants broadly regulate cell-cell communication across key processes.

Chapter 1: Introduction

Reproduction in flowering plants

The alternation of multicellular diploid and haploid generations is a unifying characteristic of the plant life cycle (Hofmeister, 1862). Throughout plant evolution, the haploid generation has undergone an immense reduction, with the most extreme found in the gametophytes of Angiosperms (flowering plants) (Graham et al., 2000). The male gametophyte (pollen) is largely made up of only three cells. A vegetative cell, which develops into a tip-elongating pollen tube (PT), and two sperm cells (the male gametes), all of which are required to complete the entire process of sperm cell delivery and double fertilization (Russell and Jones, 2015). The typical female gametophyte (embryo sac) is of the Polygonum-type (encompassing more than 70% of flowering plants) and is comprised of seven cells: an egg cell and a central cell (the female gametes), two synergid cells and three antipodal cells (Huang and Russell, 1992). The reduced multicellular gametophytes of higher plants are retained within sporophytic tissues and completely rely on this generation for their maintenance and development. In flowering plants, pollen is produced in anthers while the embryo sac develops within an ovule inside a carpel (Fig. 1.1); with the carpel and anther being entirely separate organs of a flower (Tucker and Koltunow, 2014; Hafidh et al., 2016). This separation and retention creates a very interesting biological problem since fertilization requires direct cellular contact between male and female gametes. The solution to this problem involves the invasive growth of a PT through this sporophytic tissue, attraction to and targeting of the PT to an opening in the ovule (the micropyle) to gain access to the embryo sac, and signaling between the PT and female gametophytic cells facilitating reception of the PT and release of the sperm cells (Fig. 1.2A-B) (Kessler and Grossniklaus, 2011; Beale and Johnson, 2013; Higashiyama and Takeuchi, 2015; Qu et al., 2015). Thus, cell-cell communication is essential for

regulating the entire process of pollination and fertilization in flowering plants (Chevalier et al., 2011).

Pollen tube attraction and reception

While significant strides toward understanding the signaling between these specialized cell types have been made, the molecular components regulating the final stages of this process have only recently began to be identified. The PT is attracted to the micropyle of the ovule by two synergid cells, accessory cells located at the far micropylar end of the embryo sac (Higashiyama and Takeuchi, 2015). Synergids are a highly polarized cell type with a large vacuole at the chalazal end of the cell (away from the micropyle of the ovule) and a region of proliferated plasma membrane and wall-ingrowths called the filiform apparatus (FA) at the micropylar end of the cell (Jensen, 1965; Huang and Russell, 1992). Small cysteine-rich peptides called LUREs are secreted from synergid cells driving PT tip-elongation towards the micropyle of an ovule (a process called PT attraction) (Okuda et al., 2009). Direct contact between the PT and a synergid first occurs at the FA after PT arrival (Leshem et al., 2013). The PT then undergoes a slow growth phase; eliciting sharp oscillations of cytoplasmic calcium within the synergid cells, indicative of active signaling between the PT and synergids (Iwano et al., 2012; Hamamura et al., 2014; Ngo et al., 2014). The process of PT reception initiates as one the two synergids degenerates, the PT enters the embryo sac and ruptures to release the two sperm cells required for double fertilization (Russell, 1992). PT reception is regulated by components found in both the PT and in the synergid cells (Beale and Johnson, 2013). Mutants for PT reception components have normal PT attraction but have defects in both synergid degeneration and PT rupture (Kessler and Grossniklaus, 2011). This lapse in communication leads to PT

overgrowth, the elongation of the PT within the embryo sac with no release of sperms cells, and reduces the overall fertility of the plant (Fig. 1.2C-D). With the majority of identified PT reception components predominately found in synergids, it is clear that this specialized cell type controls the fate of the PT and thus successful reproduction.

MLO-mediated cell-to-cell communication

Mechanisms mediating invasive PT growth have often been compared to those regulating biotic interactions in plants (Chen et al., 2015; Bircheneder and Dresselhaus, 2016). This is because many similarities exist between components involved in processes such as defense responses and those that directly regulate reproduction. One prevalent example of this is the MILDEW RESISTANCE LOCUS O (MLO) protein family, a plant-specific family of seven transmembrane proteins (Acevedo-Garcia et al., 2014). Originally described as negative regulators of defense response in barley (*Hordeum vulgare* L.) (Buschges et al., 1997), MLOs are now understood to have conserved roles in pathogen susceptibility (in both monocots and eudicots) as well as in regulating cell communication in other physiological responses. There are 15 MLO proteins in *Arabidopsis thaliana* representing five of the seven known clades of MLOs across plant species (Devoto et al., 2003; Acevedo-Garcia et al., 2014). In *A. thaliana* MLOs have roles in pathogen susceptibility, root thigmomorphogenesis (directional growth in response to a mechanical stimulus), and in PT reception (Acevedo-Garcia et al., 2014). MLO2, 6, and 12 (Clade V) contribute unequally to *mlo* susceptibility (Consonni et al., 2006), while MLO4 and 11 (Clade I) are both involved in the thigmotropic signaling in roots (Chen et al., 2009). Only a single Clade III MLO, NORTIA (NTA; MLO7), has been shown to be involved in PT reception (Kessler et al., 2010). Overall the molecular function of MLO proteins

remains relatively unresolved, but understanding how MLOs regulate cell-cell communication could provide unique insight into broadly conserved signaling pathways within plants.

NORTIA is an integral part of the pollen tube reception pathway

NTA is expressed specifically in synergid cells where it regulates PT reception. In *nta-1* mutants, ~30% of ovules remain unfertilized due to PT overgrowth (Kessler et al., 2010). NTA localizes to the endomembrane system of the synergid and is distributed throughout the entire cell prior to PT arrival. Interestingly, NTA is actively redistributed to the FA sometime during PT reception (Kessler et al., 2010). MLO redistribution is a conserved trait as barley MLO (HvMLO) also redistributes within the host epidermal cell during fungal infection, toward the site of penetration (Bhat et al., 2005). NTA's redistribution is dependent on other known components that regulate PT reception. FERONIA (FER) is a receptor-like kinase belonging to the CrRLK1L subfamily (Escobar-Restrepo et al., 2007). FER was the first PT reception component described, with fertilization reduced by approximately half in heterozygous *fer* mutants due to PT overgrowth (Huck et al., 2003; Rotman et al., 2003). Widely expressed, except in pollen, FER preferentially localizes to the FA of the synergid cell and contains a single transmembrane domain. FER has an active kinase domain in its intracellular domain, but does not require kinase activity for PT reception (Kessler et al., 2015). FER's ligand-binding extracellular domain is necessary for FER-mediated PT reception and is thought to provide specificity via direct interaction with a pollen-borne ligand. NTA's redistribution is dependent on FER placing NTA's function likely downstream of FER-mediated signaling (Kessler et al., 2010). LORELEI (LRE), a glucosylphosphatidylinositol (GPI)-anchored protein, is another key component

regulating PT reception from within the synergid cell (Capron et al., 2008; Tsukamoto et al., 2010). *LRE* is expressed specifically in synergids before fertilization, and localizes to the FA of the synergid cell where it is hypothesized to form a complex with FER and mediate their trafficking from the endoplasmic reticulum to the FA (Li et al., 2015; Lindner et al., 2015). Complementation experiments that expressed LRE specifically in PTs revealed that its function likely resides at the interface of the PT and the synergid cell during early reception signaling, indicating that the FER/LRE receptor complex may be the earliest component of the synergid PT reception pathway (Liu et al., 2016).

Initiation of cytoplasmic calcium oscillations within the synergid cell during PT reception is dependent on the function of the FER/LRE receptor complex (Ngo et al., 2014). NTA, while not required for the initiation of these calcium oscillations, may play a role in modulating this secondary messenger within the synergid as the overall amplitude of calcium is lower in the synergids of *nta* mutants during PT reception (Ngo et al., 2014). This may also explain the lower penetrance of NTA's PT reception phenotype compared to FER/LRE, as ~70% of *nta* ovules do successfully receive a PT. MLO proteins have a conserved calmodulin (CaM)-binding domain (CaMBD) in their C-terminal intracellular tails (Kim et al., 2002). The activity of the CaMBD is critical for HvMLO function during powdery mildew susceptibility (Kim et al., 2002). Thus the need for calcium (and CaM-binding) may be a key similarity between MLO mediated pathways and could provide a means to understanding potential downstream MLO signaling outputs.

Examining MLO-mediated pollen tube reception

Our understanding of PT reception, and especially the role an MLO plays in this signaling pathway, is still in its infancy. The overall goal of this dissertation is to determine NTA's molecular function in mediating PT reception. By understanding the requirements for MLO-mediated PT reception we gain insight into the broader roles MLO proteins play in cell-to-cell communication pathways intrinsic to the plant. The chapters of this dissertation add to our overall understanding of sexual reproduction in flowering plants and to MLO protein function in intercellular communication. In Chapter 2, I utilized a structure-function analysis using closely related MLO proteins to NTA in order to determine which domains are important for NTA's function in PT reception. Here, I found that the C-terminal intracellular tail and an N-terminal domain were crucial for NTA's function. Disruption of NTA's N-terminal domain also inhibited homo-oligomer formation in a FRET assay, suggesting that oligomerization is important for MLO function. I also found that localization within Golgi-associated compartments of the synergid cell correlated with which MLO proteins were able to function in PT reception indicating that distribution within the cell impacts MLO function. Chapter 3 describes the differential subcellular distribution observed when MLOs are expressed in different cell-types, suggesting local cellular environments may influence MLO protein localization. In Chapter 4 I describe a suite of informative subcellular markers labeling the secretory pathway of synergid cells and utilize them in a co-localization analysis with the PT reception components LRE and NTA. Chapter 5 explores the importance of the NTA's CaM-binding domain for its function during PT reception. Finally Chapter 6 looks into the expression patterns and potential function of the closely related MLOs, MLO10 and MLO8.

Figures

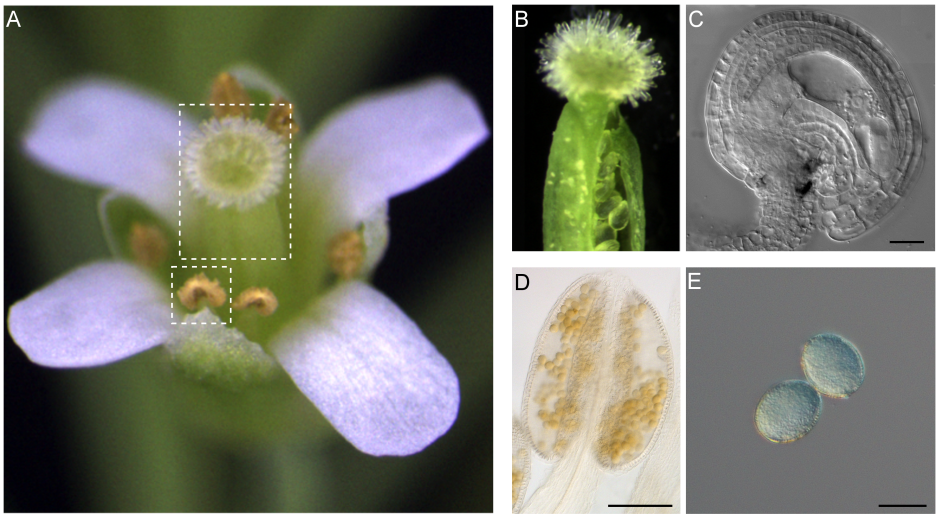

Figure 1.1 - Retention of male and female gametophytes in the flower of *Arabidopsis thaliana*. A) Mature flower of *A. thaliana* showing all four whorls of floral organs: sepals, petals, anthers, and carpels (outside to inside). B) Many ovules develop inside the carpel where they are retained through fertilization until seed dispersal C) A single multicellular embryo sac (female gametophyte) develops inside an ovule. D-E) Six anthers produce thousands of pollen grains (male gametophytes). Bar = 20μm (B, E); 100μm (D).

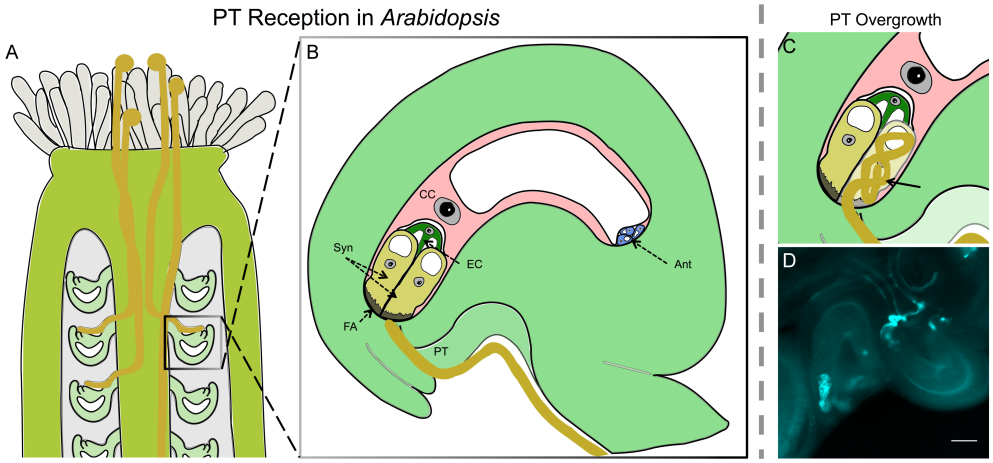

Figure 1.2 - Pollination, PT Reception and PT Overgrowth A) Pollen grains land on a receptive stigma, hydrate, and produce a PT that grows through the transmitting tract of a pistil and targets individual ovules in order to deliver the male gametes. B) The PT arrives at and enters the micropylar end of the ovule where reception into the embryo sac initiates. C) Depiction of PT overgrowth (arrow) in a mutant ovule. D) Aniline blue labeling of pollen tubes reveals PT overgrowth (arrow) in *nta-1* ovules. CC-central cell, EC-egg cell, Syn-synergid, FA-filiform apparatus, PT-pollen tube. Bar = 30μm (D).

Chapter 2: MILDEW RESISTANCE LOCUS O Function in Pollen Tube Reception Is Linked to Its Oligomerization and Subcellular Distribution

Daniel S. Jones[1], Jing Yuan[1, 2], Benjamin E. Smith[1, 3], Andrew C. Willoughby[1], Emily L. Kumimoto[1], Sharon A. Kessler[1, 2, 4]

[1]Department of Microbiology and Plant Biology, The University of Oklahoma, Norman, OK 73069, USA
[2]Department of Botany and Plant Pathology, Purdue University, West Lafayette, IN 47907, USA
[3] Vision Science, University of California, Berkley, CA 94720, USA
[4] Center for Plant Biology, Purdue University, West Lafayette, IN 47907, USA

This chapter was published in *Plant Physiology*.

Jones, D. S., Yuan, J., Smith, B. E., Willoughby, A. C., Kumimoto, E. L., & Kessler, S. A. (2017). MILDEW RESISTANCE LOCUS O Function in Pollen Tube Reception Is Linked to Its Oligomerization and Subcellular Distribution. *Plant Physiology, 175*(1), 172-185.

Contributions

Jing Yuan maintained the stable transgenic lines for TM5, IL1, and IL2 domain swaps and performed ovule counts with these plants. Benjamin E. Smith helped design FRET experiments and wrote the Fiji MACRO used to analyze FRET data. Andrew C. Willoughby did ovule counts in Supplemental Fig. 2.3. Emily L. Kumimoto cloned full-length MLO entry and $MYB98_{pro}$ expression vectors for NTA, MLO10, MLO8, and MLO2.

Summary

Sexual reproduction in flowering plants requires communication between synergid cells and a tip-elongating pollen tube (PT) for the successful delivery of sperm cells to the embryo sac. The reception of the PT relies on signaling within the synergid cell that ultimately leads to the degeneration of the receptive synergid and PT rupture, releasing the sperm cells for double fertilization. In *Arabidopsis thaliana*, NORTIA (NTA), a member of the Mildew resistance Locus O (MLO) family of proteins, plays a critical role in the communication processes regulating PT reception. In this study, we determined that MLO function in PT reception is dependent on MLO protein localization into a Golgi-associated compartment before PT arrival, indicating that PT-triggered regulation of the synergid secretory system is important for synergid function during pollination. Additionally, a structure-function analysis revealed that MLO homo-oligomerization, mediated by the N-terminal region of the protein, and C-terminal tail identity both contribute to MLO activity during PT reception.

Introduction

Intercellular communication is central to the development and maintenance of all multicellular organisms. In plants, communication between cells controls processes ranging from organ development and tissue patterning (Chaiwanon et al., 2016; Otero et al., 2016) to defense responses (Yi and Valent, 2013; Stahl and Faulkner, 2016) and reproduction (Higashiyama and Takeuchi, 2015; Bircheneder and Dresselhaus, 2016). The importance of cell-cell communication is evident during reproduction in flowering plants as the attraction and reception of the male gametophyte (pollen tube (PT)) by the synergid cells of the female gametophyte (also known as the embryo sac) are essential for reproductive success (Beale and Johnson, 2013; Higashiyama and Takeuchi, 2015). The synergid cells have two primary functions in reproduction: PT attraction and intercellular communication during PT reception (Russell, 1992; Higashiyama et al., 1998). Synergid cells are responsible for emitting LURE peptides that are perceived by the approaching PTs to guide them to the embryo sac (Okuda et al., 2009). PT reception then initiates as the PT makes contact with the synergid cells and pauses its growth to communicate with the receptive synergid at the filiform apparatus, a membrane-rich region at the micropylar end of synergid cells (Denninger et al., 2014; Hamamura et al., 2014; Ngo et al., 2014). Signal transduction pathways in the synergid and the PT lead to PT rupture, releasing the sperm cells for double fertilization, and to the degeneration of the receptive synergid.

PT reception is a complex process with key genes expressed in both the synergid cell and PT facilitating this communication (Kessler and Grossniklaus, 2011; Beale and Johnson, 2013). The synergid FERONIA/LORELEI receptor complex plays a role early in PT reception (Escobar-Restrepo et al., 2007; Li et al., 2015; Liu et al., 2016), while NORTIA (NTA, also known as AtMLO7), a member of the Mildew resistance locus O

(MLO) family of proteins, acts downstream of the receptor complex to facilitate PT reception by an unknown mechanism. In *nortia* homozygous mutants, PT-synergid communication is disrupted. Instead of bursting to release the sperm cells, PTs continue to grow within the embryo sac, a phenotype known as PT overgrowth (Kessler et al., 2010). Recently it was found that calcium oscillations in the synergid cells begin upon the arrival of the PT at the filiform apparatus (Denninger et al., 2014; Hamamura et al., 2014; Ngo et al., 2014). The PT reception components FERONIA and LORELEI are both necessary for the signaling process that initiates these calcium oscillations. In contrast, *nta-1* mutant ovules retain these oscillations but at lower amplitudes, suggesting that NTA could play a part in modulating these calcium signals, but not in initiating them (Ngo et al., 2014). The incomplete expressivity of the *nta* mutant phenotype in which some ovules carrying the mutation are fertilized normally, suggests that a threshold level of calcium (or some other signaling molecule) in synergids is necessary for PT reception.

MLOs are seven-transmembrane proteins first identified as susceptibility factors for the fungal pathogen powdery mildew (Buschges et al., 1997). The MLO family was first described in barley (*Hordeum vulgare* L.) where mutations in the *mlo* locus conferred resistance to powdery mildew (Buschges et al., 1997). MLOs have a conserved calmodulin-binding domain (CaMBD) in their C-terminal cytosolic tail that actively binds calmodulin in a Ca^{2+}-dependent manner both *in vitro* and *in vivo* (Kim et al., 2002; Bhat et al., 2005). There are 15 MLO proteins in *Arabidopsis thaliana* with representatives from five of the seven MLO clades in the plant kingdom (Devoto et al., 2003; Kusch et al., 2016). MLO proteins have been shown to function as a part of dynamic signaling pathways in response to various stimuli. Both NTA and Barley MLO (HvMLO) actively redistribute within their respective cell types to the site of invasion/penetration (the

filiform apparatus in synergids or powdery mildew penetration sites) (Bhat et al., 2005; Kessler et al., 2010). However, the functional significance of such redistribution remains to be elucidated. Similarities between MLO function in pathogen susceptibility and PT reception make determining the role MLO proteins play in either system invaluable to understanding widely conserved intercellular communication pathways within plant cells.

Taking advantage of the diversity within the *Arabidopsis* MLO family (Supplemental Fig. 2.1), we determined that the localization of AtMLO proteins within a Golgi-associated compartment in the synergid cell before PT arrival correlates with but does not completely explain MLO function in PT reception. This suggests that many coincidental characteristics influence MLO function within this pathway. A structure-function analysis via domain swap experiments revealed that the N-terminal region of NTA is sufficient to confer NTA activity on MLO8 and may play a role in homo-oligomerization. Additionally, we found that the identity of NTA's C-terminal tail is important for MLO-mediated PT reception and controls specificity of function even between closely-related MLO proteins.

Results

Expression of MLO Proteins in the Synergids of *nta-1* Reveals Differences in their Ability to Mediate Pollen Tube Reception

Previous work with AtMLO (MLO) proteins involved in powdery mildew infection showed that MLO2, MLO6, and MLO12, all members of the same monophyletic clade, were involved in powdery mildew susceptibility (Consonni et al., 2006). By analogy to the "powdery mildew clade", we wondered if MLO10 and MLO8, both part of the same

clade as NTA (Fig. 2.1A, clade III), could have redundant functions within PT reception. We first asked whether these closely related MLOs are expressed in synergid cells as NTA is. Native promoter genomic GUS (Fig. 2.1, C–E) and GFP (Fig. 2.1, H–K) fusions of MLO10 and MLO8 were analyzed and compared to NTA to determine their expression patterns in unfertilized ovules. NTA was limited to synergids in both GUS (Fig. 2.1C) and GFP (Fig. 2.1, H–I) expressing lines, similar to previous reports (Kessler et al., 2010). MLO10 (Fig. 2.1D) and MLO8 (Fig. 2.1E) were expressed in ovules, but only MLO8 was expressed near the synergids. Additional analysis with MLO_{pro}:MLO-GFP constructs revealed no GFP accumulation within the synergid cells of either MLO10 (Fig. 2.1J) or MLO8 (Fig. 2.1K) expression lines. However, MLO8-GFP was detected just outside of the synergids, in inner integument cells closely associated with the filiform apparatus (Fig. 2.1K; Supplemental Fig. 2.2).

In order to better understand how NTA functions in PT reception, we utilized the sequence diversity found within the MLO family by testing divergent MLOs for their ability to function in MLO-mediated PT reception (Fig. 2.2A). In addition to NTA, MLO10, and MLO8, we also chose MLO2 (from clade V) and MLO1 (from clade II), as even more distant proteins within the MLO phylogeny in respect to NTA. All MLO proteins tested in our experiment have the same predicted topology, with 7 membrane spanning domains and a calmodulin-binding domain in the C-terminal cytoplasmic tail (Supplemental Fig. 2.1). MLO2 and MLO1 are both expressed in ovules, but not in synergid cells (Fig. 2.1, F–G and L–M). All five of these MLOs were then ectopically expressed in the synergid cells of *nta-1* using $MYB98_{pro}$, a synergid-selective promoter (Kasahara et al., 2005), in order to assay their ability to rescue the *nta-1* PT reception phenotype. These constructs also incorporated a C-terminal GFP fusion onto each

MLO ($MYB98_{pro}$::MLO-GFP) in order to confirm expression and determine distribution/localization within the synergid cell.

In *nta-1* mutants, ovules remain unfertilized due to PT overgrowth during PT reception (Kessler et al., 2010), thus the percentage of unfertilized ovules can be used as a measure for the ability of an introduced construct to complement the *nta-1* phenotype. Unfertilized ovule counts revealed that NTA-GFP expressed under $MYB98_{pro}$ could fully rescue *nta-1* in comparison to NTA-GFP expressed under its native promoter (Supplemental Fig. 2.3), indicating that the $MYB98_{pro}$ drives expression in the synergid cells at sufficient levels for NTA activity. Both MLO10-GFP and MLO2-GFP significantly rescued *nta-1* when expressed in synergids, while MLO8-GFP and MLO1-GFP did not significantly reduce the percentage of unfertilized ovules compared to *nta-1* (Fig. 2.2A). MLO10 has the highest sequence similarity and is the most closely related to NTA according to phylogenetic analysis (Fig. 2.1A). Interestingly, MLO8 cannot rescue *nta-1*, although it is in the same sub-clade as NTA, while MLO2, a clade V MLO, does complement *nta-1*. This suggests that MLO-mediated PT reception requires specific properties of an MLO and that not all MLO proteins can function in the pathway.

MLOs Differ in their Distribution within Synergids and in their Localization in the Endomembrane System

We hypothesized that an MLO's ability to complement the *nta-1* phenotype when expressed in synergids may be dependent on whether it is localized within the appropriate subcellular location. To assay MLO distribution in the synergid cell prior to PT arrival, unfertilized ovules from lines transformed with each MLO-GFP construct were imaged using confocal laser scanning microscopy (CLSM). As was previously reported (Kessler et al., 2010), NTA accumulated within the endomembrane system of

the synergid cell and was distributed throughout the entire cell but was excluded from the filiform apparatus prior to PT arrival (Fig. 2.2B). MLO10 and MLO2 distribution were similar to NTA; however, some GFP signal was also detected in the filiform apparatus (Fig. 2.2, C, E). MLO8 was predominately distributed toward the filiform apparatus with additional GFP signal detected throughout the rest of the cell (Fig. 2.2D), while MLO1 was primarily localized to the filiform apparatus (Fig. 2.2F). Quantification of MLO-GFP distribution within the synergid cell confirmed that MLO10 and NTA are significantly less distributed toward the filiform apparatus than either MLO8 or MLO1 (Supplementary Fig. 2.4). Interestingly MLO2 varied in its distribution, with some synergids having GFP distributed towards the filiform apparatus and others being more cytoplasmic (Supplementary Fig. 2.4, I–K). Overall, the presence of the ectopically expressed MLOs in the filiform apparatus of synergids in unfertilized ovules made it difficult to assess whether active redistribution in response to PT arrival was conserved among the proteins analyzed. However, these results demonstrate that the presence of an MLO protein at the filiform apparatus during PT reception is not sufficient to rescue *nta-1* (MLO8 and MLO1), and that either an MLO's localization within the specific compartments that NTA localizes within or the active process of redistribution to the filiform apparatus may be key to MLO function in PT reception.

While MLO distribution within the synergid cell varies, the ability of MLO10, MLO8, and MLO2 to localize within cytoplasmic compartments similar to those seen in NTA-GFP lines may represent an important characteristic for MLO function in this pathway (Fig. 2.2, B–E). Therefore, determining the identity of the NTA-localized compartment may be important for understanding MLO function. To this end, the subcellular localization of NTA was defined using a stable co-expression assay in synergids with markers for specific organelles. Previously reported markers for Golgi, Endoplasmic Reticulum, and

Peroxisomes (Liu et al., 2016) were co-expressed with $MYB98_{pro}$:NTA-GFP in synergid cells (Fig. 2.3, A–C). NTA predominantly co-localized with the Golgi marker, with additional GFP signal detected outside the range of the mCherry channel (Fig. 2.3A). This suggests that NTA is localized within Golgi bodies and may also be associated with post-Golgi vesicular trafficking. We then performed a co-localization analysis using the same Golgi marker co-expressed with the MLOs used in this study to determine if the others accumulate in this compartment similar to NTA (Fig. 2.4). MLO10 (Fig. 2.4A) partially co-localized with the Golgi marker at similar levels as NTA. MLO2 (Fig. 2.4C) co-localized with the Golgi marker to a lesser extent than either MLO10 or NTA, while MLO8 (Fig. 2.4B) and MLO1 (Fig. 2.4D) showed no overlap with the Golgi marker in synergid cells.

Since the differences detected in subcellular localization between closely related MLOs correlated well with their ability to rescue *nta-1* (neither MLO8 nor MLO1 co-localized with the Golgi marker), we wanted to further elucidate the identity of the MLO8-localized compartment and compare it to NTA. To this end, $MYB98_{pro}$::SYP61-mCherry, a trans-Golgi Network (TGN) localized marker (Sanderfoot et al., 2001; Viotti et al., 2010), was co-expressed in synergids with NTA-GFP, MLO10-GFP, and MLO8-GFP in order to determine if these closely related MLOs differentially co-localized within TGN-associated compartments (Fig. 2.5). NTA had no overlap (Fig. 2.5A) while MLO10 and MLO8 both partially co-localized with the TGN marker in synergids (Fig. 2.5, B–C). This further demonstrates a distinct difference between NTA and MLO8, revealing that localization within the proper compartment could be functionally significant. Interestingly, the partial co-localization of MLO10 (which fully rescues *nta-1*) with both Golgi and TGN markers suggests that the presence of an MLO within

endomembrane compartments outside of the range of NTA does not have a negative impact on function.

These distribution/localization experiments revealed that MLO proteins are trafficked differentially within synergid cells. Multi-spanning membrane proteins can be initially directed into the membrane through a variety of different mechanisms, typically encoded as signals within the protein (Goder and Spiess, 2001). In an effort to predict the presence of signal peptides in MLO proteins, sequences of all 15 MLOs were examined using the SignalP 4.0 prediction server (Petersen et al., 2011). Interestingly, we found that out of the 15 *Arabidopsis* MLOs only NTA, MLO10, and MLO8 had significantly predicted cleavable N-terminal signal peptides (Supplemental Fig. 2.5). This suggests that this subclade (NTA, MLO10, and MLO8) of the clade III MLOs may be type I multi-spanning membrane proteins (Goder and Spiess, 2001) further differentiating them from the other 12 *Arabidopsis* MLOs. To determine if NTA's predicted signal peptide influences its localization and function within PT reception, we cloned NTA without this signal peptide (NORTIA Δsp) and expressed it in the synergid cells of *nta-1* under control of $MYB98_{pro}$ (Supplemental Fig. 2.6). Removing NTA's signal peptide appeared to have no effect on its function or distribution in the synergid cell prior to PT arrival (Supplemental Fig. 2.6, A–D). We then generated $35S_{pro}$::NTA-GFP and $35S_{pro}$::NORTIA Δsp-GFP constructs and performed a transient co-expression assay in *Nicotiana benthamiana* epidermal cells with a previously published Golgi-mCherry marker (Nelson et al., 2007). Similar to its localization in synergids, NTA partially co-localized with the Golgi marker (Supplemental Fig. 2.6, H–J), while NORTIA Δsp-GFP predominately accumulated in subdomains of the plasma membrane with no overlap with the Golgi marker (Supplemental Fig. 2.6, E–G). The presence of a signal peptide could help explain the MLO localization/distribution

patterns observed within synergid cells, however, this is not enough to account for function in PT reception or for localization within Golgi-associated compartments, as MLO8 does not rescue the *nta-1* PT reception phenotype and localization within Golgi was not detected (Figs. 2.2A and 2.4B). Additionally MLO2, which has no predicted signal peptide, and NORTIA Δsp are able to rescue *nta-1*'s PT reception phenotype and are distributed similarly to full length NTA in the synergid cell. This suggests that synergids may have cell-type specific mechanisms that determine the localization of this class of membrane proteins.

The N- and C-Terminal Domains of NTA are Important for Function

MLO8 is closely related to NTA, sharing 61% identity and 73% similarity at the amino acid level. The differential subcellular localization patterns and inability to complement the *nta-1* PT reception phenotype make MLO8 a good tool for dissecting regions of the NTA protein that are important for its function in PT reception. In order to identify functionally significant regions in the NTA protein, we performed a targeted structure-function analysis of NTA via domain swap experiments with MLO8. Regions swapped were chosen based both on sequence dissimilarity between the two MLOs and on domains previously found to be important for MLO function (Elliott et al., 2005; Chen et al., 2009). Chimeric MLOs were expressed in the *nta-1* mutant background under control of $MYB98_{pro}$ and ovule counts from T2 homozygous transgenic lines were used as a proxy for determining functionality in PT reception. Protein-GFP fusion distribution was analyzed for each line and revealed significant accumulation of all chimeric proteins with varying localization patterns in comparison to the full length MLOs (Supplemental Figs. 2.7, 2.8 and 2.9). Chimeric proteins that were able to complement *nta-1* were not primarily confined to the Golgi-associated compartment as seen with NTA; in addition to Golgi localization, proteins accumulated within the synergid

vacuole. Comparable variations in localization have been previously reported in a similar structure-function analysis of MLO family proteins (Chen et al., 2009), indicating that chimeric fusions of MLOs may partially disrupt intramolecular interactions within the chimeric proteins and subsequent regulation of their trafficking within the cell.

An N-terminal swap, including the N-terminus through the first extracellular loop (NEL1, Fig. 2.6B), demonstrated this region to be functionally significant for MLO-mediated PT reception. NTA[NEL1]-MLO8 could partially rescue *nta-1* in comparison to full length NTA while MLO8[NEL1]-NTA was not significantly different than full length MLO8 in its ability to complement the *nta-1* phenotype (Fig. 2.6B). This domain was further subdivided into swaps of only intracellular loop 1 (IL1) and extracellular loop 1 (EL1). Interestingly, constructs with either MLO's EL1 (NTA-MLO8[EL1]-NTA and MLO8-NTA[EL1]-MLO8) were capable of rescuing *nta-1* (Fig. 2.6C) while swaps of IL1 conferred no significant changes from the full-length proteins' ability to rescue (Supplemental Fig. 2.9A), indicating that NTA's EL1 is sufficient to confer NTA activity on MLO8, but the MLO8 EL1 does not compromise NTA's function unless it is combined with the MLO8 IL1 and N-terminus. Additionally, swaps of intracellular loop 2 (IL2), a prominent domain in both size and variability, had no significant impact on either MLO's function (Supplemental Fig. 2.9F). In a previous study it was shown that the NEL1 domain of MLO4 could confer partial function to MLO2 in rescuing the root curling phenotype of *mlo4-1*; however, the reciprocal swap placing MLO2's NEL1 domain onto MLO4 remained functional (Chen et al., 2009). Here we have identified the NEL1 domain of NTA as necessary for its role in PT reception and sufficient in conferring function to MLO8.

The C-terminal tails of MLO proteins have been described as intrinsically disordered, a characteristic that may contribute to specificity in function between closely related MLOs (Kusch et al., 2016). In comparison to NTA, MLO8 has a longer C-terminal tail following the conserved Calmodulin Binding Domain (CaMBD) (Supplemental Fig. 2.1). To test if their C-terminal intracellular domains provide functional specificity, NTA/MLO8 C-terminal domain swaps were analyzed in *nta-1*. NTA's C-terminus on MLO8 (MLO8-NTA[CTerm]) rescued *nta-1* at similar levels as full length NTA whereas MLO8's C-terminus on NTA (NTA-MLO8[CTerm]) rescued at an intermediate level and was significantly different than NTA (Fig. 2.6E). When this domain swap was expanded, incorporating both the third intracellular loop (IL3) and the third extracellular loop (EL3), similar results were observed in which NTA[TM5]-MLO8 did not fully rescue and MLO8[TM5]-NTA rescued *nta-1* compared to full length NTA (Fig. 2.6D), demonstrating that there is no change in the effect on function with these additional domains. This suggests that the identity of NTA's C-terminal tail domain is crucial for its function and that this domain is necessary and sufficient for MLO-mediated PT reception.

In our analysis of full-length MLO proteins expressed in synergid cells, distribution within the synergid cell and co-localization with a Golgi marker correlated well with their ability to function in PT reception. Based upon these observations, we hypothesized that the functional NTA/MLO8 domain swaps were primarily distributed throughout the cell and not toward the filiform apparatus and that they would localize within Golgi in a similar manner as NTA, MLO10, or MLO2. To test this, we quantified MLO-GFP distribution for the NEL1 and CTerm domain swaps within the synergid cell and also performed a co-localization analysis with the same Golgi marker expressed in synergid cells (Supplemental Fig. 2.8 and Fig. 2.7, respectively). Interestingly, the domain

swaps that failed to fully function in PT reception (MLO8[NEL1]-NTA and NTA-MLO8[CTerm]) were more similar to NTA in their distribution than their functional reciprocal swaps (Supplemental Fig. 2.8). Additionally, partial co-localization with the Golgi marker was detected with all four swaps analyzed (Fig. 2.7) and we could not identify MLO8-like exclusion of any of the chimeric protein-GFP fusions from the Golgi-associated compartments. Even MLO chimeric proteins with disrupted function (NTA[NEL1]-MLO8 and NTA-MLO8[CTerm]) partially co-localized with the Golgi marker in synergids. This suggests that an MLO's ability to function in PT reception is not solely dependent on localization within a specific part of the endomembrane system (although at least some accumulation appears to be required as MLO1 does not rescue *nta-1*) but requires some additional characteristic of the protein influenced by their N- and C-terminal domains.

The N-Terminal Domain of NTA Influences Efficient Homo-Oligomerization

The domain swap constructs that were compromised in their ability to complement *nta-1* did not show MLO8-like exclusion from the Golgi compartment, indicating that other molecular properties may have been disrupted in these chimeric proteins. MLO proteins have previously been shown to homo-oligomerize and conserved cysteine residues residing within EL1 were proposed to play a role in this interaction (Elliott et al., 2005). Since the replacement of the NTA NEL1 domain with MLO8's NEL1 fully disrupted its ability to function, we hypothesized that homo-oligomerization was important for NTA's function and that the NEL1 domain swap inhibited this interaction. Using a FRET-based assay in *N. benthamiana* epidermal cells, we tested whether NTA and MLO8 were able to homo- or hetero-oligomerize *in planta* and whether the NEL1 chimeric proteins generated could successfully recapitulate this characteristic. FRET was determined using a correlation analysis comparing the fluorescence emission of

the donor (mCerulean3 (Cer3) (Markwardt et al., 2011)) to the emission of the acceptor (YFP (Nagai et al., 2002)) detected after four subsequent rounds of acceptor photobleaching. Fluorescence emission from both channels was compared using a Pearson product-moment correlation analysis in which the more negative the correlation coefficient the stronger the FRET signal, as this would indicate a proportional increase in donor fluorescence and corresponding decreases in acceptor fluorescence (Supplemental Fig. 2.10; See Materials and Methods). Since NTA localized within Golgi compartments in *N. benthamiana* epidermal cells (Supplemental Fig. 2.6, H–J), we generated a positive control for the detection of FRET via acceptor photobleaching in NTA-localized compartments, in which Cer3 and YFP were fused in tandem onto NTA's C-terminal tail (NTA-Cer3-YFP). This ideal standard had a median donor-acceptor correlation coefficient of -0.9864 confirming that FRET could be reproducibly detected within NTA-associated Golgi and post-Golgi vesicles (Fig. 2.8). NTA-Cer3 was co-expressed with GUS-YFP and analyzed in each experiment as a negative control (with a median coefficient of 0.5217). FRET was detected at similar levels in test pairs that included: NTA-Cer3 + NTA-YFP and NTA[NEL1]–MLO8-Cer3 + NTA[NEL1]–MLO8-YFP (with median coefficients of -0.93405 and -0.8906, respectively). FRET was detected at significantly lower levels than the first group in the test pairs: MLO8-Cer3 + MLO8-YFP, NTA-Cer3 + MLO8-YFP, and MLO8[NEL1]–NTA-Cer3 + MLO8[NEL1]–NTA-YFP (with median coefficients of -0.6815, -0.5859, and -0.4126) (Fig. 2.8). While all pairs examined were significantly different than the negative control, this experiment indicates that MLO8[NEL1]–NTA, which does not rescue *nta-1*, homo-oligomerizes less efficiently than full length NTA under our experimental conditions. Reciprocally, no difference was detected between homo-oligomerization efficiencies of NTA or NTA[NEL1]–MLO8, which both rescue *nta-1*. Taken together, these data suggest that the homo-oligomerization of NTA could be an

intrinsic part of its function in PT reception and that disruption of NTA's NEL1 domain may reduce the efficiency of this interaction, thus compromising its function.

Discussion

PT reception requires a chain of signaling events in both the arriving pollen tube and within the receptive synergid cell (Kessler and Grossniklaus, 2011). In this study, we have further defined the role of NTA, an MLO protein involved in the female side of this signaling process. The analysis of MLOs closely related to NTA revealed a divergence in expression patterns within reproductive tissues and in their ability to function within PT reception. Previous studies of *Arabidopsis* MLOs have identified functional redundancy and co-functional relationships within discrete monophyletic clades of the MLO family (Consonni et al., 2006; Chen et al., 2009). Our data indicates that, of the MLOs presented in this study, NTA is the only MLO that is specifically expressed within synergid cells and likely functions independently from other closely related MLOs. The ectopic expression of full-length MLO proteins in the synergid cells of *nta-1* revealed that specific characteristics of an MLO are required for function in PT reception. The closely related MLO8 (clade III) does not complement *nta-1* while the more distantly related MLO2 (clade V) could, further demonstrating this divergence in function.

Our data showed that the ability of other MLO proteins to complement the *nta-1* PT reception phenotype was closely correlated with the ability of the synergid-expressed MLO to accumulate in a Golgi-associated compartment before PT arrival. However, analysis of chimeric MLO proteins during a structure-function analysis revealed that localization/retention within this Golgi-associated compartment is not the sole determinant of MLO function in PT reception. Accumulation within the synergid

endomembrane system prior to PT arrival is conserved between those MLOs (and chimeric constructs) capable of functioning in this pathway. Previous work showed that NTA redistributes to the filiform apparatus during PT reception, indicating that precise control of the synergid secretory system and polarized transport may be necessary for MLO function in this pathway (Kessler et al., 2010). Instances of enhanced trafficking of vesicles and induction of specialized secretory mechanisms in response to pathogens have been widely reported in plants (Kwon et al., 2008; Nielsen et al., 2012; Ding et al., 2014), including responses specific to powdery mildew infection (An et al., 2006; An et al., 2006). Polar redistribution events observed in NTA-mediated PT reception and in MLO-mediated fungal penetration suggests a conservation of signal-induced MLO transport. Additionally, the SNARE proteins ROR2 (barley) and PEN1 (*Arabidopsis*) are required for *mlo* pathogen resistance, providing evidence that MLO-mediated responses require activation of the secretory pathway with reported focal accumulation of ROR2 occurring at the site of infection (Bhat et al., 2005; Hückelhoven and Panstruga, 2011). NTA seems to follow a similar paradigm, with NTA's redistribution dependent on signaling via FERONIA (FER), a member of the CrRLK1L-type family of receptor like kinases and a key player in the early stages of PT reception (Escobar-Restrepo et al., 2007; Kessler et al., 2010; Ngo et al., 2014).

Secretory pathway regulation has also been shown to be important for controlling intercellular signaling during compatibility responses in *Brassica* species (Samuel et al., 2009; Safavian and Goring, 2013). In early pollen recognition events, an induction of secretory activity in stigmatic papillae was observed during compatible pollinations while an active inhibition of trafficking was noted in incompatible pollinations (Safavian and Goring, 2013). This increase in secretory activity occurs in a polarized manner toward the pollen grain upon successful signal transduction within the receptive papilla

cell, and is directly associated with the hydrating pollen grain. The parallels between secretory regulation of polarization during pollen:stigma and PT:synergid interactions suggest that precise control of the secretory pathway in response to extracellular signals may be an important characteristic of multiple levels of pollen:pistil interactions during pollination. It will be interesting to determine if similar inhibition of trafficking activity occurs during instances of PT overgrowth as described during incompatible pollinations and if MLO-mediated processes are involved in both.

Our experiments expressing full-length MLO proteins in synergid cells shows that one important determinant of MLO functionality in PT reception is the ability to localize within an endomembrane-associated compartment prior to PT arrival and thus presumably before FER-mediated signaling occurs. While distribution and localization within the synergid cell varied between MLOs, the accumulation of MLO proteins involved in PT reception within endomembrane compartments of the synergid cell could be required for multiple reasons. One hypothesis is that proper timing of polar redistribution to the filiform apparatus is critical for PT reception and that the retention of MLOs within either the Golgi or TGN prevents this redistribution until proper signaling is achieved as a PT communicates with the receptive synergid. This suggests that the presence of an MLO (or an MLO-associated compartment) at the filiform apparatus prior to PT arrival is not ideal and may even be inhibitory to the synergid cell by functioning too early. However the data presented here does not support this hypothesis since MLO2 and several chimeric MLO fusions rescued *nta-1* even though instances of MLO-GFP distribution toward the filiform apparatus prior to PT arrival were observed. A second possibility is that NTA retention facilitates its co-localization and/or interaction with some unknown co-factor required for MLO-mediated PT reception. This co-factor could be involved in forming a complex with NTA and/or other components of

the PT reception machinery or could be a secreted signaling molecule that needs to be escorted to the filiform apparatus for communication with the arriving PT. Further dissection of the required components involved in MLO-mediated processes will help elucidate the exact mechanism of MLO function.

The differences observed in MLO distribution within the synergid cell and localization between multiple cell types (NTA vs. NORTIA Δsp localization in the synergid compared to tobacco epidermal cells) may represent cell-type specific processes regulating the incorporation and retention of MLOs within the required endomembrane compartments of the synergid cell; data that supports the second hypothesis proposed above. Mechanisms regulating membrane protein polarization in plant cells have been well described, especially related to the asymmetric distribution of *Arabidopsis* PIN-FORMED (PIN)-type auxin transport proteins (Luschnig and Vert, 2014). However, it is unclear just how conserved such polarization mechanisms are within the synergid cell. Synergids are highly polarized cells that have two purposes in plant reproduction. Before PT arrival, the synergid cells secrete small LURE peptides in order to attract the PT to the micropyle of the ovule (Higashiyama, 2002; Okuda et al., 2009). The second purpose of synergids is to recognize when a PT has arrived and communicate with it facilitating the release of sperm cells so that double fertilization can occur. These distinct purposes necessitate a change in synergid cell biology from an “attractant state” with high level of protein secretion to a “signaling state” where calcium oscillations and FER-mediated signal transduction cascades prepare the synergid for PT reception (Kessler and Grossniklaus, 2011; Hamamura et al., 2014; Ngo et al., 2014; Higashiyama and Takeuchi, 2015). Interestingly, no PT reception mutants have been reported as having defects in PT attraction, providing evidence for distinct processes regulating both pathways (Huck et al., 2003; Escobar-Restrepo et al., 2007;

Kessler et al., 2010; Tsukamoto et al., 2010; Lindner et al., 2015). This suggests that a change in secretory mechanisms occurs as the PT arrives and FER-mediated PT reception initiates. Overall, more work must be done to determine the conservation of mechanisms regulating membrane polarization and protein secretion that govern these distinct roles of the synergid cell.

Homo and hetero-oligomerization has been demonstrated to be functionally important in various multispanning membrane protein families, where oligomerization is critical for processes such as signal transduction (Maurel et al., 2008), pore or channel formation (Musil and Goodenough, 1993; Véry and Sentenac, 2002), as well as subcellular localization within the endomembrane system (Weisz et al., 1993). While the homo-oligomerization of MLO proteins was previously established (Elliott et al., 2005), the functional significance of this interaction and the domains contributing to dimerization were not described. Here we have shown the homo-oligomerization of NTA *in planta* with a FRET-based interaction assay and demonstrated a reduction of this dimerization upon disruption of an N-terminal domain (NEL1). Further confirmation of the NEL1 domain's importance in the effective dimerization of NTA was established in the reciprocal detection of efficient homo-oligomerization of the NTA[NEL1]-MLO8 chimeric protein, which fully complements the *nta-1* unfertilized ovule phenotype. It should be noted that since this experiment was based on a transient assay in *N. benthamania* epidermal cells and not in the synergid cells of *A. thaliana* where NTA functions in PT reception, care must be taken in the interpretation of these interaction data. However, similar localization of NTA-GFP within the Golgi of both cell types demonstrates some conservation of its native characteristics in our assay. Furthermore, the data presented in this study suggests a reduction in the *efficiency* of interactions between those MLOs incapable of functioning in PT reception (MLO8 and

MLO8[NEL1]–NTA) and as such more validation is required to fully elucidate the role of homo-oligomerization in MLO-mediated PT reception.

Calcium is an important signaling molecule in plants with reported roles in systemic responses, cell-cell communication, and intracellular signaling (Dodd et al., 2010; Gilroy et al., 2014). Oscillation of calcium in the synergid cell upon PT arrival is dependent on FER-mediated signaling during PT reception (Hamamura et al., 2014; Ngo et al., 2014). In *nta-1* mutants, PT reception is not impaired in every ovule. Incomplete penetrance of the *nta-1* phenotype suggests that some ovules have normal fertilization if calcium oscillations within the synergid cell can reach a certain threshold (Ngo et al., 2014). CaM-binding capacity of NTA may in some way modulate calcium signaling during PT reception. In this study, we found that swapping the C-terminal tail (which contains the conserved MLO CaMBD) of NTA with MLO8's partially disrupted its ability to function in this pathway. However, NTA's C-terminal tail on MLO8 was able to function in MLO-mediated PT reception, therefore we speculate that this domain may confer the ability to modulate calcium signaling within the synergid cell above this threshold when it is present in a closely related MLO. The MLO C-terminal tail was recently described as intrinsically disordered, suggesting that this domain influences functional specificity throughout the family (Kusch et al., 2016). These data further support the hypothesis that fundamental differences affecting function exist in the C-terminal domains of MLO proteins.

While this study significantly contributes to our understanding of MLO-mediated PT reception, an exact mechanism of NTA's function throughout gametophytic interaction remains to be determined. NTA itself could be involved in signaling with the PT to trigger release of the sperm cells, or, alternatively, other factors contained in the NTA-

associated compartments could be delivered to the filiform apparatus along with NTA to assist in communication with the PT. Our domain swap experiments have indicated that both homo-oligomerization, influenced by the N-terminal domain of NTA, and C-terminal tail identity are important for NTA function in PT reception. Future work on NTA's active redistribution during PT reception and its relationship to calcium oscillations within the synergid cell will provide more insight into how MLO proteins function during cell-cell communication.

Methods and Materials

Plant Growth Conditions

Full length MLOs and domain swap constructs were transformed into homozygous *nta-1* insertion mutants in the Wassilewskija (Ws-2) background. Wild-type Ws-2 (Ws) and *nta-1* were used as the controls for all ovule count experiments. Native promoter GUS and GFP fusion constructs were transformed into the Col-0 ecotype. All *Arabidopsis thaliana* were grown at 22°C in long day conditions (16 hours of light and 8 hours of dark) in a custom built grow room. Seeds were sterilized and plated on ½ MS plates with transgenic lines either grown on ½ MS plates supplemented with 20mg/L hygromycin (full length MLO and domain swap ovule count lines and native promoter lines) or planted directly on soil (endomembrane marker co-expression lines) and kept in the dark at 4°C for two days for cold-stratification. 5-7d old seedlings were transplanted from plates to soil (ProMix Flex supplemented with 40g MARATHON pesticide and Peter's 20:20:20 (NPK) fertilizer at recommended levels) and grown until flowering for further analysis. Seeds sown directly on soil were treated with BASTA herbicide spray for three successive days starting at 5 days after germination and

resistant plants were maintained for analysis. *Nicotiana benthamiana* was grown on soil in long day conditions at 22°C in a Conviron ATC13 growth chamber.

Cloning and Generation of Transgenic Lines

PCR with PHUSION High-Fidelity Polymerase (NEB, M0535S) was utilized to generate all constructs in this study. Genes were amplified with primers that had attB1 and attB2 sites for recombination via BP reaction into the Gateway-compatible entry vector pDONR207 (Supplemental Table 2.1). Native promoter constructs were amplified from Col-0 genomic DNA, while full-length MLO and domain swap constructs were amplified from cDNA derived from rosette leaves or flowers of Col-0. Native promoter entry vectors were recombined via LR reactions into pMDC107 (GFP) and pMDC163 (GUS) (Curtis, 2003) to generate reporter fusion expression vectors. Full-length MLO cDNA entry vectors were recombined via LR reactions into the pMDC83 backbone with the $MYB98_{pro}$ promoter (Muller et al., 2016) to drive synergid-selective expression with a C-terminal GFP fusion. Domain swap and site-directed mutagenesis constructs were made using primers listed in Supplemental Table 2.1 to generate overlapping fragments of specific regions from full-length NTA and MLO8 entry vector cDNA template described above. AttB sites were included on the ends of the chimeric constructs and fragments were pieced together using a PCR-pasting protocol. Amplified chimeras were recombined via BP reaction into pDONR207 and entry vectors were subsequently recombined via LR reaction into the modified pMDC83 backbone described previously. All entry vectors were sequenced to ensure swaps were present within each construct.

$MYB98_{pro}$::SYP61-mCherry construct was generated in a single reaction using a 3 fragment Gibson Assembly, with Gibson Assembly Master Mix NEB E2611S (Gibson

et al., 2009). SYP61 was amplified from Col-0 flower cDNA and $MYB98_{pro}$ was amplified using the pMDC83 backbone previously described (Lindner et al., 2015). Fragments were assembled into the pEarlyGate301 backbone following digestion with PacI (NEB R0547S) and BamHI (NEB R3136S) and subsequent gel purification. Primers with overlaps used for amplification are listed in Supplemental Table 2.1.

Constructs for transient expression in *N. benthamiana* were generated using entry vectors of full-length MLOs recombined via LR reaction into pMDC83, which has a 2× 35S viral promoter and C-terminal GFP fusion (Curtis, 2003). Gateway-compatible destination vectors with C-terminal mCerulean3 (mCer3), C-terminal YFP and N-terminal YFP were used for all FRET analyses (Myers et al., 2016). Entries described above were recombined into their respective FRET vectors via LR reaction.

***nta-1* Complementation Assays**

Expression vectors were transformed into the *Agrobacterium tumefaciens* strain GV3101 and subsequently transformed into *nta-1* via the floral-dip method (Bent, 2006). The resulting seeds were plated on ½ MS plates supplemented with 20mg/L hygromycin for selection of transgenic plants. 3-4 different insertion lines for each construct were taken to the T2 generation and homozygous plants were identified using fluorescence microscopy to ensure synergid expression of GFP in every ovule. Fertilization rates of self-pollinated flowers were counted in at least 3 plants from each line. Counts of unfertilized vs. fertilized ovules were performed and compared to controls in order to determine complementation status of each construct in the *nta-1* background. Aniline blue staining of pollen tubes in pollinated pistils was used to confirm that unfertilized ovules in the complementation lines were the result of *nta* mutant-induced pollen tube overgrowth and not other problems with female

gametophyte development or pollen tube attraction. Data was graphed and statistically analyzed using Prism (www.graphpad.com). Significance was determined using Analysis of Variance (ANOVA) and Dunnett's multiple comparison test. Full-length MLO complementation lines were compared to both *nta-1* and WS unfertilized ovule counts, resulting in the same significance with both tests (constructs that complement the nta-1 phenotype were significantly different than the *nta-1* control but not significantly different than the WS control, but only statistical tests with *nta-1* comparisons are shown in the figures for simplicity). Domain swap complementation lines were compared to full-length NTA and MLO8 unfertilized ovule counts.

GUS Staining of Ovules

Flowers from 2-3 T1 plants of each native promoter line were emasculated. At 2 days after emasculation, pistils were slit down the septum prior to being fixed for 45 min in 90% acetone at -20°C. Exposed ovules were vacuum infiltrated and incubated overnight in GUS staining solution (10 mM EDTA, 0.1% Triton X-100, 2 mM $Fe^{2+}CN$, 2 mM $Fe^{3+}CN$, 1 mg mL^{-1} X-GLUC (GoldBio) in 100 mM sodium phosphate buffer pH 7.2) at 37°C. Ovules were dissected out of the pistils into chloral hydrate:glycerol:water solution (8:1:2, w:v:v) and imaged using Differential Interference Contrast (DIC) optics on a Nikon Eclipse Ni-U compound microscope.

Transient Expression in *N. benthamiana*

Leaves from 4-6 week old *N. benthamiana* were co-infiltrated with *A. tumefaciens* strain GV3101 harboring either an MLO-GFP construct and –mCherry secretory marker discussed or Cer3 and YFP-fused proteins for analysis of FRET, along with the *A. tumefaciens* strain C58C1 containing the viral silencing suppressor helper complex pCH32 (Hamilton, 1997). For colocalization experiments, *A. tumefaciens* overnight

cultures were pre-treated as in (Myers et al., 2016). For FRET analysis, *A. tumefaciens* overnight cultures were centrifuged for 5 min at 4000*g* and resuspended/washed in 10mM $MgCl_2$ twice. A final suspension of each *Agrobacterium* in 10mM $MgCl_2$ was then co-infiltrated into the leaf. Plants were maintained in the growth chamber and all further analyses took place 2-4 days after infiltration.

Microscopy

Young flowers from lines with NTA-GFP driven by NTA's native promoter and $MYB98_{pro}$ were dissected out in water on a clean microscope slide. Ovules were imaged using a 40× dry objective (NA = 0.75) on a Nikon Eclipse Ni-U compound epifluorescent microscope equipped with an X-Cite 120 LED fluorescent lamp and narrow band eGFP filter cube. Brightfield images were taken using DIC optics and overlaid with fluorescence to determine where NTA-GFP was detected.

Ovules from MLO-GFP lines were dissected out 2 days after emasculating the flower and were removed but retained on the septum for analysis of GFP localization and distribution on a confocal scanning laser microscope (CSLM). Freshly dissected ovules were incubated on a slide in 20μM FM464 (Molecular Probes, T3166) in PIPES Buffer (50mM PIPES, 5mM EGTA and 1mM $MgSO_4$ at pH = 6.8) for 10 min on ice in a humid chamber (pipette tip box with ice in the bottom and moist kimwipes under the slide on the top). Cover slips were placed right before the samples were taken to the microscope and excessive staining solution was removed with a clean kimwipe. Images were taken on a Leica TCS SP8 CSLM using a HC PL APO 40× water immersion objective (NA = 1.10) with GFP excited by a 488nm argon laser and FM464 excited by a 561nm diode laser in sequential mode. Fluorescent signals were detected

using two HyD detectors in photon counting mode (single sections) and normal mode (z-series).

Co-localization of secretory markers in mature ovules used similar settings but a more narrow detection window for mCherry fluorescence. Ovules were dissected out but retained on the septum and placed in PIPES Buffer and imaged immediately. For transient co-localization experiments in *N. benthamiana*, leaf discs were collected near the site of infiltration, placed in PIPES Buffer and GFP and mCherry signals were imaged in cells expressing both constructs.

FRET Detection via Acceptor Photobleaching

Due to the rapid trafficking of NTA and MLO8-localized compartments within the epidermal cells of *N. benthamiana*, leaf discs were treated with 20µg/mL Cytochalasin B (Sigma-Aldrich, C6762) in PIPES Buffer for 10 min at room temperature prior to acceptor photobleaching. Epidermal cells co-expressing the two constructs to be assayed were chosen with mCer3 (donor) excited at 458nm and detected using a HyD detector from 459nm to 512nm, while YFP (acceptor) was excited at 514nm and detected with a PMT from 512 to 562nm, while using a 458/514 notch filter. Three images of both mCer3 and YFP were taken before photobleaching and in between each subsequent period of photobleaching (5 sec of high intensity 514 nm). After four rounds of photobleaching a final set of three images were taken of both mCer3 and YFP fluorescence.

Overall drift of punctate fluorescent compartments also made the analysis of FRET via a calculation of FRET Efficiency (as in previous studies (Karpova et al., 2003; Bhat et al., 2005)) inaccurate, as increases in fluorescence intensity could be a result of axial

shifts of the sample being imaged. Thus all data gathered was analyzed through the use of a custom Macro in Fiji (Schindelin et al., 2012). Fluorescence of mCer3 and YFP in the photobleached region were graphed and compared by determining their Pearson product-moment correlation coefficient. This enabled the accurate detection of mCer3 fluorescence signal changes over time in response to acceptor photobleaching. The distributions of the correlation coefficients from all assayed pairs within each experiment were compared using the non-parametric Kruskal-Wallis test with FDR-corrected multiple pairwise comparisons determined using the Dunn Test. Statistical analyses for FRET data were all carried out in R, version 3.1.2 (Team, 2014) using the packages dplyr (Wickham and Francois, 2015) and DescTools (Signorell, 2015).

Figure Construction and Image Processing

All images were edited using Fiji (Schindelin et al., 2012). MLO protein and ovule diagrams were made in Inkscape v0.91. All graphs were generated in Prism (www.graphpad.com) and figures were constructed in Gimp v2.8.14.

Figures and Tables

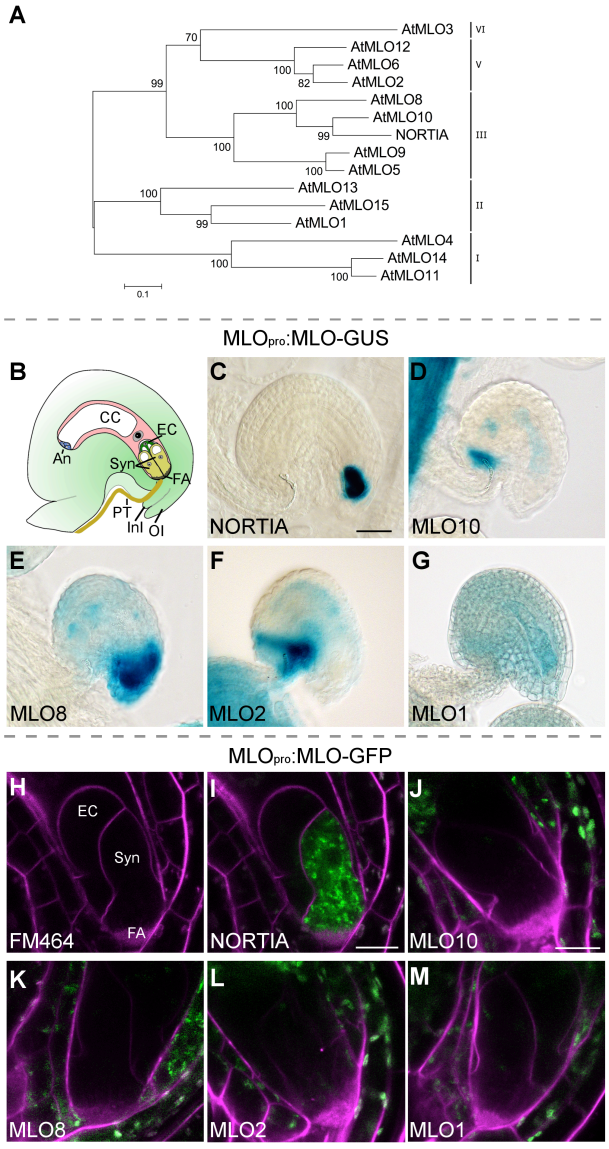

Figure 2.1 - Native MLO expression patterns in *Arabidopsis* ovules. A) Maximum-likelihood phylogenetic tree from an amino acid alignment of the 15 MLO proteins in *Arabidopsis thaliana* generated using MEGA6 (Tamura et al., 2013). Roman numerals refer to previously defined clades within the MLO family (Devoto et al., 2003; Kusch et al., 2016). B) Diagram of an *A. thaliana* ovule at PT arrival. CC - central cell, EC - egg cell, Syn - synergid, FA - filiform apparatus, PT - pollen tube, InI – inner integument, OI – outer integument, An - antipodals. C-G) GUS stained mature ovules of native promoter genomic MLO fusion proteins. H-M) Mature ovules of native promoter driven MLO-GFP protein fusion lines labeled with the membrane-localized dye FM464 to reveal the full outline of the synergid cell (I). Bars = 20μm (C-G), 10μm (H-M).

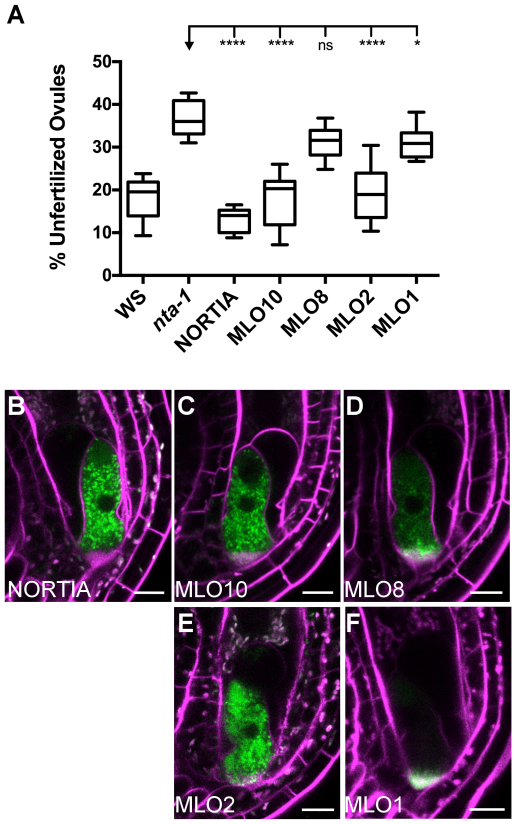

Figure 2.2 - **Analysis of MLO proteins expressed in synergids of *nta-1.*** A) Boxplot of unfertilized ovule counts in T3 plants homozygous for indicated $MYB98_{pro}$:MLO-GFP constructs in *nta-1* mutants. Boxplot represents full range of each dataset with median at the center. B-F) $MYB98_{pro}$:MLO-GFP (green) distribution in synergid cells of unfertilized mature ovules merged with FM464 labeling (magenta). Adj. P-values - " **** " = < 0.0001, " * " = 0.05-0.01, "ns" = >0.05. Bars = 10µm (B-F).

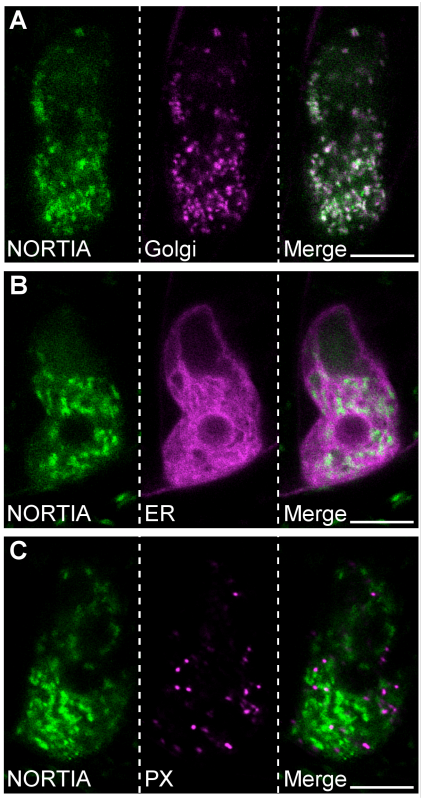

Figure 2.3 - NTA co-localization with secretory markers in synergids. A-C) Co-localization of $MYB98_{pro}$:NTA-GFP (green) with the Golgi (A; Man49-mCherry), ER (B; SP-mCherry-HDEL), and Peroxisome (C; mCherry-PTS1) markers (magenta) expressed under the synergid selective promoter of LRE (Liu et al., 2016) in the synergid cell. Bars = 10µm.

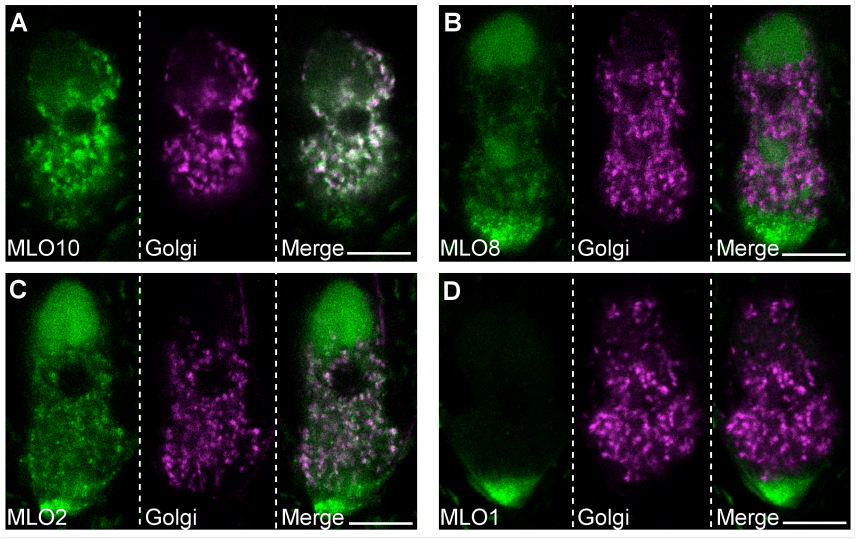

Fig 2.4. MLO co-localization with a Golgi marker in synergids. A-D) $MYB98_{pro}$:MLO-GFP (green) co-expressed with the Golgi marker (LRE_{pro}:Man49-mCherry; magenta) in the synergid cell. Bars = 10μm.

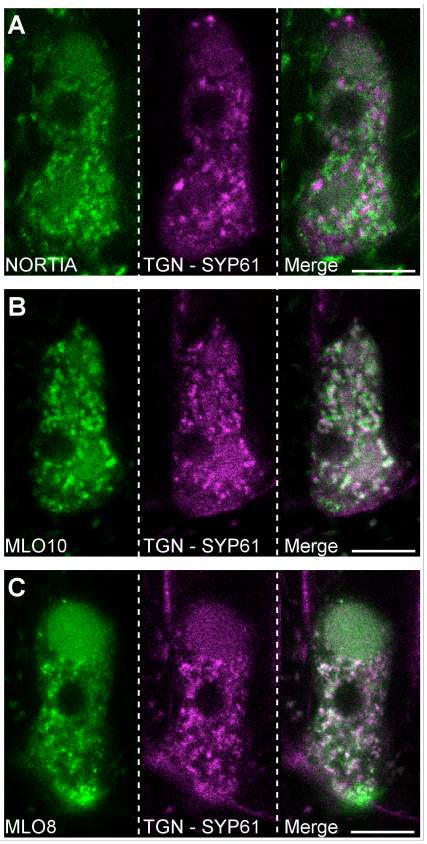

Fig 2.5. NTA, MLO10, and MLO8 co-localization with a trans-Golgi network (TGN) marker in synergids. A-D) $MYB98_{pro}$:MLO-GFP (green) co-expressed with the TGN marker ($MYB98_{pro}$::SYP61-mCherry; magenta) in the synergid cell. Bars = 10μm.

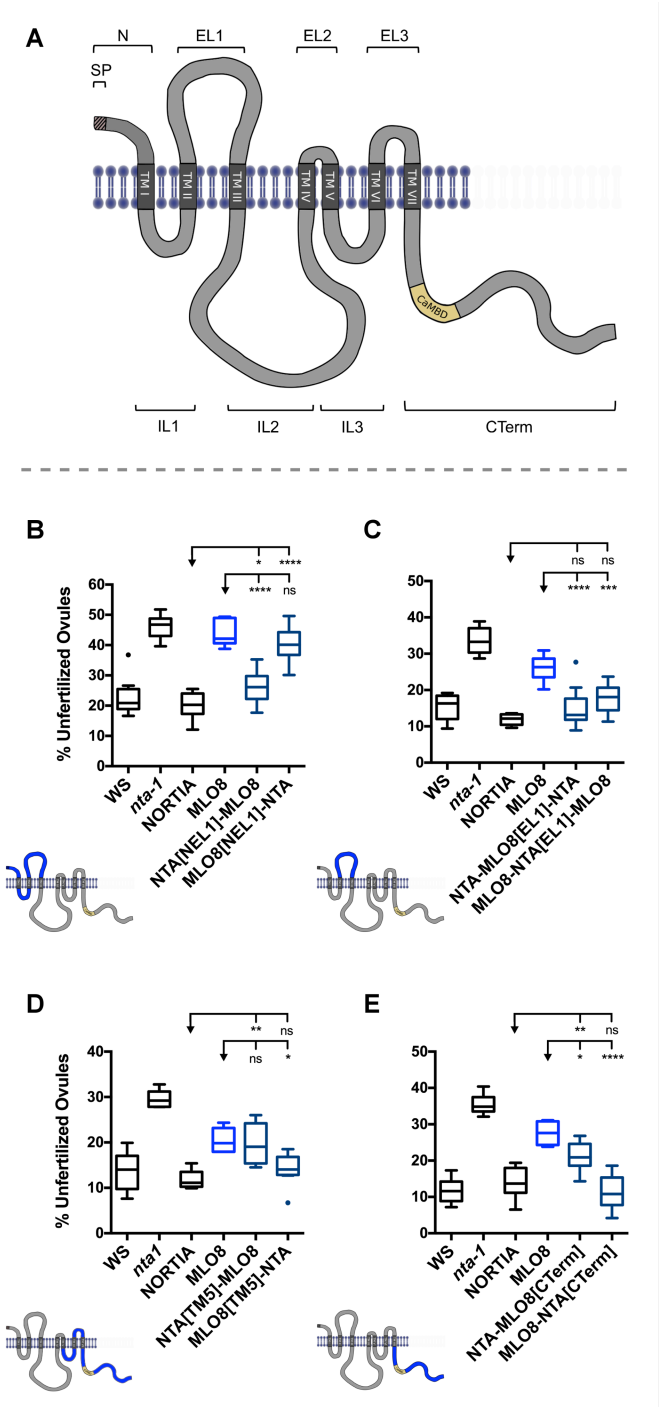

Fig 2.6. Analysis of domain swaps between MLO8 and NTA.
Legend on next page

Fig 2.6. Analysis of domain swaps between MLO8 and NTA. A) Diagram of an MLO protein with described domains and regions annotated. N - N-terminal domain, SP - signal peptide, EL - extracellular loops 1-3, IL - intracellular loops 1-3, CTerm - C-Terminal intracellular tail, CaMBD - calmodulin-binding domain. B-E) Boxplots of unfertilized ovule counts of T2 homozygous lines of $MYB98_{pro}$ expressed domain swap constructs in the *nta-1* background. B) N-Terminus through the first extracellular loop [NEL1] domain swap between NTA and MLO8 C) extracellular loop 1 [EL1] domain swap between NTA and MLO8. D) C-Terminal swap including intracellular loop 3, extracellular loop 3, and the C-terminal tail [TM5] between NTA and MLO8. E) C-Terminal [CTerm] domain swaps between NTA and MLO8. Adj. P-values - " **** " = < 0.0001, " *** " = 0.001-0.0001, " * " = 0.05-0.01, "ns" = >0.05.

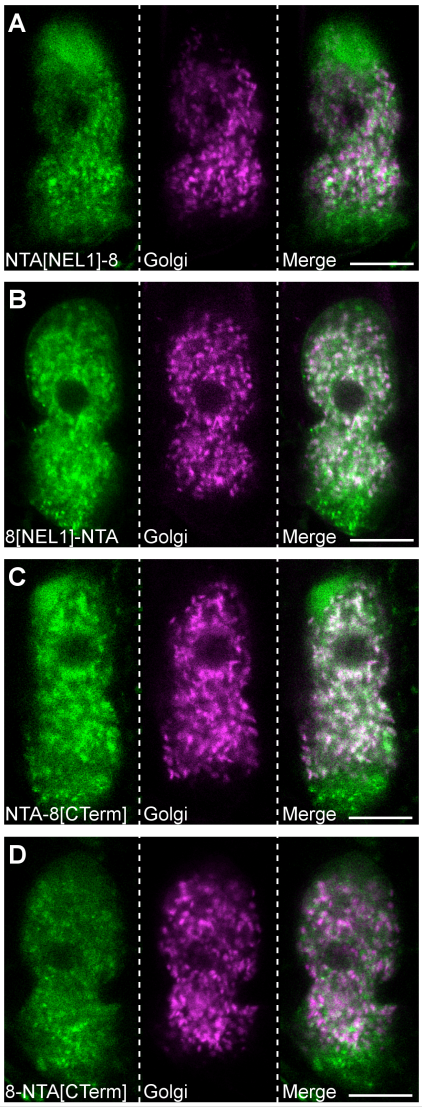

Fig 2.7. Co-localization of NEL1 and CTerm swaps with a Golgi marker in synergids. A-D) $MYB98_{pro}$:MLO-GFP (green) co-expressed with the Golgi marker (LRE_{pro}:Man49-mCherry; magenta) in the synergid cell. Bars = 10μm.

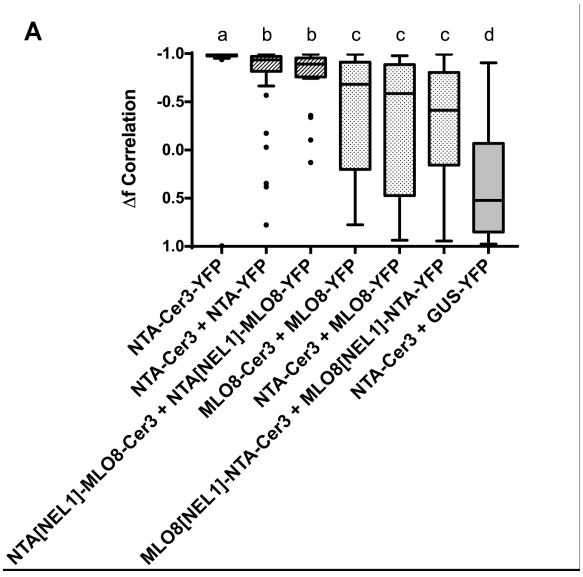

Fig 2.8. Detection of oligomerization of MLO constructs via FRET analysis. Boxplot of correlation coefficients from FRET analysis of homo- and hetero- oligomerization of constructs indicated. Groupings of “a”, “b”, “c”, and “d” based on significant differences between each dataset’s distribution as determined using a Kruskal-Wallis test. See also Supplemental Fig. 2.9. Datasets in all boxplots represent full range of data with median at the center.

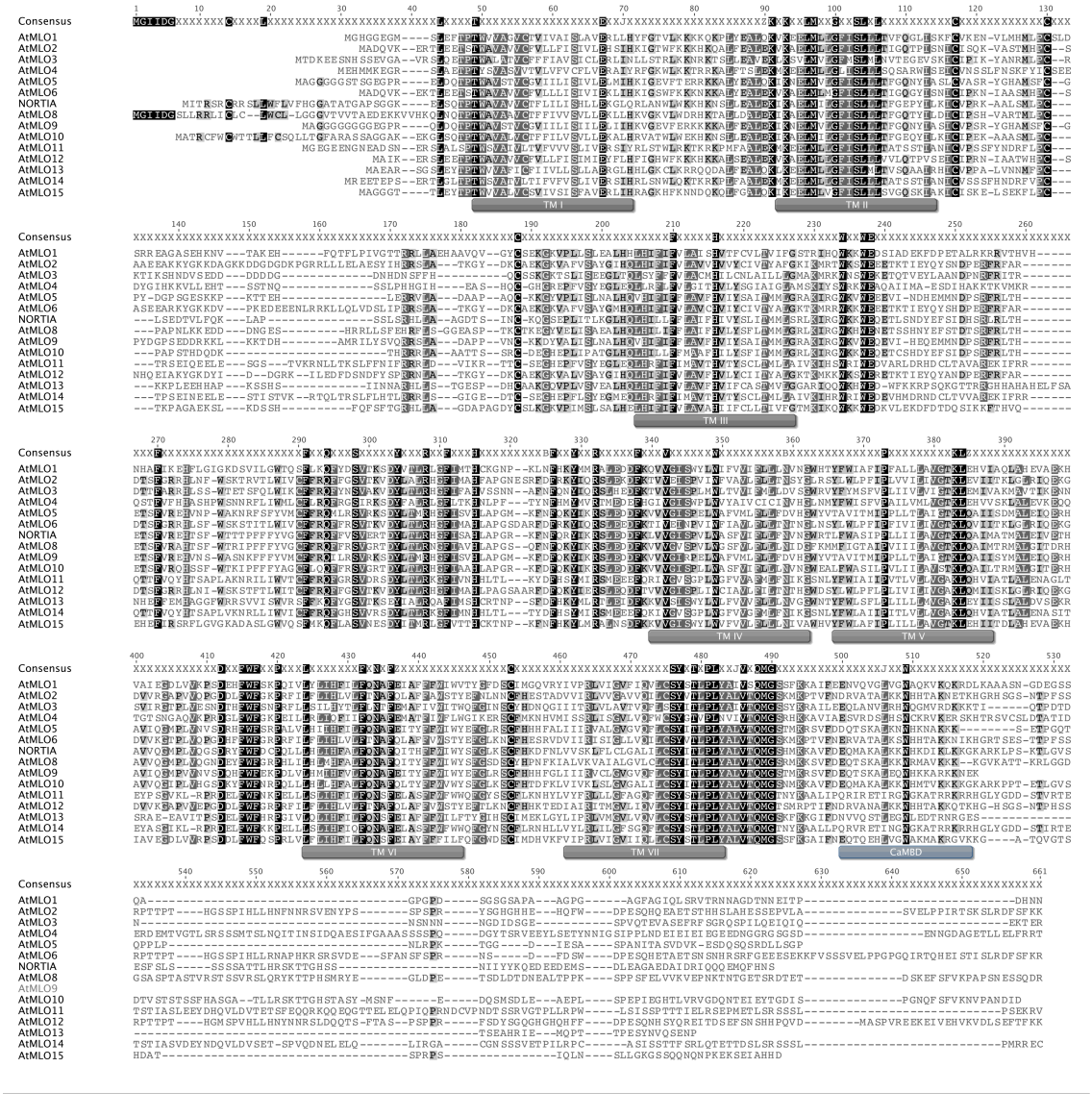

Supplemental Fig. 2.1 Protein alignment of the *Arabidopsis thaliana* MLO family A) Amino acid alignment of all 15 MLOs from *A. thaliana*. Conserved transmembrane domains (TMI-TMVII) and the calmodulin binding domain (CaMBD) are labeled as defined in previous analyses (Panstruga 2005; Kusch et al., 2016). Alignment was constructed using Geneious ver. 7. B) Diagrams of MLO proteins chosen for functional analysis in pollen tube reception. The 5 MLO proteins share common domain structures, with a 7 membrane spanning regions ™ and a cytoplasmic C-terminal tail. (EL, Extracellular Loop; IL, Intracellular Loop; CaMBD, Calmodulin Binding Domain).

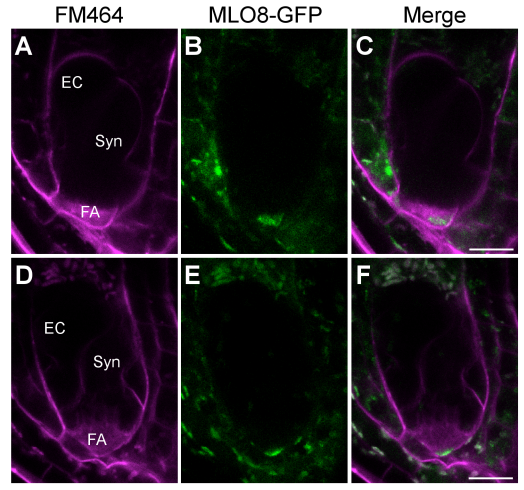

Supplemental Fig. 2.2 $MLO8_{pro}$::MLO8-GFP expression pattern in mature ovules. A-F) MLO8-GFP (green) accumulation around FM464 (magenta) labeled synergid cells of ovules before PT arrival. EC - egg cell, Syn - synergid, FA - filiform apparatus. Bars = 10µm.

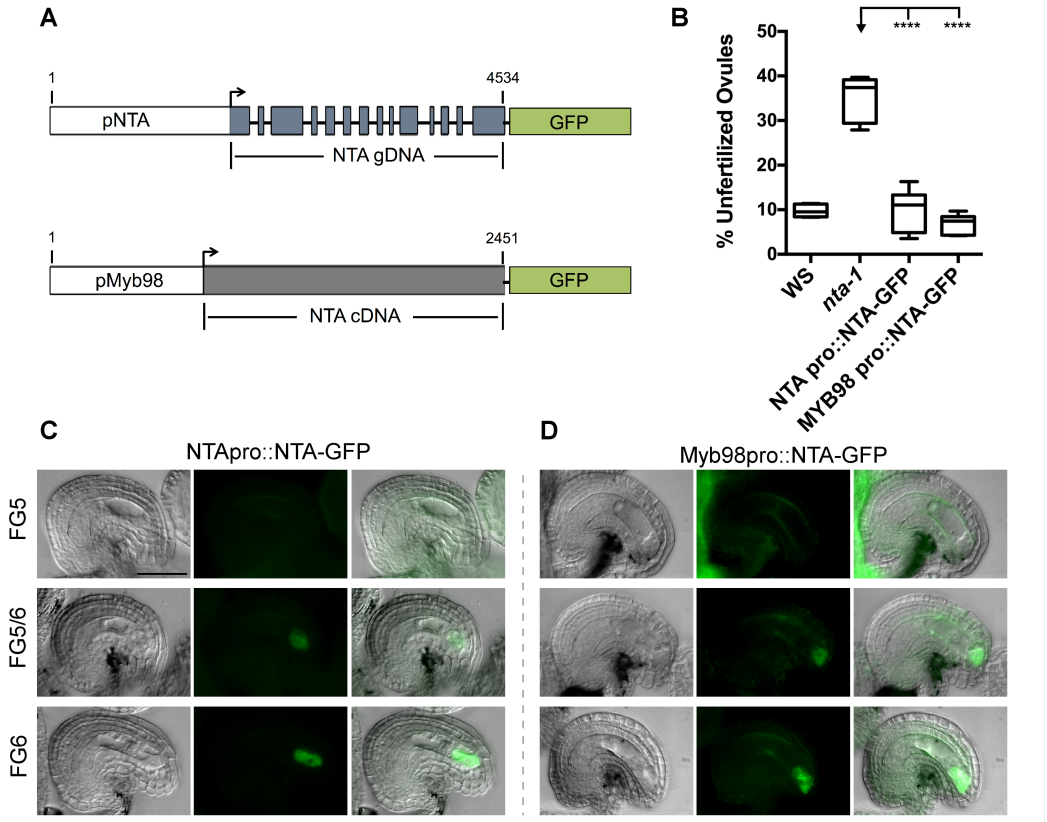

Supplemental Fig. 2.3 Comparison of NTA_{pro}::NTA-GFP and $MYB98_{pro}$::NTA-GFP expression in *nta-1*. A) Diagram of NTA_{pro}::NTA gDNA-GFP and $MYB98_{pro}$::NTAcDNA-GFP constructs. B) Boxplot of unfertilized ovule counts in T2 plants homozygous for $MYB98_{pro}$::NTA-GFP in the *nta-1* background compared to NTA_{pro}::NTA-GFP (Kessler et al 2010). C-D) Accumulation of NTA-GFP in developing ovules (developmental staging as in Christensen et al) expressed under the NTA_{pro} (C) and $MYB98_{pro}$ (D). Bar = 50µm. Adj. P-values - " **** " = < 0.0001.

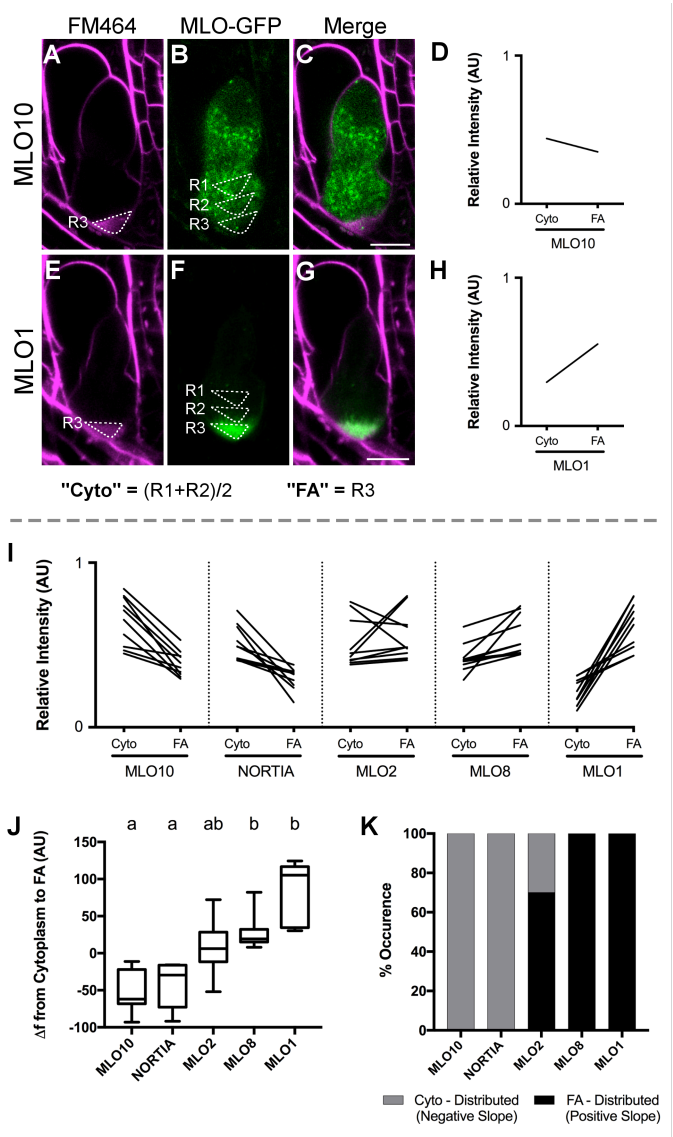

Supplemental Fig 2.4. Analysis of full length MLO distribution in synergid cells. A-H) Examples of fluorescence intensity measurements taken from MYB98$_{pro}$:MLO-GFP lines to determine GFP distribution in synergid cells of unfertilized mature ovules. R3 represents an ROI set to the area of the FA. Mean relative intensity (Arbitrary Units (AU)) measurements were taken at the FA then in two more places sequentially towards the chalazal end of the synergid cell (R2 and R1) using the same ROI to ensure comparable regions for further analysis. R1 and R2 were averaged and referred to as the "Cyto" intensity (amount of GFP in the cytoplasm of the synergid) and R3 was used directly as the "FA" intensity (amount of GFP present in the filiform apparatus). I) Comparison of intensity differences between "Cyto" and "FA" of 10 synergid cells expressing the different full length MLO-GFP constructs. J) Boxplot of slope values corresponding to the change in GFP fluorescence intensity from "Cyto" to "FA". Groupings of "a" and "b" based on significant differences between each dataset's distribution as determined using a Kruskal-Wallis test. K) Frequency of either cytoplasmic distribution (negative slope values) or FA distribution (positive slope values) of GFP fluorescence from each MLO analyzed. Bars = 10μm

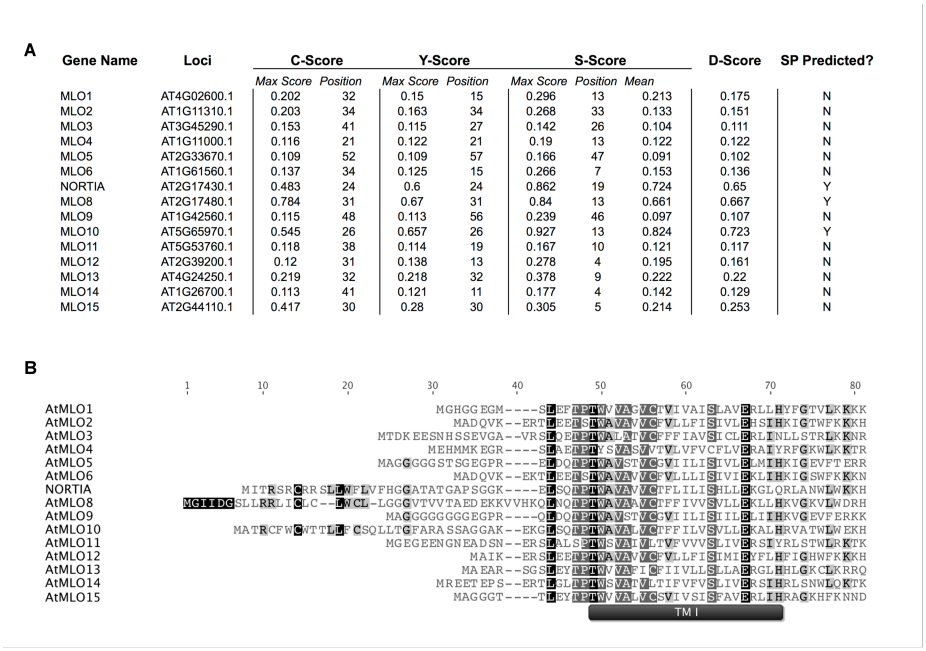

Gene Name	Loci	C-Score		Y-Score		S-Score			D-Score	SP Predicted?
		Max Score	*Position*	*Max Score*	*Position*	*Max Score*	*Position*	*Mean*		
MLO1	AT4G02600.1	0.202	32	0.15	15	0.296	13	0.213	0.175	N
MLO2	AT1G11310.1	0.203	34	0.163	34	0.268	33	0.133	0.151	N
MLO3	AT3G45290.1	0.153	41	0.115	27	0.142	26	0.104	0.111	N
MLO4	AT1G11000.1	0.116	21	0.122	21	0.19	13	0.122	0.122	N
MLO5	AT2G33670.1	0.109	52	0.109	57	0.166	47	0.091	0.102	N
MLO6	AT1G61560.1	0.137	34	0.125	15	0.266	7	0.153	0.136	N
NORTIA	AT2G17430.1	0.483	24	0.6	24	0.862	19	0.724	0.65	Y
MLO8	AT2G17480.1	0.784	31	0.67	31	0.84	13	0.661	0.667	Y
MLO9	AT1G42560.1	0.115	48	0.113	56	0.239	46	0.097	0.107	N
MLO10	AT5G65970.1	0.545	26	0.657	26	0.927	13	0.824	0.723	Y
MLO11	AT5G53760.1	0.118	38	0.114	19	0.167	10	0.121	0.117	N
MLO12	AT2G39200.1	0.12	31	0.138	13	0.278	4	0.195	0.161	N
MLO13	AT4G24250.1	0.219	32	0.218	32	0.378	9	0.222	0.22	N
MLO14	AT1G26700.1	0.113	41	0.121	11	0.177	4	0.142	0.129	N
MLO15	AT2G44110.1	0.417	30	0.28	30	0.305	5	0.214	0.253	N

Supplemental Fig 2.5. SignalP 4.0 Prediction results and N-terminal peptide alignment for all 15 MLO proteins in *Arabidopsis thaliana.*
A) The calculated C-Score (raw cleavage site score), Y-Score (combined cleavage site score), S-score (signal peptide score) and D-score (discrimination score) for all 15 MLOs analyzed. Scores calculated as in (Petersen et al., 2011) and described at the SignalP server website. Analysis performed with a D-score cutoff of 0.5 or greater and utilized the SignalP-TM network for all inputs. B) Amino acid alignment of all 15 MLOs through the first transmembrane domain (TM1). Alignment was constructed using Geneious ver. 7.

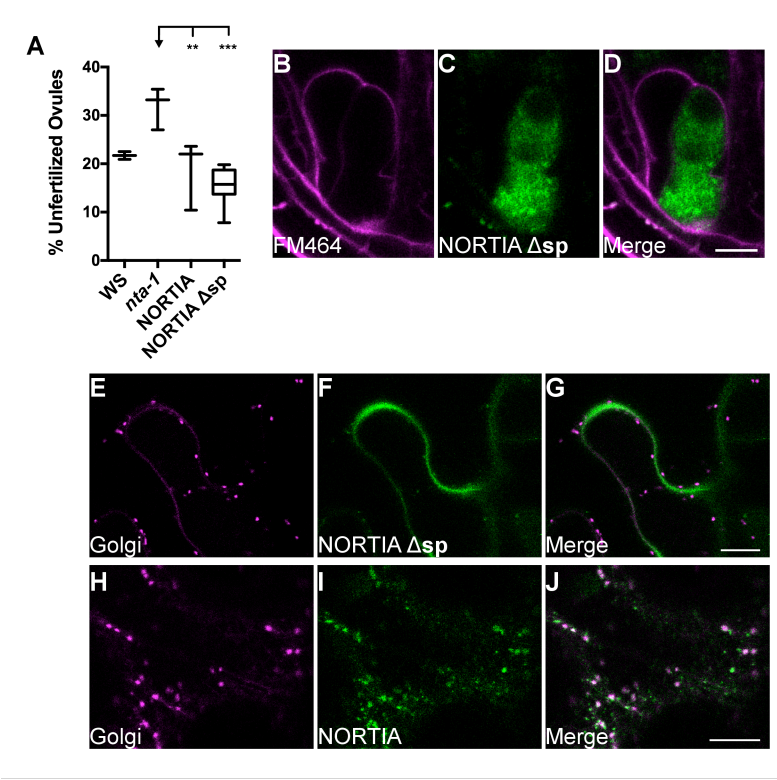

Supplemental Fig. 2.6 Analysis of NTA without its predicted signal peptide (sp). A) Boxplot of unfertilized ovule counts of T2 homozygous lines of MYB98$_{pro}$::NORTIAΔsp-GFP in the *nta-1* background. B-D) Distribution of NORTIA Δsp-GFP (green) in the synergid cell prior to PT arrival counterstained with FM464 (magenta). E-J) Co-localization of 35S$_{pro}$::NORTIA Δsp-GFP and 35S$_{pro}$::NORTIA-GFP (green) with the Man49-mCherry Golgi marker in *N. benthamiana* epidermal cells. Bars = 10μm (E-G) and 20μm (H-J). Adj. P-values - " *** " = 0.001-0.0001, " **" = 0.01-0.001.

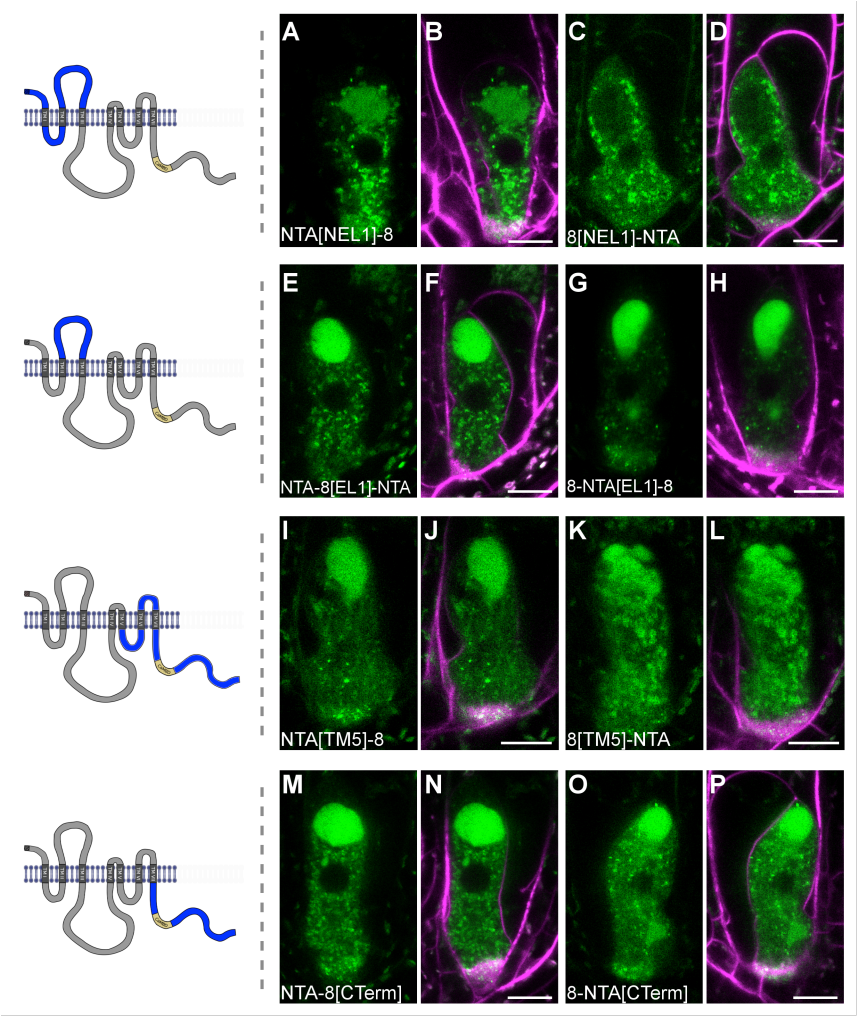

Supplemental Fig. 2.7 MLO-GFP distributions of domain swaps and truncations within synergids. Distribution of indicated chimeric MLO-GFP (green) domain swaps (A-P) in synergids of unfertilized ovules co-labeled with FM464 (magenta). Bars = 10μm.

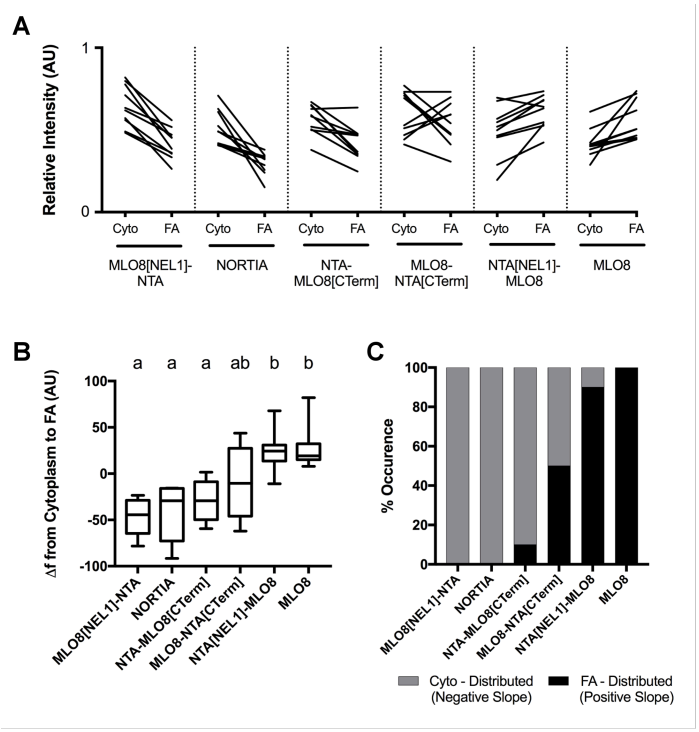

Supplemental Fig 2.8. Analysis of NEL1 and CTerm domain swap distribution in synergid cells. A) Comparison of intensity differences between "Cyto" and "FA" of 10 synergid cells expressing the NEL1 and CTerm domain swap MLO-GFP constructs (same measurements of full length NORTIA and MLO8 from Supplemental Fig. S4 were incorporated into this analysis). B) Boxplot of slope values corresponding to the change in GFP fluorescence intensity from "Cyto" to "FA". Groupings of "a" and "b" based on significant differences between each dataset's distribution as determined using a Kruskal-Wallis test. C) Frequency of either cytoplasmic distribution (negative slope values) or FA distribution (positive slope values) of GFP fluorescence from each construct analyzed.

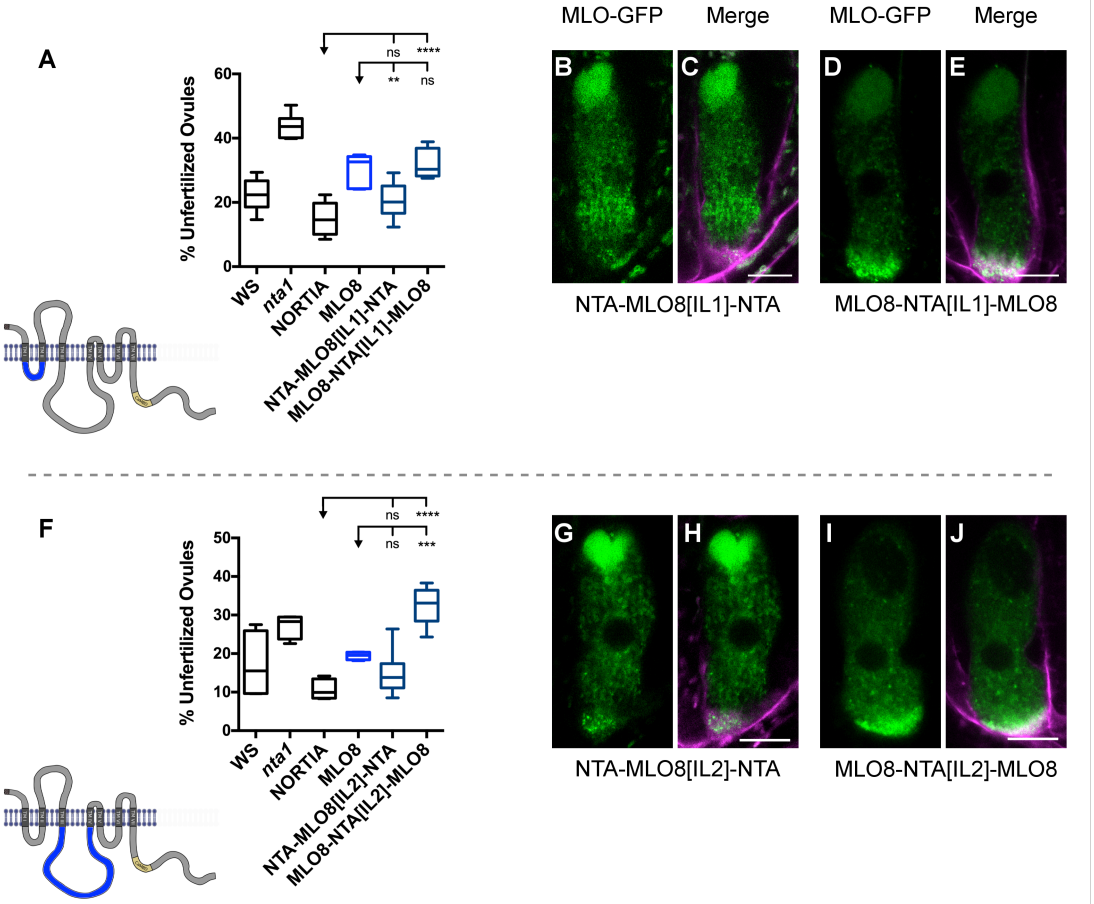

Supplemental Fig 2.9. Analysis of IL1 and IL2 domain swaps between MLO8 and NTA. A, F) Boxplots of unfertilized ovule counts of T2 homozygous lines of pMYB98 expressed domain swap constructs in the *nta-1* background. A) Intracellular loop 1 [IL1] domain swap between NTA and MLO8. F) Intracellular loop 2 [IL2] domain swap between NTA and MLO8. B-E, G-J) Distribution of indicated IL1 (B-E) and IL2 (G-J) swap chimeric GFP fusions (green) in the synergids of unfertilized ovules co-labeled with FM464 (magenta). Bars = 10µm. Adj. P-values - " **** " = < 0.0001, " *** " = 0.001-0.0001, " ** " = 0.01-0.001, "ns" = >0.05.

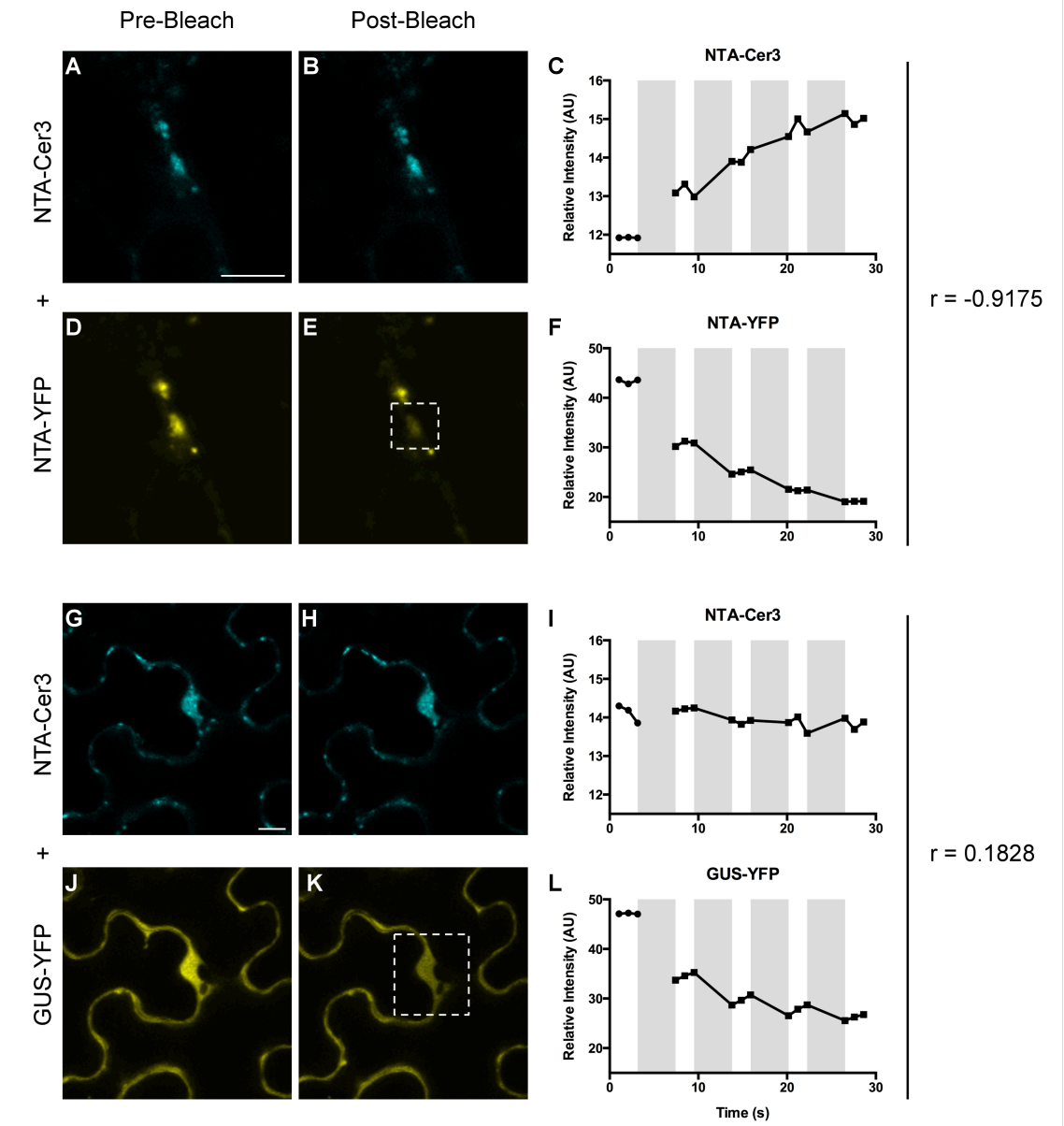

Supplemental Fig 2.10. FRET detection via acceptor photobleaching. Examples of a positive FRET detection (NTA-YFP + NTA-Cer3, A-F) and a negative FRET detection (GUS-YFP + NTA-Cer3, G-L) in transient co-expression assay in *N. benthamiana* epidermal cells. C,F,I,L) Fluorescent intensity measurements corresponding to the measured intensity with the indicated region (white box (E,K)) throughout four subsequent rounds of photobleaching (gray bars on graphs). Pearson product-moment correlation value for each experiment indicated on right (see Experimental Procedures). Bars = 10μm.

Full Length MLOs (MYB98pro, Native Promoter Constructs)	**Primer Name**	**Primer Sequence (attB cloning sites in italics)**
pMLO1 - start of native promoter	DJ_MLO1_F1	*GGGGACAAGTTTGTACAAAAAAGCAGGCTTCACC* CGGGAAATAGATTTACAAGG
35S/pMYB98::MLO-GFP Construct	DJ_MLO1_F2	*GGGGACAAGTTTGTACAAAAAAGCAGGCTTCACC* ATGGGTCACGGAGGAGAAG
3' End of MLO1	DJ_MLO1_R1	*GGGGACCACTTTGTACAAGAAAGCTGGGTG* GTTGTTATGATCAGGTGTAATCTCA
pMLO2 - start of native promoter	DJ_MLO2_F1	*GGGGACAAGTTTGTACAAAAAAGCAGGCTTCACC* GTTGTGTCCAATTGTGTCAGTC
35S/pMYB98::MLO-GFP Construct	EKMLO2-1F_attB1	*GGGGACAAGTTTGTACAAAAAAGCAGGCTTCACC* ATGGCAGATCAAGTAAAAGAGC
3' End of MLO2	EKMLO2-2R_attB2	*GGGGACCACTTTGTACAAGAAAGCTGGGTG* TTTCTTAAAAGAAAAATCTC
pMLO8 - start of native promoter	DJ_MLO8_F1	*GGGGACAAGTTTGTACAAAAAAGCAGGCTTCACC* GGTCGGCATAGACTAATAGTATG
35S/pMYB98::MLO-GFP Construct	EKMLO8-1F_attB1	*GGGGACAAGTTTGTACAAAAAAGCAGGCTTCACC* ATGGGAATCATCGACGGTTC
3' End of MLO8	EKMLO8-2R_attB2	*GGGGACCACTTTGTACAAGAAAGCTGGGTG* CCGGTCTTGAGATGATTCAT
pMLO10 - start of native promoter	DJ_MLO10_F1	*GGGGACAAGTTTGTACAAAAAAGCAGGCTTCACC* GAGAAGCAGTCAAGGTTAAAG
35S/pMYB98::MLO-GFP Construct	EKMLO10-1F_attB1	*GGGGACAAGTTTGTACAAAAAAGCAGGCTTCACC* ATGGCCACAAGATGCTTTTGG
3' End of MLO10	EKMLO10-2R_attB2	*GGGGACCACTTTGTACAAGAAAGCTGGGTG* GTCAATATCATTAGCAGGAACG
35S/pMYB98::MLO-GFP Construct	NTA_B1_F	*GGGGACAAGTTTGTACAAAAAAGCAGGCTTCACC* ATGATCACAAGAAGCAGGTGT
3' End of NORTIA	DJ_MLO7_R1	*GGGGACCACTTTGTACAAGAAAGCTGGGTG* AGAGTTGTGGAATTGCATCTC

Domain Swap Constructs		(Green letters indicate sequence overlaps between the fragments used for cloning)
NTA[NEL1]- MLO8	DJ_MLO7_R5	ATAAGGATGTGCAATTGGTGCAAGCCTTTCAATGTTATGAG
	DJ_MLO8_F4	TTGCACATCCTTATATTCTTCTTAGCC
MLO8[NEL1]- NTA	DJ_MLO8_R2	CAACAAGATGTGAAGCTGATGGAGTGCCTCGG
	DJ_MLO7_F2	CTTCACATCTTGTTGTTCTTCTTG
NTA - MLO8[EL1]- NTA	DJ_MLO8_F3	GGAGAACCATATATTTTGGATATTTGTATCCCTTCAC
	DJ_MLO8_R2	CAACAAGATGTGAAGCTGATGGAGTGCCTCGG
	DJ_MLO7_R3	AATATATGGTTCTCCAAAAGTGAG
	DJ_MLO7_F2	CTTCACATCTTGTTGTTCTTCTTG
MLO8 - NTA[EL1]- MLO8	DJ_MLO7_F4	GGACAAACCTACATTCTCAAGATCTGTGTTCCTCG
	DJ_MLO7_R5	ATAAGGATGTGCAATTGGTGCAAGCCTTTCAATGTTATGAG
	DJ_MLO8_R3	AATGTAGGTTTGTCCAAATGTCAG
	DJ_MLO8_F4	TTGCACATCCTTATATTCTTCTTAGCC
NTA[TM5]- MLO8	DJ_MLO7_R6	TGTCATAATCGCTTGAAGCTTTGTTCCAACAGCTAG
	DJ_MLO8_F5	CAAGCGATTATGACAAGGATG
MLO8[TM5]- NTA	DJ_MLO7_F7	CAAGCAATTATGGCAACAATGGC
	DJ_MLO8_R4	TGCCATAATTGCTTGAAGCTTTGTCCCTACAGCTA
NTA-MLO8[Cterm]	DJ_MLO7_R7	TGCTTTTGACGTTTGCTCATCAAACACTGCTTTCTTC
	DJ_MLO8_F6	CAAACGTCAAAAGCACTCAAG
MLO8-NTA[Cterm]	DJ_MLO7_F8	CAAATGGCAAAGGCATTGAAG
	DJ_MLO8_R5	TGCCTTTGCCATTTGTTCATCGAATACCGATTTTTTCATCC
MLO8 - NTA[IL1]- MLO8	DJ_MLO7_F9	TCTGTTCTTCTTGAAAAGGGTCTTCAAAGACTCGC
	DJ_MLO7_R9	CATCAGCTCTGCTTTGATTTTCTCTAAGGCTTCAAGGAGAG
	DJ_MLO8_F7	AAAGCAGAGCTGATGGTTCTTGG
	DJ_MLO8_R6	TTCAAGAAGAACAGAAACAACGATGAAG
NTA - MLO8[IL1]- NTA	DJ_MLO7_F10	AAAGCTGAGCTGATGATCCTTG
	DJ_MLO7_R10	TTCAAGGAGATGGGAAATGAGG
	DJ_MLO8_F8	TCCCATCTCCTTGAAAAACTTCTTCACAAAGTTGGAAAGG
	DJ_MLO8_R7	CATCAGCTCAGCTTTGATCTTCTCCAAAGCGTCAAGAAG
MLO8 - NTA[IL2]- MLO8	DJ_MLO7_F11	TTCTTAACTATGATGCTTAGCAGGCTCAAGATTCGTG
	DJ_MLO7_R11	GACTACCTTGAAATCATCCTCGAGAGATCTTTTGATATATCTC
	DJ_MLO8_F9	GATTTCAAGGTAGTCGTTGGAG
	DJ_MLO8_R8	CATCATAGTTAAGAAGCTGTAAAGAACG
NTA - MLO8[IL2]- NTA	DJ_MLO7_F12	GACTTATTCCAACTACCAACTTGAAATC
	DJ_MLO7_R12	CATCATGGTGATTAAACTATATACGATATG
	DJ_MLO8_F10	TTAATCACCATGATGCTTGGAAGGTTGAAGATTCGCG
	DJ_MLO8_R9	TACCAACTTGAAATCATCCTCCAACGATCTTTTAATGTATTTTTGG

MY98pro::NTA Δsp-GFP		
NTA Δsp	DJ_MLO7_F5	*GGGGACAAGTTTGTACAAAAAAGCAGGCTTCACC* ATGGCTCCCTCTGGTGGGAAAGAGC

Gibson Assembly of MYB98pro::SYP61-mCherry		
MYB98pro::SYP61-mCherry	DJ_Syp61_F2	CTCTCCAACCACCATATGTCTTCAGCTCAAGATCCATTC
	DJ_Syp61_R2	GGCCGCTGCACCTGAGGTCAAGAAGACAAGAACGAATAGG
	DJ_linkmCher_F1	TCAGGTGCAGCGGCCGCTTC
	DJ_pMyb98_R2	ATGGTGGTTGGAGAGCCTGCT
	DJ_pEarlyGate_F1	GTTAATTAAGAATTAGCTTGC
	DJ_pEarlyGate_R1	TGAGCTACACATGCTCAGG

Positive Control for FRET:		
NTA - Cer3 - YFP	DJ_NTA_118_F	GAGAGGACACGCTCGAGATCACAAG
	DJ_Cer3_R	CTCCTCCTCCTCCTCCTGACTTGTACAGCTCGTCCATGC
	DJ_linkYFP_F	TCAGGAGGAGGAGGAGGAG
	DJ_YFP_118_R	GAAGCTTGAGCTCGAGAATTCGGTCTCAGCAGTTACTTG

Supplemental Table 2.1. Primers Used for Cloning.

Chapter 3: Cell Type-Dependent Localization of MLO Proteins

Daniel S. Jones[1] and Sharon A. Kessler[2, 3]

This chapter was published in *Plant Signaling and Behavior*.

Jones, D. S., & Kessler, S. A. (2017). Cell Type-Dependent Localization of MLO Proteins. *Plant Signaling & Behavior*, 00-00. doi:10.1080/15592324.2017.1393135

[1]Department of Microbiology and Plant Biology, The University of Oklahoma, Norman, OK 73069, USA
[3]Department of Botany and Plant Pathology, Purdue University, West Lafayette, IN 47907, USA
[4]Center for Plant Biology, Purdue University, West Lafayette, IN 47907, USA

Summary

Mildew resistance locus O (MLO) proteins are transmembrane proteins that mediate cell-cell communication in plants. We recently demonstrated the importance of subcellular localization to MLO function during pollen tube reception. NORTIA (NTA), the MLO protein involved in this process, localizes to the Golgi of the synergid cell before interaction with the pollen tube. MLO proteins that can substitute for NTA's function in this pathway all partially localize with the same Golgi marker in the synergid cell. In this study, we report that MLO subcellular localization is cell type-dependent, with different distributions of some MLOs observed when ectopically expressed in the epidermal cells of tobacco and Arabidopsis compared to synergids. This dependency may be due to co-factors that influence MLO function within a given cell type, providing an intriguing new target for understanding MLO distribution and subsequent function in their respective processes.

Introduction

Mildew resistance locus O (MLO) proteins are a plant-specific family of seven-spanning transmembrane proteins that mediates cell-cell communication in response to various stimuli[1]. Most notably MLOs were first identified as susceptibility factors involved in powdery mildew infection as part of a conserved signaling pathway found in both monocots and dicots[2, 3]. In *Arabidopsis thaliana,* MLOs have since been found to regulate root thigmomorphogenesis and the process of pollen tube (PT) reception[4, 5]. PT reception occurs in the final stages of sexual reproduction in flowering plants as the tip-elongating PT interacts with the synergid cells of the female gametophyte initiating a signaling cascade that results in one of two synergids degenerating and PT rupture, releasing two sperm cells into the embryo sac[6]. NORTIA (NTA) is an MLO protein that mediates this communication from within the synergid cell. In *nortia* homozygous mutants, PT-synergid communication is disrupted resulting in an overall reduction in fertilization[5].

As with other MLOs, the molecular function of NTA within its pathway has remained elusive. NTA localizes within Golgi-associated compartments prior to interaction with the PT but polarly redistributes toward a region of invaginated plasma membrane, called the filiform apparatus, sometime during PT reception[5, 7]. This redistribution is dependent on the activity of the receptor-like kinase FERONIA, an upstream component regulating PT reception, and may be important for NTA's role in regulating PT-synergid communication[5]. The barley MLO protein also redistributes in response to fungal penetration to become polarly localized to the site of infection[8]. In both PT reception and powdery mildew infection contact between a plant cell and a tip-growing cell triggers MLO redistribution, presumably following the perception of some signal. This signal-dependent polarization may be a conserved trait amongst MLOs, thus

understanding the regulation of MLO subcellular trafficking may provide insight into MLO function. In a recent study, we found a divergence in the ability of related Arabidopsis MLO proteins to function in PT reception when ectopically expressed in the synergid cells of the *nortia* (*nta-1*) mutant[7]. MLO function in this pathway correlated with their subcellular localization prior to PT arrival. The MLOs tested that could rescue *nta-1* also co-localized with a fluorescent Golgi marker in the synergid cell (MLO10 and MLO2), whereas those that couldn't rescue *nta-1* did not overlap with the same marker (MLO8 and MLO1). This implies that MLO localization within Golgi-associated compartments of synergids is important for their function in PT reception.

Results and Discussion

Here we report that MLO localization may be dependent on the cell type in which the proteins are expressed. Co-localization experiments in tobacco epidermal cells reveal that some MLOs show common subcellular distributions in synergid cells and epidermal cells, while others exhibit different subcellular localizations when ectopically expressed in the two cell types. NTA, MLO10, and MLO8 all displayed similar localization patterns in synergids and tobacco epidermal cells. NTA-GFP partially co-localized with a Golgi marker and had no overlap with markers for either the endoplasmic reticulum or peroxisomes in both cell types (Fig. 3.1)[7]. MLO10 and MLO8 also showed no appreciable difference in localization between the two cell types, with MLO10 co-localizing with the Golgi marker and MLO8 accumulating in punctate compartments similar to those seen in synergid cells (Fig. 3.2A–B)[7]. However, both MLO2 and MLO1 had unique distribution patterns in tobacco, localizing to the periphery of the epidermal cells with no detectable accumulation in punctate compartments (Fig. 3.2C–D). Whereas MLO2 partially co-localized with the Golgi

marker in synergid cells, MLO2 accumulated only within specific subdomains (potentially in the plasma membrane) associated with epidermal cell lobes (Fig. 3.2C). In contrast to MLO1's polar distribution at the filiform apparatus in synergid cells, MLO1-GFP was evenly distributed around the periphery of tobacco epidermal cells (Fig. 3.2D). In order to determine if the observed cell type-dependent localization was due to our transient assay being done in a heterologous system, we also generated stable overexpression lines of MLO1 and NTA in the Columbia ecotype (Col-0) of *A. thaliana* (Fig. 3.3). As in our transient assay, MLO1-YFP localized predominantly to the periphery of epidermal pavement cells in a pattern similar to that seen in tobacco (Fig. 3.3A-B vs. Fig. 3.2D), while NTA-YFP accumulated in punctate compartments consistent with the endomembrane system (Fig. 3.3C-D).

In summary, NTA, MLO10, and MLO8 were incorporated into endomembrane-associated compartments within both synergid cells and tobacco epidermal cells, while MLO2 and MLO1 had cell type-dependent localization patterns. We also demonstrated that NTA and MLO1 maintained their respective epidermal cell distributions when stably transformed into *A. thaliana*. NTA, MLO10, and MLO8 are closely related and are all a part of Clade III within the MLO family[9]. We recently reported a difference between these three MLOs and the rest of the family in that NTA, MLO10 and MLO8 all have predicted N-terminal signal peptides[7]. Upon removal of NTA's signal peptide (NTA Δsp), there was no difference in its function in PT reception or its localization within the synergid cell. However, when expressed in tobacco epidermal cells, NTA Δsp's distribution resembled that of MLO2's, accumulating in subdomains of epidermal cell lobes instead of partially co-localizing with the Golgi marker[7]. Since MLO2 has no predicted N-terminal signal peptide, the differences in MLO localization may represent the influence of additional co-factors involved in PT reception (in the synergid cell) or

involved in an unknown process occurring within the epidermal cell lobe. This observation fits well with the finding that both MLO2 and NTA Δsp rescue *nta-1* and thus can function in PT reception[7]. Co-factors influencing localization may be of functional significance within these pathways/processes and remain a target of interest for understanding the role of MLO localization (as well as polar redistribution). As MLO proteins have a conserved calmodulin-binding domain in their C-terminal intracellular tail, and interaction with calmodulin is required for MLO function in powdery mildew susceptibility[10], an obvious candidate for the co-factor influencing MLO distribution is calmodulin. In barley, interactions between MLO and calmodulin differ along the cell periphery in epidermal cells, with positive interactions occurring within subdomains of this cell type[8]. This provides some evidence for differential processes involving MLOs occurring within subdomains of the epidermal cell; however, the functional significance of these spatial limitations remains unknown.

Overall the observed cell type-dependent localization patterns of MLOs indicate a reliance on additional components within the cell for their distribution. With the recent finding that the ability of MLOs to function in PT reception correlates with their protein localization to a Golgi-associated compartment, we propose that regulation of subcellular distribution of MLO proteins within a cell may be a mechanism for controlling MLO function in response to various external stimuli. Synergid cells are very unique among plant cells. Before PT arrival they act as secretory factories that pump out LURE peptides from the filiform apparatus to attract PTs[11]. After attraction, the PT halts its growth and communicates with the receptive synergid cell, inducing subcellular changes in the synergid involving calcium oscillations and NTA redistribution to the filiform apparatus[5, 12]. While the molecular mechanism and functional relevance behind the redistribution of NTA during PT reception is still under investigation, our results

suggest that the ability to regulate MLO trafficking may provide plasticity within the MLO pathway in a given cell type and provides evidence for a more complex regulation of MLO-mediated intercellular communication.

Figures

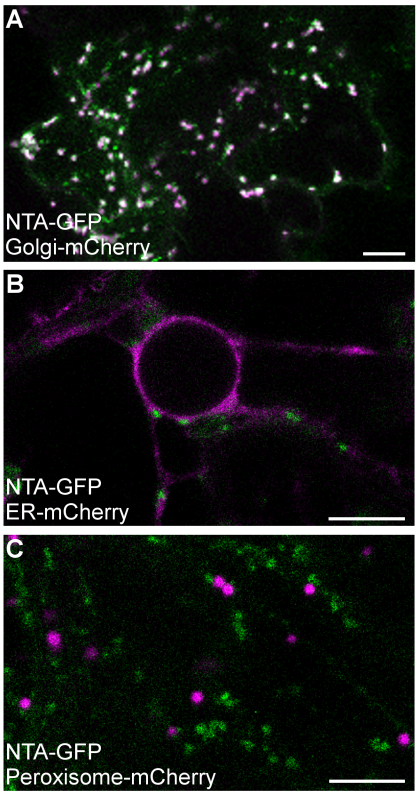

Figure 3.1 Transient co-expression of $35S_{pro}$:NTA-GFP (green signal) with mCherry-labeled secretory markers (magenta signal) in in tobacco epidermal cells[13]. A) NTA-GFP (green) colocalizes with Golgi (Man49-mCherry) (white indicates overlapping GFP and mCherry signals). B) NTA-GFP does not colocalize with an Endoplasmic Reticulum marker (SP-mCherry-HDEL). C. NTA-GFP does not colocalize with peroxisomes (mCherry-PTS1). Four- to Six-week-old *Nicotiana benthamiana* plants were used in all transient co-expression assays. *Agrobacterium tumefaciens* (GV3101) harboring the NTA-GFP (or other MLO) and respective marker constructs were co-infiltrated into mature leaves. Imaging was done using a Leica SP8 confocal microscope three days after infiltration similar to our previous study[7]. Bars = 10µm.

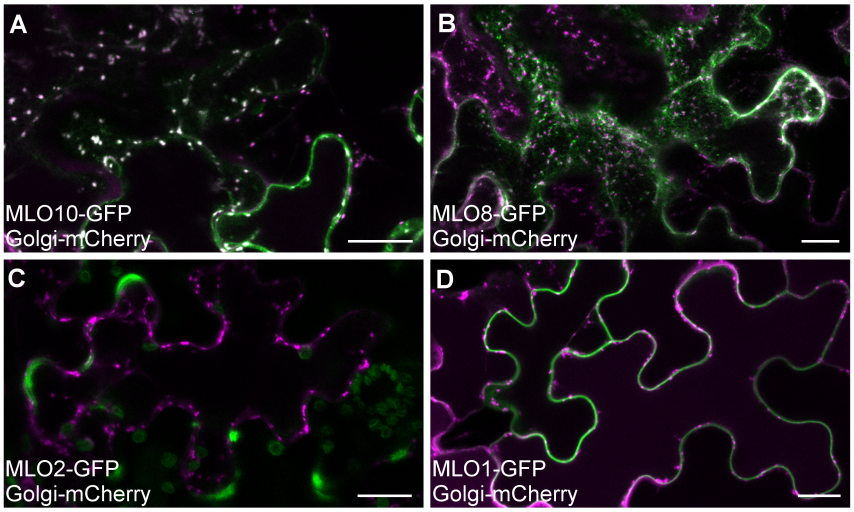

Figure 3.2 MLO co-localization with a Golgi marker in tobacco epidermal cells. A-D) $35S_{pro}$:MLO-GFP (green) transient co-expression with the Man49-mCherry Golgi marker (magenta). A) MLO10-GFP colocalizes with the Golgi marker (white spots indicate co-localization). B) MLO8-GFP is distributed in punctate pattern that does not overlap with Golgi. C) MLO2-GFP localizes to the periphery of epidermal lobes and does not overlap with Golgi. D) MLO1-GFP localizes with the periphery of the cells and does not overlap with Golgi. Bars = 20µm.

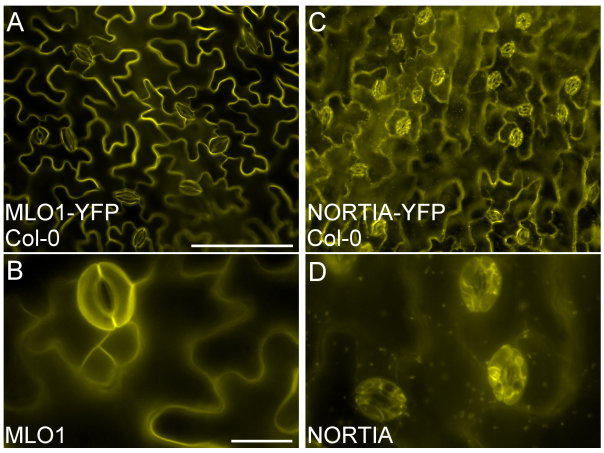

Figure 3.3 Distribution of ectopically expressed MLO1 and NTA in the epidermal cells of *Arabidopsis thaliana.* A-B) $35S_{pro}$:MLO1-YFP localizes to the periphery of epidermal pavement cells (yellow signal). C-D) $35S_{pro}$:NTA-YFP localizes in a punctate pattern consistent with the endomembrane system in epidermal pavement cells (yellow signal). Stable lines were generated via floral dip transformation[14] of Col-0 using the GV3101 strain of *A. tumefaciens* harboring each construct. $35S_{pro}$:NTA-YFP cloning was described previously[7] and the $35S_{pro}$:MLO1-YFP construct was cloned using the MLO1 cDNA Gateway compatible vector previously reported[7] in a manner similar to NTA's construction. T1 plants were grown on soil and lines were selected following 4 days of BASTA herbicide application. Rosette leaves were imaged from 15-20d old plants after screening for YFP, on a Nikon Eclipse Ni-U compound epifluorescent microscope equipped with an X-Cite LED fluorescent lamp and YFP dichroic filter. Bars = A, C) 100µm; B, D) 20µm.

Chapter 4: Analysis of the secretory pathway in the haploid synergid cells of *Arabidopsis thaliana*

Daniel S. Jones[1], Xunliang Liu[2], Andrew C. Willoughby[1], Ravishankar Palanivelu[2], and Sharon A. Kessler[3, 4]

[1]Department of Microbiology and Plant Biology, The University of Oklahoma, Norman, OK 73069, USA
[2]School of Plant Sciences, University of Arizona, Tucson, Arizona 85721
[3]Department of Botany and Plant Pathology, Purdue University, West Lafayette, IN 47907, USA
[4]Center for Plant Biology, Purdue University, West Lafayette, IN 47907, USA

This chapter is under review for publication in *The Plant Journal*.

Jones, D. S., Liu, X., Willoughby, A., Palanivelu, R., & Kessler, S. A. (under review). Analysis of the secretory pathway in the haploid synergid cells of Arabidopsis thaliana. *The Plant Journal*.

Contributions:

Xunliang Liu cloned ER, Golgi, recycling endosome, and peroxisome markers used in this study and generated/characterized the stable co-expression lines of LRE_{pro}::LRE-YFP with SYP61, recycling endosome and EXPO (Fig. 4.3). Andrew C. Willoughby imaged several lines used in Figs. 4.3 and 4.4.

Summary

In flowering plants, cell-cell communication plays a key role in reproductive success, as both pollination and fertilization require pathways that regulate interactions between many different cell types. Some of the most critical of these interactions are those between the pollen tube (PT) and the embryo sac, which ensure the delivery of the sperm cells required for double fertilization. Synergid cells function to attract the PT through the secretion of small peptides and in PT reception via membrane-bound proteins associated with the endomembrane system and the surface of the cell. While many synergid-expressed components regulating PT attraction and reception have been identified, few tools exist to study the localization of membrane-bound proteins and the components of the endomembrane system in this cell-type. In this study, we describe the localization and distribution of seven fluorescent markers labeling components of the secretory pathway in synergid cells of *Arabidopsis thaliana.* These markers were used in co-localization experiments to investigate the subcellular distribution of the two PT reception components LORELEI, a GPI-anchored surface protein, and NORTIA, a MILDEW RESISTANCE LOCUS O protein, both found within the endomembrane system of the synergid cell. These secretory markers are useful tools for both reproductive and cell biologists, enabling the analysis of membrane-associated trafficking within a haploid cell actively involved in polar transport.

Introduction

Sexual reproduction in flowering plants requires communication between highly specialized cells to ensure the successful delivery, reception, and fusion of gametes (Russell, 1992; Chevalier et al., 2011). This need for cell-cell communication is primarily due to the complex nature of their reproductive development. Multicellular gametophytes (the gamete-producing generation) of flowering plants develop deep within the tissues of entirely separate floral organs (male gametophytes in anthers and female gametophytes in ovules) (Tucker and Koltunow, 2014; Hafidh et al., 2016). In order to reproduce, the male gametophyte (pollen) must land on a receptive stigma of a flower and produce a tip-elongating pollen tube (PT) to transport the male gamete(s) through the pistil to the female gametophyte (embryo sac). The mature pollen grain of *Arabidopsis thaliana* is tricellular, made up of two sperm cells and a vegetative cell, while the mature embryo sac is composed of seven cells: the egg cell and central cell (the two female gametes), along with five accessory cells consisting of two synergids and three antipodals (Fig. 4.1A) (Drews and Yadegari, 2002). The two synergids are located at the micropylar end of the embryo sac and have critical roles in mediating both the attraction and reception of the PT. Synergids secrete small cysteine-rich peptides (LUREs) that attract the PT and guide its growth toward the ovule micropyle (Higashiyama and Takeuchi, 2015). After arriving and communicating with the receptive synergid cell, PT reception initiates as the PT pauses its growth. The PT then enters the embryo sac and ruptures, releasing the two sperm cells required for double fertilization (Kessler and Grossniklaus, 2011; Beale and Johnson, 2013). These complex and dynamic interactions have made it difficult to understand the cellular processes, occurring in the synergid cells, regulating both PT attraction and reception.

The synergid cell is highly polarized with a large vacuole at one end and a region of

extensive membrane invaginations and cell wall in-growths in the micropylar end, known as the filiform apparatus (FA) (Mansfield et al., 1991; Huang and Russell, 1992). This region of invagination greatly increases the surface area of the synergid's plasma membrane at the micropylar interface and gives "transfer cell" like qualities to the synergid cells (Jensen, 1965; Gunning and Pate, 1969; Sumner and Caeseele, 1989; Mansfield et al., 1991; Huang and Russell, 1992). The FA is the first site of contact between the PT and embryo sac and although the structure and morphology of the FA differs across taxa, the conservation of the FA's positioning at the entrance of the embryo sac suggests that this site is important for communication with the PT upon arrival (Mansfield et al., 1991; Leshem et al., 2013). Additionally, many proteins involved in regulating both attraction and reception of the PT localize to the FA. The cysteine-rich LURE peptides localize to the FA within synergids of both *Torenia fournieri* and *A. thaliana* (Okuda et al., 2009; Takeuchi and Higashiyama, 2012). LUREs are also detected throughout the ovule integument cells surrounding the micropyle, demonstrating that they are actively secreted from the FA into the apoplast of the micropyle (Takeuchi and Higashiyama, 2012). The receptor-like kinase FERONIA (FER), and the glycosylphosphatidylinositol (GPI)-anchored surface protein LORELEI (LRE) both polarly localize to the FA of the synergid cell where they function in PT reception (Escobar-Restrepo et al., 2007; Lindner et al., 2015; Liu et al., 2016). FER's localization to the FA is at least partially dependent on LRE-mediated chaperoning from the endoplasmic reticulum (ER) and LRE/FER may function together in this pathway as a complex (Li et al., 2015; Liu et al., 2016). The MILDEW RESISTANCE LOCUS O (MLO) family protein NORTIA (NTA), a seven-spanning transmembrane protein also involved in mediating PT reception, initially localizes to Golgi distributed throughout the synergid cell in a mature embryo sac and redistributes to the FA in a FER-dependent manner after PT arrival (Kessler et al., 2010; Jones et

al., 2017). In a recent structure-function analysis of NTA's role in PT reception, it was found that closely related MLO proteins could substitute for NTA in this pathway if they localized to the Golgi, suggesting that MLO localization in Golgi prior to PT arrival is a pre-requisite for their function in PT reception (Jones et al., 2017).

Proteins localized in the plasma membrane of plant cells mediate communication between multiple cells within a tissue as well as between a cell and its environment. These proteins are targeted to the plasma membrane from within the cell via the secretory pathway. Polar trafficking, the directional transport of proteins to the plasma membrane, utilizes the endomembrane system to recycle proteins and restrict their diffusion within a specific region of the plasma membrane ensuring a polarized distribution (Naramoto, 2017). Both polarized trafficking and secretion are involved in PT attraction and reception indicating that the synergid secretory pathway plays a critical role in regulating these processes. Characterizing the secretory pathway in the synergid cell and identifying compartments directly involved in either PT attraction or reception will be a vital step towards understanding key regulatory mechanisms in flowering plant reproduction.

While subcellular markers have been used to describe the localization of both LRE and NTA, both experiments also revealed fluorescent signal beyond the organelle markers used (Liu et al., 2016; Jones et al., 2017). In this study, we used confocal laser scanning microscopy (CLSM) to perform co-localization experiments in the synergid cell with a set of fluorescent markers labeling components of the secretory pathway in an attempt to more thoroughly define the distributions of LRE and NTA in the synergid cell before PT arrival. We generated markers based on established proteins or signals (signal peptides and/or retention motifs) that can localize a fluorescent reporter protein

to specific compartments within the endomembrane system. These markers enabled co-localization analyses with known components involved in PT reception and assisted in the elucidation of endomembrane compartment distribution within synergid cells *in vivo* using CLSM. This suite of markers was stably transformed into the Columbia-0 (Col-0) ecotype and characterized in a wildtype background (i.e. solely expressed in synergid cells and not in conjunction with other reporter fusion proteins), so that it can serve as a tool to study the secretory pathway of synergid cells by the reproductive and cell biology communities.

Results

Distribution of secretory pathway markers in synergid cells

Synergids are specialized cells that function in PT attraction and reception, both processes that require the complex regulation of their secretory pathway for the trafficking of cargo. While the biological function of these cells has become clearer, comprehensive analysis of the cellular components directly involved in these processes remains difficult. To bridge this knowledge gap and better describe the secretory pathway of the synergid cell, seven markers identifying different components of the secretory pathway, expressed under the synergid-selective promoters of *LORELEI* and *MYB98*, were stably transformed into the Col-0 background (Fig. 4.2; Supplemental Table 4.1). Synergid-expressed markers for the ER, Golgi, peroxisomes and the trans-Golgi Network (TGN; SYP61) had all previously been used in co-localization analyses with LRE and NTA (Liu et al., 2016; Jones et al., 2017); however, none of these markers had been solely expressed in synergid cells to determine organelle distribution in the absence of other fluorescent markers, which could adversely affect organelle marker localization. No discernable differences were

detected in marker distribution in the wildtype background (Fig. 4.2B-D, H) compared to the previous findings (Liu et al., 2016; Jones et al., 2017), indicating that these markers consistently and correctly localized in the expected organelle and are not noticeably influenced by the presence of either LRE or NTA-reporter fusion proteins.

The ER marker (SP-mCherry-HDEL (Nelson et al., 2007; Liu et al., 2016)) was distributed throughout the synergid cell but was predominantly excluded from the FA (Fig. 4.2B). The reticulate nature of the ER was obvious in synergids, with transvacuolar strands detected in the chalazal vacuole and a perinuclear envelope observed in all cells imaged. Both the Golgi (Man49-mCherry (Nelson et al., 2007; Liu et al., 2016)) and TGN (SYP61 and VHA-a1 (Sanderfoot et al., 2001; Dettmer et al., 2006; Jones et al., 2017)) markers were present in punctate compartments throughout the synergid cell (Fig. 4.2C-E), as previously noted (Liu et al., 2016; Jones et al., 2017). The Golgi marker was never detected in the FA nor was there any polarly distributed signal towards this region of the synergid cells. This localization pattern was markedly different from the TGN markers, which exhibited two types of distribution. The first type had signal in the FA (as well as in compartments throughout the cell), while the other only accumulated in punctate compartments and was predominantly excluded from the FA (Fig. 4.2D-D'; Supplemental Table 4.2). The recycling endosome marker (RabA1g (Rutherford and Moore, 2002; Geldner et al., 2009)) was distributed throughout the synergid cell with both diffuse signal and punctate compartmentalization (Fig. 4.2F). Focal accumulations of this marker occurred around the FA, but not necessarily within it. These focal accumulations rarely occurred across the entire FA evenly but instead appeared to be distributed to just one side. Like the TGN markers, the exocyst positive organelle marker (EXPO; Exo70E2 (Wang et al., 2010)) varied in both expression level and distribution within the synergid cell. Punctate

compartmentalization of this marker was regularly observed and at least some signal was polarly distributed toward the FA (Fig. 4.2G). The majority of synergids imaged had the EXPO marker present within the FA; however, a few synergids differed with signal in a line at the top edge of the FA and not within the FA (see Fig. 4.3H). Those that differed typically had much larger accumulations of the marker aggregating as well. These aggregates were much brighter and thus may be associated with synergids that had higher expression levels of the marker. The peroxisome marker (mCherry-SKL (Nelson et al., 2007; Liu et al., 2016)) accumulated within spherical compartments that were distributed throughout the synergid cell cytosol, but were excluded from the FA (Fig. 4.2H).

LORELEI partially co-localizes with trans-Golgi markers in the filiform apparatus

In unfertilized embryo sacs, LRE primarily accumulates in the FA of the synergid cells; however, LRE also localizes within intracellular compartments distributed throughout the cell (Fig. 4.1B) (Capron et al., 2008; Tsukamoto et al., 2010; Liu et al., 2016). Previous co-localization analyses in synergid cells found that LRE did not overlap with markers localized to the ER, Golgi or peroxisomes (Liu et al., 2016). To determine the identity of these intracellular compartments, translational fusion of LRE and citrine yellow fluorescent protein (cYFP) was co-expressed with fluorescent markers labeling additional components of the secretory pathway in the synergid cell. Four marker proteins that localize to the TGN, recycling endosomes, or the EXPO fused to mCherry were co-expressed with LRE-cYFP in synergid cells (Fig. 4.3; Supplemental Table 4.3). These markers correspond to a number of endomembrane-associated compartments involved in endo- and exocytic trafficking of soluble and membrane-bound cargo (Foresti and Denecke, 2008; Geldner et al., 2009; Drakakaki and Dandekar, 2013). As LRE-cYFP is highly enriched at the FA, saturation of this signal typically occurs before

the LRE-associated intracellular compartments were easily visualized during post-image processing. In order to better analyze this data, images of whole synergids were cropped to remove the FA, enlarged, and fluorescent signal adjusted to make more informed comparisons between signals corresponding to the YFP and mCherry channels. Overall, no appreciable overlap was observed between LRE-associated intracellular compartments and any of the four markers used in this analysis (Fig. 4.3 insets).

Three markers were distributed toward the FA of synergid cells in a manner similar to or associated with LRE-cYFP. Of the two distribution patterns observed with the TGN markers, only the TGN signal that accumulated in the FA had any overlap with LRE, indicating that some TGN-associated components may have a role in LRE's distribution to this region (Fig. 4.3B, D). The recycling endosome marker was mostly diffuse with some accumulation in punctate compartments throughout the synergid cell and had no detectable overlap with LRE-cYFP (Fig. 4.3E-F). Although the polarly localized EXPO distribution appeared at first to localize within the FA in a manner similar to LRE, the two signals formed distinct subdomains with relatively little overlap (Supplemental Fig. 4.1). This finding not only indicates that LRE likely does not localize within the EXPO but also suggests that multiple domains may exist within the FA of *A. thaliana*, an observation made previously about the synergid cells of cotton (*Gossipium hirsutum*) (Jensen, 1965).

NORTIA partially co-localizes with an endosome marker in the synergid cell

When expressed from its native promoter, NTA accumulates specifically in the synergid cells where it mediates PT-synergid communication during PT reception (Fig. 4.1C) (Kessler et al., 2010). NTA predominantly co-localizes with a Golgi marker in the

synergid cell (Jones et al., 2017); however, NTA-GFP was also detected in other parts of the synergid cell besides the Golgi, suggesting it accumulates within other membrane-bound compartments as well. A previous study found no overlap between NTA-GFP signal and markers for the ER, peroxisomes, or TGN (SYP61) (Jones et al., 2017). If conventional trafficking pathways mediate NTA's initial retention within the Golgi or its active redistribution following PT arrival, then these non-Golgi compartments are presumably associated with the secretory pathway and we may be able to detect overlap between NTA and the additional markers generated in this study. To this end, a translational fusion of NTA-GFP was co-expressed in synergid cells alongside three markers for components of the secretory pathway previously uncharacterized alongside NTA (Fig. 4.4; Supplemental Table 4.3).

Similar to the NTA-GFP and TGN marker (SYP61) co-localization pattern previously reported (Jones et al., 2017), no direct overlap was detected between NTA and VHA-a1 (Fig. 4.4A-B), further demonstrating NTA's exclusion from the TGN prior to PT arrival. However, NTA-GFP and TGN distribution do appear to be closely associated, which agrees with previous reports comparing Golgi and TGN dynamics using fluorescent markers for each organelle in hypocotyl cells (Viotti et al., 2010). Co-localization of NTA-GFP and the recycling endosome marker revealed some overlap between the two signals; however, this was only observed in a portion of the more punctate accumulations of this marker (Fig. 4.4C-D). Since the recycling endosome marker's primary distribution was more diffuse within the cell, we cannot say whether there is additional overlap with the more diffuse NTA-GFP signal or not. Due to this, there may be some cases of co-localization between the two signals that remains below the resolution limits of this system. No overlap was detected in the case of the EXPO marker and NTA-GFP in unpollinated ovules (Fig. 4.4E-F).

Discussion

In vivo analysis of the synergid secretory pathway

Ultrastructural and genetic analyses have both provided extensive insight into the biological function of synergid cells from many species (Huang and Russell, 1992; Kessler and Grossniklaus, 2011; Beale and Johnson, 2013). In particular, analyses focusing on PT attraction and reception in the model system *A. thaliana* have produced much of what is known about the complex molecular pathways regulating these critical processes (Kessler and Grossniklaus, 2011; Beale and Johnson, 2013; Higashiyama and Takeuchi, 2015). While the synergid cell's function is dependent on the active secretion of attractant molecules (PT attraction) and the polar distribution of membrane bound proteins to the FA (PT reception), few tools, if any, exist to study the secretory pathway within this cell type *in vivo*. Constitutively expressed markers for secretory pathway compartments have been generated using both the 35S and UBQ10 promoters (Nelson et al., 2007; Geldner et al., 2009). While these marker lines have proven to be extremely useful for sporophytic tissues, their utility in female gametophytes is limited due to the weak expression of the 35S promoter in these cells and the fact that the female gametophyte is buried under several layers of sporophytic tissue impeding CLSM analysis of these cell types. Highly specific and strong expression of secretory pathway markers in the synergids of *A. thaliana* provides an invaluable tool for the analysis of the cellular processes regulating its function.

The specialized nature of the synergid cell requires a thorough description of the distribution of secretory pathway components in this cell. We found no discernable differences in the distributions of the seven secretory markers assayed when co-expressed with fluorescently labeled PT reception components (LRE and NTA) or when expressed independently. These data suggest that this suite of secretory

markers can be used as effective tools for co-localization analyses of synergid expressed proteins. Additionally, these markers enable the comparative analysis of endomembrane distribution between wildtype and more complex genetic backgrounds, such as mutants for essential components involved in regulating the secretory pathway. With many parallels drawn between cell-cell communication during sexual reproduction and responses to pathogens, tools like these markers could demonstrate more similarities between conserved intracellular communication pathways. This is especially true in comparing reproductive signaling to defense responses since much is known about the role of the secretory pathway in response to fungal pathogen infection in plants (Hückelhoven and Panstruga, 2011). Investigation of the synergid secretory pathway in PT reception deficient mutants would allow us to explore additional levels of conservation between these two systems. However, the benefits of comparative analyses in synergid cells go beyond understanding the function of synergid-regulated processes. As gametophytic cells, synergids are haploid, enabling the analysis of loss-of-function and dominant negative mutations that are lethal or have deleterious effects on normal plant growth and development by studying them in a heterozygous background.

While the majority of secretory markers used in this study maintained predictable distribution patterns in synergid cells when compared to previous descriptions (Sanderfoot et al., 2001; Geldner et al., 2003; Dettmer et al., 2006; Nelson et al., 2007; Geldner et al., 2009), there was some variation in marker distribution in our analysis. The TGN marker varied in its distribution in synergid cells between exclusion from the FA and incorporation in the FA (Supplemental Table 4.2). Individuals exhibited consistent TGN distribution, with little to no variation between synergids within a single flower. Although the cause of these different distributions is not immediately clear, they

were observed across many independent transgenic lines with different levels of marker accumulation, suggesting that it is not an artifact of insertion bias of the transgene. Both TGN markers used are full-length proteins and, although ectopically expressed in the synergid, could be influenced by other components within the cell. While every flower analyzed was imaged two days after emasculation (see methods), we cannot rule out environmental factors such as time of day or age of a specific synergid cell in influencing the distribution of these markers. Since two different markers for the TGN were analyzed, and both showed variation in distribution within the cell, it is likely that this variability is biologically relevant and could represent an unknown switch in the synergid cell's secretory function (i.e. trafficking processes regulating PT attraction vs. reception). We also observed some differences in distribution of the recycling endosome marker (RabA1g) compared to what was previously reported (Geldner et al., 2009). While punctate accumulations were detected, much of the marker's signal was more diffuse (Fig. 4.2F). This may represent differences in either expression level between our system and that previously reported or a biological difference in how synergid cells sort and regulate this class of proteins. As another indicator of the synergid cell's complexity, multiple domains within the FA were observed in synergids co-expressing LRE and the EXPO marker (Supplemental Fig. 4.1). Distinct domains within an FA were previously described in cotton as two "phases" of the synergid FA, a highly organized region with striations and an amorphous region, but no functional significance for these domains is known (Jensen, 1965). Our analysis reveals that this characteristic may extend to the FA of *A. thaliana* synergid cells.

The role of the synergid endomembrane system in the distribution of pollen tube reception components

LRE primarily localizes to the FA of the synergid and functions with FER to mediate interactions between the PT and synergid cell during PT reception (Capron et al., 2008; Tsukamoto et al., 2010; Li et al., 2015; Lindner et al., 2015). A recent study exploring LRE function and localization within the synergid also demonstrated its accumulation in additional unknown intracellular compartments throughout the cell (Liu et al., 2016). Based on the nature of LRE's polar distribution, and its role in trafficking FER from the ER to the FA, our original hypothesis was that these LRE-associated intracellular compartments were a component of the secretory pathway (Li et al., 2015; Liu et al., 2016). Co-localization analyses using a set of secretory pathway markers expressed in the synergid cell did not reveal the identity of LRE's intracellular compartment; however, this study did provide some evidence for LRE-related trafficking. The overlap between LRE and markers for the TGN at the FA supports the notion that LRE's polar distribution is achieved, in some part, through conventional trafficking processes involving transport through the TGN to the plasma membrane. Additionally, while no direct overlap with recycling endosome markers was found, the unique distribution of the endosome marker maxima at the FA suggests some relationship with FA-localized proteins (Fig. 4.3E-F). The role of endosomal compartments in polar trafficking has been proposed for the recycling of the PIN-FORMED (PIN) auxin efflux proteins at the plasma membrane and it is possible that the polar accumulation of PT reception components in the FA of the synergid cell could be maintained in this way (Geldner et al., 2003; Reyes et al., 2011; Naramoto, 2017). One function of LRE is at the PT-synergid interface, demonstrated by complementation of the *lre* mutant with ectopic expression of LRE in the PT or with LRE fused to the transmembrane domain of FER (which ensured its localization to the FA in the synergid cell without being cleaved) (Liu

et al., 2016). Since the LRE/FER receptor complex represents an upstream signaling component of the PT reception pathway, it's likely that the polar transport and maintenance of LRE/FER within the FA is critical for this important cellular function in the synergid.

NTA localizes within the Golgi of the synergid cell prior to PT arrival and redistributes toward the FA sometime during PT reception (Kessler et al., 2010; Jones et al., 2017). NTA localization in Golgi is conserved among MLO proteins that can substitute for NTA when expressed in this cell type, and may represent an interaction with an unknown component involved in MLO function during PT reception (Jones et al., 2017). Mobilization of MLO proteins to a focused domain in the plasma membrane is conserved across MLO-mediated processes. During powdery mildew infection, barley MLO redistributes to the site of fungal penetration in epidermal cells, suggesting that polarized MLO trafficking is critical for their function (Bhat et al., 2005; Kessler et al., 2010). The partial co-localization of NTA-GFP and the recycling endosome marker prior to PT arrival suggests either that NTA's retention within the Golgi or the prevention of its distribution to the FA is dependent on trafficking through endosome-associated compartments. In plants, endosomal trafficking is primarily associated with either the TGN, for transport/recycling of cargo to the plasma membrane, or multivesicular bodies (pre-vacuolar compartments), for transport related to protein degradation (Reyes et al., 2011). Interestingly, no appreciable overlap between NTA-GFP and TGN markers has been observed in the synergid cell (Fig. 4.4A-B) (Jones et al., 2017). These data support the hypothesis that NTA's presence in endosome-associated compartments is linked to its transport out of the FA (or plasma membrane), preventing its accumulation in this region before PT arrival. This hypothesis is dependent on NTA's exclusion from the TGN. We cannot, however, rule out that NTA

may still be trafficked through the TGN, but that its transport is too rapid and dynamic to detect in our *in vivo* assay (Viotti et al., 2010; Jones et al., 2017).

Conclusion

In summary, the seven secretory markers described in this study provide a tool to investigate the secretory pathway in synergid cells by the reproductive and cell biology communities. Future studies can utilize this set of markers to identify the cellular compartments involved in PT attraction and reception and more thoroughly dissect processes regulating the secretory pathway of a highly polarized haploid cell.

Methods and Materials

Cloning and Transformation

Secretory marker fusions with mCherry expressed under the *MYB98pro* (VHAa1 and Exo70E) were generated in a manner similar to the previously published *MYB98pro::SYP61-mCherry* construct (Jones et al., 2017). Expression vectors were generated in the pEarlyGate301 backbone using Gibson Assembly, Gibson Assembly Master Mix - NEB E2611S (Gibson et al., 2009). *VHAa1* and *Exo70E* were amplified with PHUSION High-Fidelity Polymerase (NEB, M0535S) from Col-0 flower cDNA and *MYB98pro* was amplified out of a modified pMDC83 vector that incorporates the *MYB98pro* (Lindner et al., 2015). Fragments were assembled after restriction digests of pEarlyGate301 with PacI (NEB R0547S) and BamHI (NEB R3136S) followed by gel purification. To generate *LREpro::mCherry-RabA1g* construct, the 959bp *LRE* promoter and *mCherry* coding sequence were amplified from previous described constructs (Liu et al., 2016), and *RabA1g* (AT3G15060) genomic sequence (from ATG to TGA) was amplified from Col-0 genomic DNA. These three fragments were then

assembled via overlapping PCR, and cloned into a pFGC19 backbone using In-Fusion HD Cloning Plus (Clontech, cat# 638909). A flexible linker (Ala-Gly-Ala-Ala-Ala-Ala-Ala-Gly-Ala) (Tian et al., 2004) was placed between *mCherry* and *RabA1g* sequences. Primers used for cloning are listed in Supplemental Table 4.4. Expression vectors containing the secretory markers were transformed into the *Agrobacterium tumefaciens* strain GV3101 and transformed into the *LREpro::LRE-cYFP*, *MYB98pro::NTA-GFP*, and Col-0 via the floral-dip method (Bent, 2006). Details of the *LREpro::LRE-cYFP* and *MYB98pro::NTA-GFP* lines used can be found in their original articles (Lindner et al., 2015; Liu et al., 2016; Jones et al., 2017).

Plant growth and transgenic selections

All *Arabidopsis thaliana* used for imaging was grown at 22°C in long day conditions (16 hours light/8 hours dark) in a custom built grow room. T1 generation plants were planted directly on soil (ProMix Flex supplemented with 40g MARATHON pesticide and Peter's 20:20:20 (NPK) fertilizer at recommended levels) and cold-stratified in the dark at 4°C for two days. Seedlings were sprayed with BASTA herbicide for three successive days starting at 5 days after germination and resistant plants were maintained for subsequent analysis. T1 plants were screened for expression of desired constructs and 2-3 independent lines were carried on to the next generation for imaging. T2 seeds were bleach sterilized, plated on ½ MS plates, and cold-stratified at 4°C in the dark for two days before being moved to the grow room described above. 5-7d old seedlings were then transplanted to soil and grown to flower for further analysis.

CLSM

All T1 lines were screened using a compound epifluorescent microscope (Nikon Eclipse Ni-U) with an X-Cite 120 LED fluorescent lamp and narrow band eGFP and

TXRed filter cubes. Mature flowers were selected and ovules dissected out retained on the septum and placed in PIPES buffer (50mM PIPES, 5mM EGTA and 1mM $MgSO_4$ at pH = 6.8) on a clean slide. Lines with varying levels of fluorescent marker accumulation were analyzed and carried forward to account for expression-level bias in marker distribution.

Final imaging was done in stable T2 lines using confocal laser scanning microscopy (CLSM). Ovules were dissected out of emasculated flowers (after 2d to ensure ovule maturity) and mounted in PIPES buffer on clean slides. Immediately after dissection, samples were imaged on a Leica TCS SP8 CLSM using a HC PL APO 40× water immersion objective (NA = 1.10) with both GFP and cYFP excited using an argon laser (488nm and 514nm, respectively) and mCherry excited with a 561nm diode laser in sequential mode. Fluorescence was detected differentially using two separate HyD detectors, both in photon counting mode, obtaining single sections of synergid cells at 4.5× zoom.

Native promoter lines were imaged similar to above but with the following changes. Ovules from *LREpro::LRE-cYFP* in the *lre* mutant background and *NTApro::NTA-GFP* in Col-0 were imaged on the Leica TCS SP8 using the 40× water immersion objective but with no zoom. Autofluorescence was detected simultaneously along with *LREpro::LRE-cYFP* using the 488nm argon laser and a separate HyD detector. The *NTApro::NTA-GFP* ovule was counterstained and imaged along with FM464 (Molecular Probes, T3166) as in previously studies (Jones et al., 2017).

Image Processing and Figure Construction

Micrographs were edited and analyzed using Fiji (Schindelin et al., 2012). Ovule diagram was made in Inkscape v0.91. Figures were all constructed using Gimp v2.8.14.

Figures and Tables

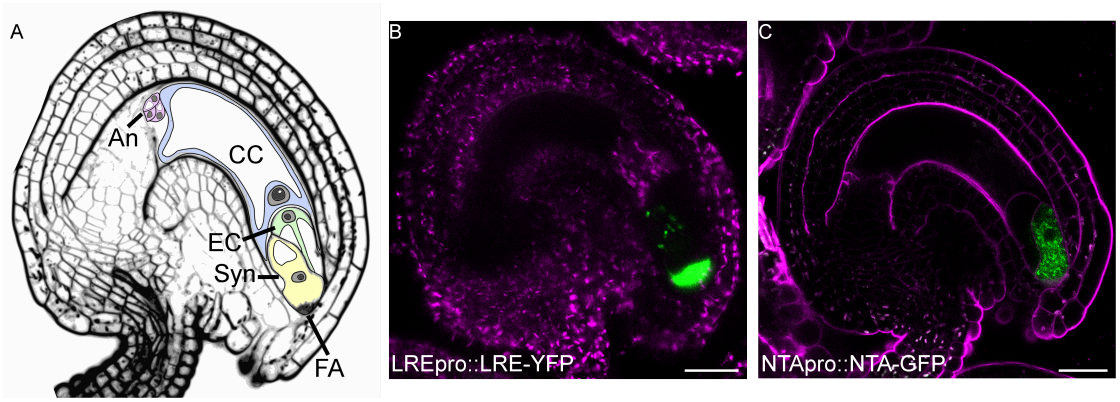

Figure 4.1 – LORELEI and NORTIA expression in the synergid cell. A) Diagram of a mature *Arabidopsis thaliana* embryo sac. An, Antipodals; CC, central cell; EC, egg cell; Syn, synergid; FA, filiform apparatus. B-C) Both LRE and NTA are expressed specifically in the synergid cells of the mature embryo sac. B) LRE-cYFP (green) in an unpollinated ovule (autofluorescence-magenta). C) NTA-GFP (green) in an unpollinated ovule labeled with FM4-64 (magenta). Bars = 20μm.

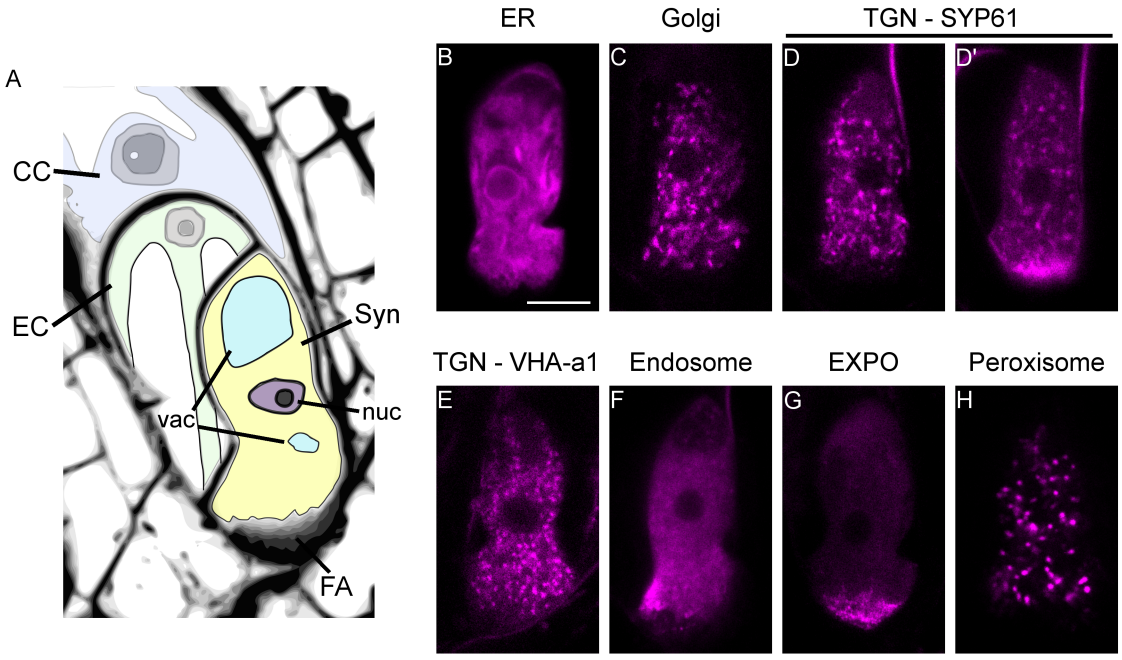

Figure 4.2 – Secretory marker distribution in Col-0 synergids. Localization of secretory markers (magenta) in synergids of Col-0 from emasculated flowers. A) Diagram of a synergid cell at the micropyle of a mature embryo sac. CC, central cell; EC, egg cell; Syn, synergid; vac, vacuoles; nuc, nucleus; FA, filiform apparatus. B) endoplasmic reticulum (ER) - SP-mCherry-HDEL. C) Golgi –SM1-mCherry. D-E) trans-Golgi network (TGN), Both the punctate distribution of the TGN markers throughout the cell (D) and their enrichment toward the filiform apparatus (D') were commonly observed: D) SYP61-mCherry, E) VHA-a1-mCherry. F) recycling endosome mCherry-RabA1g. G) exocyst-positive organelle (EXPO) –Exo70E-mCherry. H) Peroxisome –mCherry-SKL. M-N) Bar = 10μm.

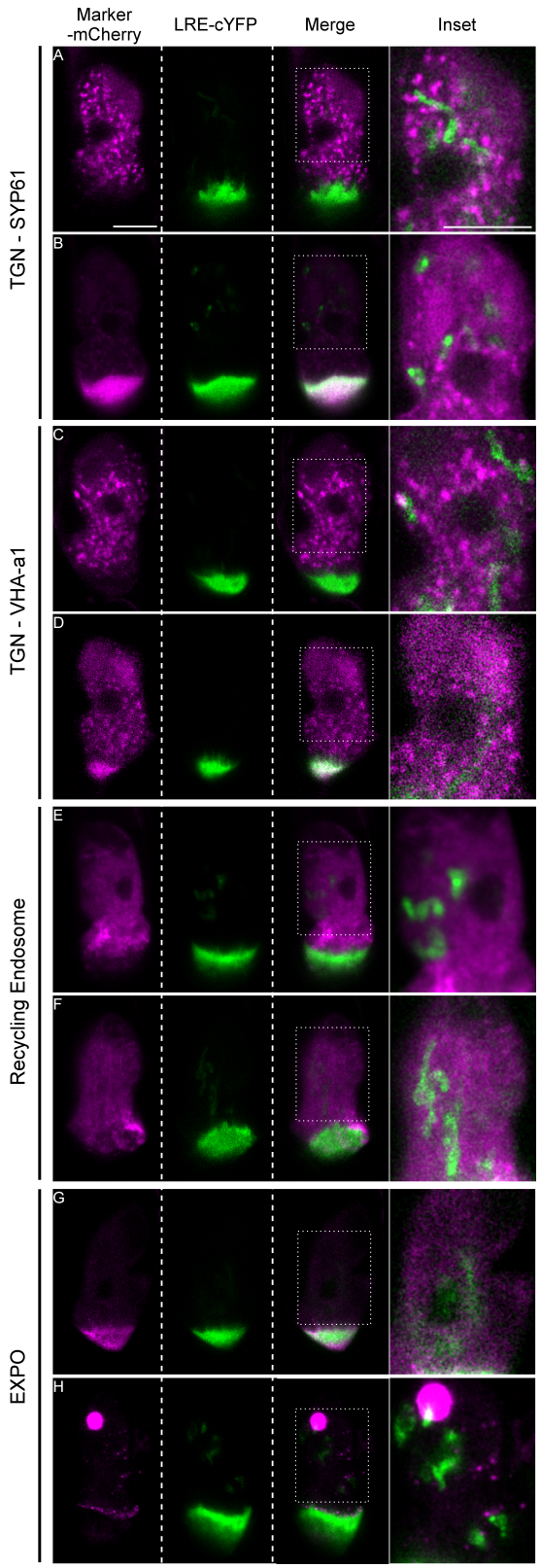

Figure 4.3 – LRE-cYFP co-localization with secretory markers in synergids.
Legend on next page

Figure 4.3 – LRE-cYFP co-localization with secretory markers in synergids. LRE-cYFP (green) co-localization with secretory markers (magenta) in synergid cells of *lre* from emasculated pistils. A-B) trans-Golgi network (TGN) - SYP61-mCherry. C-D) trans-Golgi network (TGN) - VHA-a1-mCherry. LRE-cYFP co-localized with both TGN markers at the filiform apparatus when they were polarly distributed to this region (B and D). E-F) recycling endosome - mCherry-RabA1g. G-H) exocyst-positive organelle (EXPO) - Exo70E-mCherry. Bars = 10µm (Bar on A inset used for all insets).

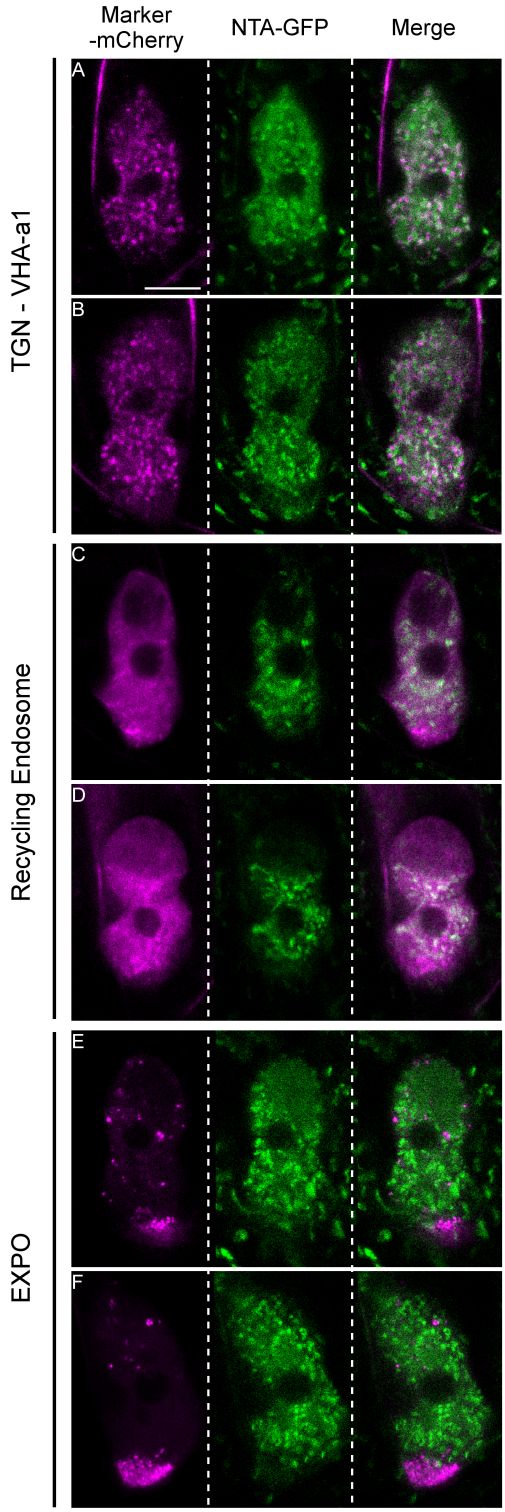

Figure 4.4 – NTA-GFP co-localization with secretory markers in synergids. *Legend on next page*

Figure 4.4 – NTA-GFP co-localization with secretory markers in synergids. NTA-GFP (green) co-localization with secretory markers (magenta) in synergid cells of *nta-1* from emasculated pistils. A-B) trans-Golgi network (TGN) - VHA-a1-mCherry. C-D) recycling endosome - mCherry-RabA1g. E-F) exocyst-positive organelle (EXPO) - Exo70E-mCherry. Bar = 10µm.

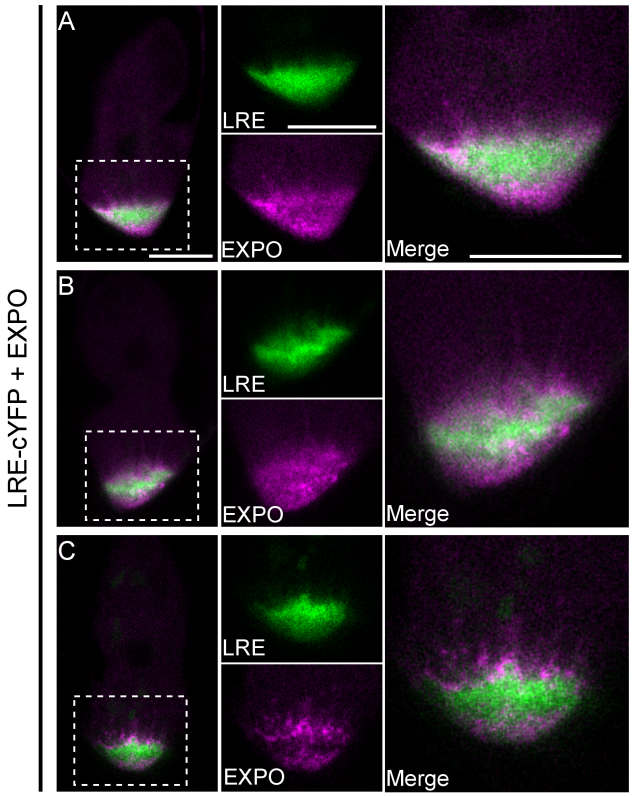

Supplemental Figure 4.1 – LRE-cYFP co-localization with EXPO in the FA of mature synergids. LRE-cYFP (green) co-localization with the EXPO marker (magenta, Exo70E-mCherry) in synergid cells of from emasculated pistils. A) Close-up of synergid used in Fig. 3G showing FA sub-domains more clearly. B-C) Synergid cells from additional lines revealing the same sub-domain patterning of LRE with the EXPO marker in the FA. Bars = 10μm (Bars corresponding to each panel of A can be used with same panels of B-C).

Secretory Compartment	Marker Construct	AGI	Number of Synergids Imaged
			Marker in Col-0
Trans Golgi Network	MYB98pro::Syp61-mCherry	At1G28490	19
Trans Golgi Network	MYB98pro::VHA-a1-mCherry	At2G28520	17
EXPO	MYB98pro::Exo70E2-mCherry	At5G61010	31
Endosome	LREpro::RabA1g-mCherry	At3g15060	29
Golgi	LREpro::SM1-mCherry	N/A	10
Endoplasmic Reticulum	LREpro::SP-mCherry-HDEL	N/A	10
Peroxisome	LREpro::mCherry-SKL	N/A	10

Supplemental Table 4.1 – Secretory markers analyzed in the Col-0 background.

Trans Golgi Network Marker	Number of Synergids with Different Localization Patterns	
	# Not in FA	# FA-localized
Syp61	32	22
VHA-a1	34	8

Supplemental Table 4.2 – Number of synergids expressing TGN markers with FA-localizaiton vs. no FA-localization.

Secretory Compartment	Marker Construct	AGI	Number of Synergids Imaged (Marker + LRE/NTA)	
			Marker with LREpro::LRE-cYFP	Marker with MYB98pro::NTA-GFP
Trans Golgi Network	MYB98pro::Syp61-mCherry	At1G28490	35	-
Trans Golgi Network	MYB98pro::VHA-a1-mCherry	At2G28520	16	17
EXPO	MYB98pro::Exo70E2-mCherry	At5G61010	42	18
Endosome	LREpro::mCherry-RabA1g	At3g15060	36	15

Supplemental Table 4.3 – Secretory markers co-expressed and imaged with LRE and NTA

Table S4 - Primers used for Cloning

DJ_VHAa1_F	CTCTCCAACCACCATATGGAGGAATTCTTAGATAAGTTGC
DJ_VHAa1_R	GGCCGCTGCACCTGAGATTAAAGCGAAAGAGAAAGGCTTG
DJ_Exo70E2_F2	CTCTCCAACCACCATATGGCAGAGTTTGATTCCAAGG
DJ_Exo70E2_R2	GGCCGCTGCACCTGATCTCTTACGAGAGCTGCGCAG
DJ_pEarlyGate301_F	GTTAATTAAGAATTAGCTTGC
DJ_pEarlyGate301_R	TGAGCTACACATGCTCAGG
DJ_linkmCher_F1	TCAGGTGCAGCGGCCGCTTC
DJ_pMyb98_R2	ATGGTGGTTGGAGAGCCTGCT
pLRE-RabA1g-F1	AAAAATCTCAGAATTATCTGTGAGTCATCCTTTCGAGGAAATC
pLRE-RabA1g-R1	CACCATGAAATTGTTGTTAAAGAAGCTTGTAACATT
pLRE-RabA1g-F2	CAACAATTTCATGGTGAGCAAGGGCGAGGAGGA
pLRE-RabA1g-R2	GGCCCCAGCGGCCGCAGCAGCACCAGCCTTGTACAGCTCGTCCATGCCGCCG
pLRE-RabA1g-F3	GCTGGTGCTGCTGCGGCCGCTGGGGCCATGGCGGCGTATAGAGCTGACGATG
pLRE-RabA1g-R3	GCTTGATATCGAATTCTCAACTTGAGCAGCATCCAACCTTC

Supplemental Table 4.4 – List of primers used for cloning secretory markers. Sequence in green corresponds with overhangs used in Gibson Assembly into the pEarlyGate301 backbone and with overhangs used in In-fusion assembly into the pFGC19 backbone (see methods). Sequence in blue corresponds with overhangs used in overlapping PCR.

Chapter 5: Interaction with calmodulin influences MLO function during pollen tube reception

Daniel S. Jones[1], Patrick B. Day[1], Sharon A. Kessler[2, 3]

Contributions:

Patrick B. Day cloned NTA truncation and W458A entry vectors, $MYB98_{pro}$:NTA(var)-GFP expression vectors and generated the stable lines and did preliminary analysis for experiments in Fig. 5.1 A, D-F.

[1]Department of Microbiology and Plant Biology, The University of Oklahoma, Norman, OK 73069, USA
[2]Department of Botany and Plant Pathology, Purdue University, West Lafayette, IN 47907, USA
[3]Center for Plant Biology, Purdue University, West Lafayette, IN 47907, USA

Summary

Many mechanisms regulating intercellular communication in plants are conserved across a wide-range of physiological processes. In some cases, this makes studying the components involved in a specific pathway relevant to understanding more broadly conserved signaling mechanisms. In *Arabidopsis thaliana*, the MILDEW RESISTANCE LOCUS O (MLO) family of proteins mediates communication in fungal pathogen susceptibility, root thigmomorphogenesis and pollen tube reception. MLO proteins have seven transmembrane domains and a conserved calmodulin (CaM)-binding domain in their C-terminal intracellular tails. CaMs are proteins that directly bind calcium and function as sensors, detecting changes in calcium concentrations within the cell. CaMs are essential components for calcium-related signaling and act through direct interactions with CaM-binding proteins. NORTIA (NTA) is an MLO protein expressed specifically in the synergid cells of the female gametophyte where it functions in pollen tube reception. During pollen tube reception, NTA polarly redistributes from Golgi-associated compartments to the site of initial cellular contact between the synergid cell and pollen tube. In this study we determined that NTA's CaM-binding domain is important for its function during pollen tube reception. Although it disrupted NTA's function, CaM-binding activity had no affect on NTA's initial localization to the Golgi or its ability to actively redistribute to the filiform apparatus. Additionally, we found that the closely related MLO8, which cannot function in pollen tube reception, does not interact with the same CaM that NTA does indicating that differential interactions with CaMs could influence MLO-mediated communication.

Introduction

Cell communication requires a mechanism for transducing external signals into a downstream response. This communication is important for an organism's capacity to respond to environmental stimuli but is also critical for developmental signaling within multicellular organisms. Signaling pathways vary dramatically in biological systems. Signals can range from small peptides or hormones that act as ligands for a specific receptor to fluxes in intracellular concentrations of small molecules such as calcium (Ca^{2+}) or reactive oxygen species (ROS) as secondary messengers (Endo et al., 2014; Gilroy et al., 2014; Haruta and Sussman, 2017; Hirakawa et al., 2017). This variability can ensure specificity of a given response within cells following transduction, but it also allows for plasticity, as the same components are utilized in many different pathways (Endo et al., 2014; Chen et al., 2015). An example of this in flowering plants is the conservation of components used in immune responses and in regulating reproductive signaling.

From self-incompatibility to gamete recognition and fusion, intercellular communication controls every aspect of reproduction in flowering plants (Rea and Nasrallah, 2004; Chevalier et al., 2011). This is, in part, due to the nature of their reproductive development. Gametophytes (the gamete-producing generation) develop deep within protective tissues, physically separating the two different sets of gametes. In order for fertilization to occur, the male gametophyte (pollen) must land on a receptive stigma and produce a tip-elongating cell, the pollen tube (PT), which travels through the pistil of the flower to deliver two sperm cells to the female gametophyte (embryo sac) (Russell, 1992). The PT is guided to an opening of the ovule, called the micropyle, via attractant molecules secreted by synergid cells, a pair of accessory cells in the embryo sac (Higashiyama and Takeuchi, 2015). When a PT arrives at the embryo sac, the

process of PT reception initiates, where one of the two synergids degenerates while the PT enters the embryo sac and ruptures, releasing the two sperm cells required for double fertilization (Russell, 1992; Kessler and Grossniklaus, 2011; Beale and Johnson, 2013). The core components regulating communication during reproduction are resonant with those involved in immune responses in plants (Dresselhaus and Márton, 2009). In this comparison, the PT's journey through the pistil of a flower represents "invasive-growth" reminiscent of fungal hyphae during either symbiotic or pathogenic infection. Members of the diverse group of cysteine-rich peptides (CRPs) are involved in PT attraction and guidance to the ovule (Higashiyama and Takeuchi, 2015; Bircheneder and Dresselhaus, 2016). Various receptor-like kinases regulate self-incompatibility, PT guidance and reception, and the secondary messengers Ca^{2+} and ROS play direct roles in polarized tip-elongation and rupture of the PT (Duan et al., 2014; Chen et al., 2015; Qu et al., 2015). Both systems utilize very similar mechanisms to regulate their respective cell-cell interactions. The fact that these general classes of signaling components are shared between both processes is not all that surprising; however, an intriguing link exists between the mechanisms regulating reproductive communication and immune response, as certain families of proteins appear to have conserved roles in each.

The MILDEW RESISTANCE LOCUS O (MLO) family of proteins represents a key similarity between plant defense and reproductive signaling with members having roles in both fungal pathogen susceptibility and in PT reception (Buschges et al., 1997; Consonni et al., 2006; Kessler et al., 2010). MLOs are seven-transmembrane proteins originally identified as negative regulators of defense responses related to the fungal pathogen powdery mildew (Buschges et al., 1997). MLO deficiency leads to broad-spectrum resistance to powdery mildew, a characteristic that is conserved across both

monocots and eudicots. In the case of *Arabidopsis thaliana*, three related *MLO* genes (*MLO2*, *6*, and *12*; Clade V) are redundant all contributing, albeit unequally, to MLO-mediated fungal susceptibility (Consonni et al., 2006). Unlike this susceptibility clade, the MLO protein NORTIA (NTA, or MLO7) is the sole *MLO* expressed in the synergid cell and is the only MLO described as regulating PT reception within this cell type (Kessler et al., 2010; Jones et al., 2017). In *nta-1* mutants, PT-synergid communication is disrupted leading to an overall reduction in fertilization. NTA functions downstream of the major PT reception components FERONIA (FER), a member of the *Catharanthus roseus* RLK1-like kinase (CrRLK1L) family, and LORELEI (LRE), a GPI-anchored protein (Kessler et al., 2010; Liu et al., 2016). Both FER and LRE are expressed in synergid cells where they localize to a specialized region of the cell called the filiform apparatus (FA), a membrane rich area located at the micropyle of the ovule (Escobar-Restrepo et al., 2007; Lindner et al., 2015). The FA is thought to be important for the secretion of attractant peptides and is the first site of interaction between the PT and synergid cell prior to PT reception (Mansfield et al., 1991; Huang and Russell, 1992; Leshem et al., 2013). After the PT arrives, calcium oscillations initiate within the synergid cells early on during PT reception-related signaling (Iwano et al., 2012; Hamamura et al., 2014). These oscillations are dependent on the FER/LRE complex and do not initiate in plants deficient for either (Ngo et al., 2014). Interestingly, the initiation of these calcium oscillations is not dependent on NTA; however, the amplitude of the oscillatory calcium peaks within *nta* mutant synergids is lower, suggesting NTA may play a role in modulating this signal in some way (Ngo et al., 2014). Prior to PT arrival, NTA is localized within Golgi-associated compartments and is distributed throughout the entire synergid cell (Kessler et al., 2010; Jones et al., 2017). During PT reception, NTA is redistributed towards the FA in a FER-dependent manner (Kessler et al., 2010). The timing and importance of NTA's redistribution is unknown; however,

subcellular redistribution is a conserved trait among MLOs as the barley MLO (HvMLO) is recruited to the site of fungal penetration during powdery mildew infection (Bhat et al., 2005).

The molecular function of MLOs remains relatively unresolved. MLO proteins are highly variable with few predicted functional domains (Devoto et al., 2003; Kusch et al., 2016). Other than their transmembrane domains, they all have a conserved calmodulin-binding domain (CaMBD) located in their C-terminal intracellular tail (Lee et al., 1997; Kim et al., 2002). Calmodulin (CaM) is a small protein that binds Ca^{2+} and is involved in signal transduction for many cellular processes (Yang and Poovaiah, 2003). CaMs are highly conserved, found in all eukaryotes, and are considered essential receptors for Ca^{2+}-linked signaling within cells. Signaling via CaM typically occurs through interactions with CaMBDs, interactions that change the conformation of a target protein in a Ca^{2+}-dependent manner (Zielinski, 1998). MLOs interact with CaM *in vivo,* and this interaction is required for MLO-mediated powdery mildew susceptibility (Kim et al., 2002). In an effort to more broadly understand the requirements for MLO-mediated processes, we wanted to determine the role of NTA's CaMBD during PT reception. Taking advantage of an MLO-mediated signaling pathway that requires only a single gene knockout for a quantitative phenotype, we assayed the influence of CaM-binding on NTA's function and subcellular distribution through C-terminal truncations and a point mutation disrupting its CaMBD. Here we show that CaM-binding is necessary for NTA's complete rescue of *nta-1*'s unfertilized ovule phenotype, revealing additional conservation of MLO-mediated processes. Additionally we show that a functional CaMBD is not required for NTA's Golgi-associated localization within the synergid or its redistribution at PT arrival. We also provide evidence for differential CaM-binding

activity in closely related MLO proteins, demonstrating a potential mechanism for specificity in MLO-mediated signaling.

Results

CaM-binding activity is important for NTA's function in PT reception

Like all MLO proteins, NTA has a predicted CaMBD in its C-terminal tail (Fig. 5.1) (Kim et al., 2002). Previous studies have found that CaM-binding activity of its conserved CaMBD influences MLO function in powdery mildew susceptibility (Kim et al., 2002). We hypothesized that CaM-binding activity is also important for NTA's function during PT reception. While the MLO CaMBD is conserved and MLO + CaM interactions are well documented (Lee et al., 1997; Kim et al., 2002; Gookin and Assmann, 2014; Kusch et al., 2016), we wanted to confirm that NTA is capable of physically interacting with CaM *in planta*. Using a previously described FRET-based assay (Jones et al., 2017), C-terminal Cer3 fusions of NTA and NTA with a W➔A point mutation predicted to disrupt this domain's CaM-binding activity (NTA W458A) (Arazi et al., 1995; Yamada et al., 1995; Kim et al., 2002) were co-expressed with an N-terminal YFP fusion of AtCaM1 (CaM1) in epidermal cells of *Nicotiana benthamiana* (Supplemental Fig. 5.1). FRET was detected between NTA and CaM1 as efficiently as our positive control (NTA-Cer3 and NTA-YFP), and there was no significant difference between the negative control (NTA-Cer3 and GUS-YFP) and NTA W458A and CaM1 (Fig. 5.1B). These data indicate that NTA can interact with CaM1 and that the W458A point mutation generated within NTA's CaMBD disrupts this interaction. We then made an attempt to confirm this interaction through the co-immunoprecipitation (Co-IP) of CaM1 (Myc-CaM1) with NTA and the NTA W458A variant (NTA–YFP-HA and NTA W458A–YFP-HA) transiently co-expressed in *N. benthamiana* leaf epidermal cells. No

interaction was detected between either NTA or NTA W458A and CaM1 using this system (Supplemental Fig. 5.2). As this is the first time Co-IP has been attempted using full-length MLO proteins, successful detection of interactions with MLOs may require testing additional conditions to optimize use of this assay. Previously we had demonstrated that MLO8, an MLO that's closely related to NTA, could not function in PT reception when expressed in the synergid cells of *nta-1* (Jones et al., 2017). In that study, we also found that domain swap constructs in which NTA's C-terminal tail domain was replaced with that of MLO8's was unable to fully rescue *nta*'s unfertilized ovule phenotype, leading us to hypothesize that MLO8's C-terminal tail may not have a functional CaMBD and that this characteristic contributes to MLO function in PT reception. To investigate this, MLO8-Cer3 was also tested for interaction with CaM1 in our FRET-based assay, where we found no significant difference between MLO8-Cer3 + YFP-CaM1 and either the negative control or the NTA W458A point mutation (Fig. 5.1B), indicating that MLO8 does not interact with CaM1 in this assay.

Next, we wanted to know whether CaM-binding activity was important for MLO-mediated PT reception. To test this, a truncation removing the C-terminal tail including the CaMBD (NTA Δ450), the W➔A point mutation disrupting CaM-binding function (NTA W458A), and a truncation removing the tail immediately following the CaMBD (NTA Δ481) were generated and expressed under the MYB98 promoter in the *nta-1* background. Ovule counts in homozygous lines revealed that all three constructs had significant reductions in unfertilized ovules compared to *nta-1*; however, only NTA Δ481 rescued at similar levels as wildtype NTA (Fig. 5.1A). Both NTA Δ450 and NTA W458A rescued *nta*-1 at intermediate levels, suggesting that either the removal or disruption of the CaMBD have a similar impact on NTA's function, while the amino acids C-terminal to the CaMBD are dispensable. These results indicate that CaM-

binding activity influences NTA's function in PT reception but is not the sole contributor, suggesting that the role of the CaMBD may be to modulate some other part of NTA's activity.

NTA's Golgi-localization and redistribution during PT reception does not require a functional CaMBD

Prior to PT arrival, NTA is distributed throughout the entire synergid cell where it is localized primarily within Golgi (Fig. 5.1C) (Kessler et al., 2010; Jones et al., 2017). When expressed in synergid cells, related MLO proteins that localize within Golgi can rescue *nta-1* whereas those that localize elsewhere do not function in PT reception. To test the effect of CaM-binding on NTA's distribution in the synergid cell, each construct used in the PT reception assay also had a C-terminal translational fusion with GFP (*MYB98pro:NTA(var)-GFP*). Confocal laser scanning microscopy (CLSM) revealed differences in the overall distribution of the NTA variants within the synergid cells of unpollinated ovules (Fig. 5.1D-F). NTA Δ450 was primarily distributed towards the FA of the synergid cell and also accumulated in vacuoles and punctate compartments throughout the rest of the cell (Fig. 5.1D). Both NTA Δ481 and NTA W458A were distributed throughout the synergid cell in punctate compartments and were predominantly maintained out of the FA (Fig. 5.1E-F); however, they also differed in that NTA Δ481 had a more diffuse distribution overall (Fig. 5.1E). Although they both partially rescued the *nta-1* unfertilized ovule phenotype at similar levels, the two variants with disrupted CaMBDs (NTA Δ450 and NTA W458A) had different distributions in the synergid cell. This suggests that differences in localization between these two variants may not be functionally relevant to PT reception, but could represent a secondary characteristic of MLOs expressed in this cell type. Due to this, we focused

primarily on NTA W458A for our downstream analyses and comparisons with wildtype NTA so as to not further complicate the interpretation of our results.

With “NTA-like” distribution in the synergid cell, we suspected that the NTA W458A variant would accumulate within Golgi-associated compartments similar to wildtype NTA. NTA W458A was co-expressed with fluorescent markers for Golgi (LREpro:Man49-mCherry, (Liu et al., 2016)) and the trans-Golgi network (TGN; MYB98pro:Syp61-mCherry, (Jones et al., 2017)) in synergid cells and unpollinated ovules were analyzed via CLSM (Fig. 5.2). The NTA W458A variant partially co-localized with the Golgi maker (Fig. 5.2A) and had no overlap with the TGN marker (Fig. 5.2B), similar to wildtype NTA localization (Jones et al., 2017). These data demonstrate that neither NTA’s distribution within the synergid cell, where it is maintained out of the FA prior to PT arrival, nor its localization within Golgi-associated compartments are dependent on having a functional CaMBD.

During PT reception, NTA is actively redistributed toward the FA. This redistribution is dependent on FER-mediated signaling, placing NTA’s role in this process downstream of FER in the PT reception pathway (Kessler et al., 2010). However, the importance of NTA’s redistribution in PT reception is unknown. The NTA W458A variant maintains a wildtype distribution and localization pattern in the synergid cell but does not fully rescue *nta-1*’s unfertilized ovule phenotype. To test whether CaM-binding is important for NTA’s redistribution, emasculated flowers of *Myb98$_{pro}$::NTA-GFP* and *Myb98$_{pro}$::NTA W458A-GFP* in the *nta-1* background were pollinated with the ACA9pro:DsRed fluorescent PT marker line and redistribution of GFP was assayed. Synergids were imaged 4-6 hours after pollination (hap) via CLSM with representative ovules prior to and after PT arrival analyzed (Fig. 5.3). Prior to PT arrival, both NTA-

GFP and NTA W458A-GFP maintained distributions out of the FA, consistent with unpollinated flowers above (Fig. 5.3A, C). At PT arrival (when a PT is first making contact with the synergids through the micropyle) a marked increase in GFP signal was detected in both lines at the FA (Fig. 5.3B, D). These data suggest that an active CaMBD is not essential for NTA's redistribution to the FA during PT reception.

Discussion

MLO proteins function within complex signaling pathways that mediate cell communication. In *A. thaliana*, disruption of MLOs affects processes related to pathogen susceptibility, root thigmomorphogenesis (change in growth due to mechanical stimulus), and PT reception (Consonni et al., 2006; Chen et al., 2009; Kessler et al., 2010). The MLO family represents a key similarity between components regulating intercellular communication linked to both pathogen infection and reproductive signaling. While the exact molecular function of MLOs in each process is unclear, common themes have emerged in recent studies providing some clues as to the mechanisms driving MLO-mediated communication.

All MLO proteins are predicted to have a CaMBD in their C-terminal intracellular tail (Kim et al., 2002). Disruption of NTA's CaMBD significantly reduced its ability to function in PT reception yet had no impact on its localization or redistribution within the synergid cell. The need for CaM-binding activity in HvMLO's redistribution during fungal infection has not been determined; however, HvMLO and CaM interactions in barley occur unevenly along the plasma membrane, suggesting HvMLO localizes along the entirety of the contact site and primarily interacts with CaM in subregions coincident with sites of successful fungal penetration into the host cell (Bhat et al., 2005). Since

recruitment of NTA to the FA is not dependent on its CaM-binding activity, there may be an additional component contributing to MLO redistribution within the synergid cell. This is consistent with the FA distribution of both NTA Δ450 (with the CaMBD completely removed) as well as the previously reported MLO8 in synergid cells prior to PT arrival (Jones et al., 2017). It is unclear whether the role of MLOs in root thigmomorphogenesis is also dependent on the CaM-binding activity of the conserved MLO CaMBD or if a polar redistribution/recruitment event occurs. Calcium signaling does however play a major role in this physiological response (Braam and Davis, 1990; Nakagawa et al., 2007). *A. thaliana* deficient for *MLO4, MLO11*, and *MLO14* have a dramatic root curling phenotype as a result of genetically predefined directional growth following a mechanical stimulus (Chen et al., 2009). Recently, it was shown that exogenous addition of Ca^{2+} partially suppressed this root curling phenotype in *mlo4-4* and *mlo11-4* seedlings (Bidzinski et al., 2014). Interestingly, addition of the Ca^{2+} chelator EGTA also partially suppressed root curling in *mlo4-4* seedlings, indicating that maintaining tight control over the physiological balance of Ca^{2+} concentrations influences this MLO-mediated process. While not a direct link, the importance of Ca^{2+} for the manifestation of the *mlo* root curling phenotype indicates there may be a role for the MLO CaMBD in this signaling pathway as well.

We now know that CaM-binding activity is important for MLO function in both powdery mildew susceptibility and in PT reception. No genetic evidence exists, however, for CaMs functioning directly within either pathway. Many proteins contain Ca^{2+}-binding EF-hand motifs that are structurally similar to CaM. With *A. thaliana* having at least 250 EF-hand proteins (Chen et al., 2015), there's a possibility that other CaM-like proteins interact with the MLO CaMBD. Interestingly, expression of a constitutively active variant of a barley Ca^{2+}-dependent protein kinase (HvCDPK4) partially restored

susceptibility in *mlo* mutants (Freymark et al., 2007). Ca^{2+}-dependent protein kinases (CPKs) are a unique family of serine/threonine kinases that contain a CaM-like domain at their C-terminus that functions as a Ca^{2+} sensor, enabling kinase activity in the presence of Ca^{2+} (Harper et al., 1991; Schulz et al., 2013). In *A. thaliana*, the CPKs 17, 34 and CPKs 11, 24 have roles in reproductive development, functioning in the regulation of the tip-focused elongation of PTs (Myers et al., 2009; Zhao et al., 2013). Partial rescue of MLO-susceptibility in barley with an active CPK (with autoinhibitory and CaM-like domains removed) suggests that phosphorylation targets of this CPK may reside downstream of MLO-related signaling (Freymark et al., 2007). In the Arabidopdsis Membrane-based Interactome Network Database (MIND1; (Jones et al., 2014)), multiple MLO proteins (MLO2, 6, 10, and 12) had interactions with CPKs. While interactions between MLO proteins and CPKs must be confirmed *in planta*, they represent an enticing link to downstream targets of MLO-mediated signaling in both PT reception and powdery mildew susceptibility.

Calcium signaling plays a key role in reproductive cell-cell communication (Ge et al., 2007). This remains a major similarity between reproductive processes and those regulating immunity and symbiotic interactions in plants (Chen et al., 2015; Zipfel and Oldroyd, 2017). This parallel has made understanding how proteins involved in both systems utilize calcium as a secondary messenger important for elucidating the complete signaling pathways in these systems. The relevance of the conserved CaMBD to MLO protein function remains an attractive target for understanding calcium-linked signaling in both PT reception and MLO fungal susceptibility. While all Arabidopsis MLO proteins have predicted CaMBDs, these domains are not completely conserved between MLO family members (Kim et al., 2002). Although closely related to NTA, MLO8 does not rescue the *nta-1* PT reception phenotype when ectopically

expressed in synergid cells. Domain swap experiments revealed that replacing NTA's C-terminal intracellular tail (which contains the predicted CaMBD) with MLO8's C-terminal tail inhibited function in PT reception, while NTA's tail on MLO8 enabled it to rescue *nta-1* (Jones et al., 2017). Here we have shown that, in our FRET-based assay, MLO8 may not interact with CaM1 *in planta*. Taken together these data suggest either that MLO8 does not contain a functional CaMBD or that MLO8 interacts with different CaMs in comparison to NTA. Many incidences of differential CaM interactions have been reported within related proteins, indicating that although CaMs are highly conserved, variation in CaMBDs (or the sequence surrounding them) contributes to specificity in interaction (Popescu et al., 2007). These differential interactions between MLOs and CaMs (or CaM-like proteins) could provide functional specificity to MLO proteins within a given process, making the identification of other components directly involved in MLO-mediated communication critical to determining the molecular role of MLO proteins.

Methods and Materials

Plant Growth Conditions

Arabidopsis thaliana was grown in a custom built grow room at 22°C in long day conditions (16hr light/8hr dark). Seeds were sterilized in a 3% (v/v) bleach solution and plated on ½ MS plates (transgenic lines on plates supplemented with 20µg/L hygromycin), cold-stratified at 4°C in the dark for two days then moved into the grow room. 7 day-old seedlings were then transplanted from plates to soil (ProMix Flex with 40g MARATHON pesticide and Peter's 20:20:20 (N:P:K) fertilizer at recommended concentrations) and grown to flowering for analysis. *Nicotiana benthamiana* seeds

were sown directly on soil (BM7 Berger) and grown in long day conditions at 22°C in a Conviron ATC13 growth chamber.

Cloning and Generation of Transgenic Lines

PCR amplification with PHUSION High-Fidelity Polymerase (NEB, M0535S) was used to generate all constructs in this study. Genes were amplified with primers that had attB1 and attB2 sites for recombination via BP reaction into the Gateway-compatible entry vector pDONR207. Full-length NTA and MLO8 entry vectors used in this study were generated as described previously (Jones et al., 2017). NTA truncations were amplified using NTA full-length entry vector as a template with previously published forward primers at NTA's start (Jones et al., 2017) with the following reverse primers: NTA450 R – GGGGACCACTTTGTACAAGAAAGCTGGGTG*CTCATCAAACACTGCTTTCTTC* and NTA481 R – GGGGACCACTTTGTACAAGAAAGCTGGGTG*TGAAACACCAAGTGTCTTGCT*. The NTAW458A point mutation was generated using the same NTA template and amplifying two fragments of NTA with desired point mutations introduced into the primers (bold): NTAW458A F – *GCATTGAAGAAG**GC**GCACAAAGACATCAAATTGAAGAAAG* + NTAstopR - GGGGACCACTTTGTACAAGAAAGCTGGGTG*AGAGTTGTGGAATTGCATCTC* and NTAstart F - GGGGACAAGTTTGTACAAAAAAGCAGGCTTCACC*ATGATCACAAGAAGCAGGTGT* + NTAW458A R – *C**GC**CTTCTTCAATGCCTTTGCCAT*. The two fragments were purified and pasted together with overlaps using a PCR-pasting protocol. The coding sequence from both truncations and the point mutation were fully sequenced in entry vectors. All entries were then recombined via LR reactions into the pMDC83 backbone

with the $MYB98_{pro}$ (Muller et al., 2016) to drive expression of each NTA variant in synergid cells with a C-terminal GFP fusion.

Constructs for interaction assays were generated using the NTA, MLO8, NTA W458A entry vectors described above and previously published (Jones et al., 2017). Additionally AtCaM1 (AT5G37780) was amplified from cDNA derived from rosette leaves and flowers. CaM1 was cloned in a two-step process to ensure specificity. Primers for 5' and 3' UTRs were used first (CaM1_F – *AAAGAGAGACGACTCTGAATCC* + CaM1_R – *CCCAACCCATCGGTTTCAATC*) and the PCR product was purified and used as a template to be amplified from the start of the gene to the stop codon with attB sites for Gateway cloning (CaM_F – GGGGACAAGTTTGTACAAAAAAGCAGGCTTCACC*ATGGCGGATCAGCTCACAGA* + CaM_R – GGGGACCACTTTGTACAAGAAAGCTGGGTG*TCACTTAGCCATCATAATCTTGACA AAC*). AtCaM1 was purified and recombined via BP reaction into pDONR207. For FRET, entries were recombined into Gateway-compatible destination vectors with C-terminal Cer3 and YFP-HA (NTA W458A) and N-terminal YFP (AtCaM1) fusions (Myers et al., 2016). For Co-immunoprecipitation (Co-IP), AtCaM1 entry was recombined into pEarlyGate203 via LR for the N-terminal Myc tag fusion.

For *nta-1* complementation assay and co-localization analyses, expression vectors were transformed into the *Agrobacterium tumefaciens* strain GV3101 and transformed into the *nta-1* mutant background or the Col-0 background (co-localization – Col-0 was stably expressing the Golgi or TGN synergid secretory markers) via the floral-dip method (Bent, 2006). Stable transgenic lines were selected using their respective selections described above. Homozygous T2 lines were used in *nta-1*

complementation assay and co-localization imaging in the synergid was done in a T1 analysis.

nta-1 Complementation Assays

3-4 independent insertion lines for each construct were taken to the T2 generation and screened for homozygosity using fluorescence microscopy to ensure transgene expression in synergids of every ovule. Unfertilized vs. fertilized ovule counts from self-pollinated flowers were assessed in at least three plants of each insertion line and compared to *nta-1*, Wassilewskija (Ws-2; wildtype), and the previously published full-length NTA ($MYB98_{pro}$::NTA-GFP in *nta-1* background, (Jones et al., 2017)). Ovule counts were statistically analyzed using Prism (www.graphpad.com) with significance determined using Analysis of Variance (ANOVA) and Dunnett's multiple comparison test. Comparisons of the NTA variants were made to full-length NTA and the *nta-1* mutant.

Transient Expression in *N. benthamiana*

Leaves from 3-4 week old *N. benthamiana* were co-infiltrated with *A. tumefaciens* strain GV3101 harboring Cer3, YFP or Myc-fused proteins for analysis via FRET or Co-IP. Each infiltration set was additionally co-infiltrated with *A. tumefaciens* strain C58C1 containing the viral silencing suppressor helper complex pCH32 (Hamilton, 1997). Overnight cultures were centrifuged for 5 min at 4000*g* and resuspended and washed in 10mM $MgCl_2$ twice. A final suspension of each *Agrobacterium* in 10mM $MgCl_2$ was then co-infiltrated into the leaf. Plants were maintained at ambient temperatures and leaves were used 3-4 days after infiltration.

Microscopy and FRET Assay

To assess GFP distribution in synergid cells, ovules from flowers of NTA full-length and NTA variant stable T2 lines were imaged 2 days after emasculation. Ovules were dissected out retained on the septum then incubated in 20μM FM464 (Molecular Probes, T3166) in PIPES Buffer (50mM PIPES, 5mM EGTA and 1mM $MgSO_4$ at pH = 6.8) for 10 min on ice labeling plasma membranes for imaging. CLSM was done using a Leica SP8 confocal microscope with an HC PL APO 40× water immersion objective (NA = 1.10). GFP excitation was done with a 488nm argon laser and FM464 excitation with a 561nm diode laser. Fluorescent signals were detected using two HyD detectors in counting mode set to detect GFP and FM464 individually and excitation/emission of the two fluorophores was done sequentially. Co-localization with secretory markers and detection of GFP distribution after PT reception were imaged with similar settings on the SP8 but with more narrow detection windows for mCherry and DsRed signals. These ovules were dissected out, retained on the septum and imaged in PIPES Buffer. For analysis following PT reception, 2 day old emasculated flowers were hand pollinated with the pollen expressing the pollen specific promoter $ACA9_{pro}$::DsRed (Francis et al., 2007) and placed back into the grow room for 4-6hrs prior to dissection and imaging.

The FRET-based interaction assay was done similar to a previous study (Jones et al., 2017). Leaf discs from *N. benthamiana*, infiltrated with the respective protein combinations, were incubated in PIPES Buffer with 20μg/mL Cytochalasin B (Sigma-Aldrich, C6762) for 10min at ambient temperatures to stop trafficking of endomembrane associated compartments. The donor/acceptor pair mCerulean3 (Cer3) (Markwardt et al., 2011) and YFP were used in this experiment. Epidermal cells

co-expressing the proteins to be assayed were imaged prior to photobleaching and after each round of subsequent photobleaching (3 rounds total). YFP (acceptor) was bleached for 5 sec with the argon laser at 514nm at high intensity. Fluorescent data gathered during imaging was analyzed using a custom macro in Fiji (Schindelin et al., 2012). mCer3 and YFP signals were graphed and compared using a Pearson product-moment correlation coefficient. Differences in correlation coefficients between protein pairs were statistically compared using the non-parametric Kruskal-Wallis test with multiple comparisons corrected using the Dunn Test. FRET statistics were all done in R, version 3.1.2 (Team, 2014) with the packages dplyr (Wickham and Francois, 2015) and DescTools (Signorell, 2015).

Co-Immunoprecipitation and Western Blot

Total protein was extracted from infiltrated *N. benthamiana* leaves by grinding whole leaves (from three different infiltrations) in liquid nitrogen and suspending in non-denaturing lysis buffer (100mM Tis-HCl pH-7.5, 150nM NaCl, 5mM EDTA, 10mM 2-mercaptoethanol, 10% glycerol, 0.1% Triton X-100) (Popescu et al., 2007) supplemented with fresh 5mM DTT, 1x plant protease inhibitor cocktail (0.2mM AEBSF - GoldBio #A-5440-500, 0.7μM Bestatin - A.G. Scientific #B1075, 0.7μM Pepstatin A - Sigma #P4265, 10μM Leupeptin - A.G. Scientific #L-1165, 1.4μM E-64 - A.G. Scientific #E2030, 1.4μM Phenanthroline - Sigma #P9375) and 10mM $CaCl_2$. 800μg of total protein was incubated with anti-HA magnetic beads (μMACS, HA Isolation Kit – Miltenyi 130-091-122) and HA tagged proteins were immunoprecipitated using magnetic columns (μ Columns – Miltenyi 130-042-701). Input and IP samples were visualized using standard SDS-PAGE methods (12% gel). Western blot detection was performed after protein was transferred to a PDVF membrane (Hybond-P, GE Healthcare/Amersham Biosciences, cat# RPN2020F). HA-conjugated proteins were

detected using high affinity anti-HA primary antibody (Roche - 11 867 423 001) and goat anti-rat secondary antibody (Santa Cruz - SC-2032). Myc-conjugated proteins were detected using anti-Myc primary antibody (Abcam – ab9106) and goat anti-rabbit secondary antibody (Abcam – ab205718). All secondary anitbodies conjugated to horseradish peroxidase were visualized using ECL Plus Reagent (GE Healthcare/Amersham - cat# RPN2132) and imaged with a Bio-Rad ChemiDoc XRS imaging system.

Figure Construction and Image Processing

Figures were all constructed using Gimp v. 2.8.14. Graphs were generated using Prism (www.graphpad.com) and diagrams made with Inkscape v0.91. All images were processed and edited in Fiji (Schindelin et al., 2012).

Figures

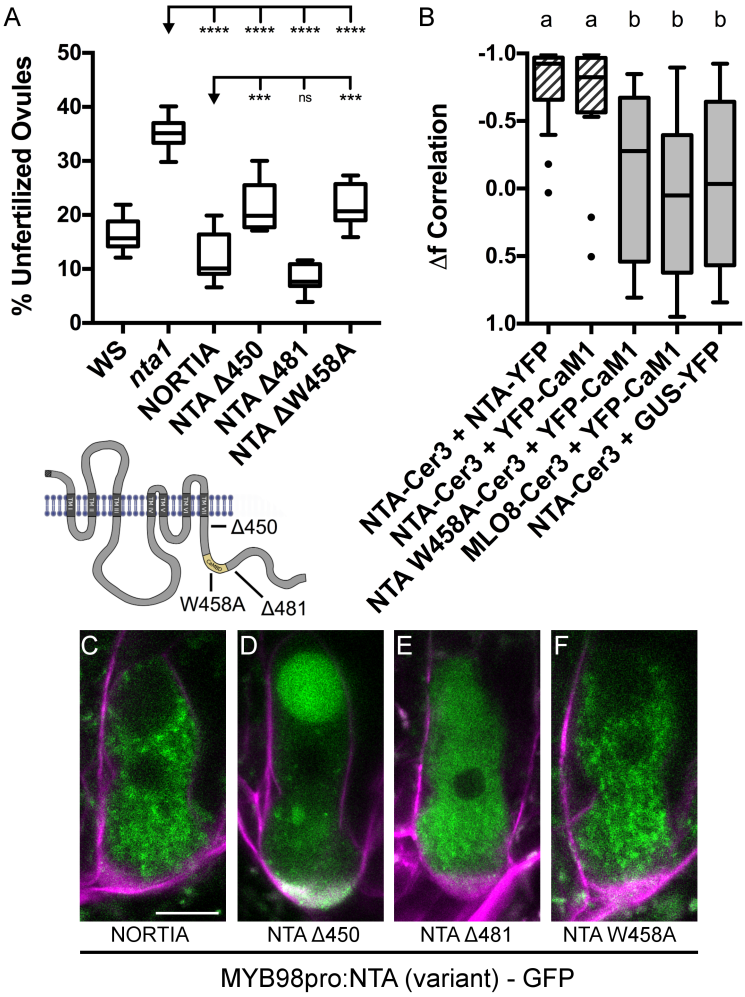

Figure 5.1 - Analysis of NTA variants expressed in synergids of *nta-1*
A) Unfertilized ovule counts in T2 plants homozygous for *MYB98*$_{pro}$*:NTA(variant)-GFP* constructs in *nta-1* mutants. WS, Wassilewskija. B) Detection of AtCaM1 interaction with MLO constructs via FRET analysis. Box plots show the correlation coefficients from FRET analysis of MLOs, AtCaM1, and GUS. Groupings of "a" and "b" are based on significant differences between each distribution as determined using the Kruskal-Wallis test. C-F) NTA(variant)-GFP (green) distribution in synergid cells of unfertilized ovules merged with FM464 (magenta). Bars = 10 μm. Adjusted P values are as follows: **** = P < 0.0001; ***, P = 0.001 to 0.0001; and n.s. = P > 0.05.

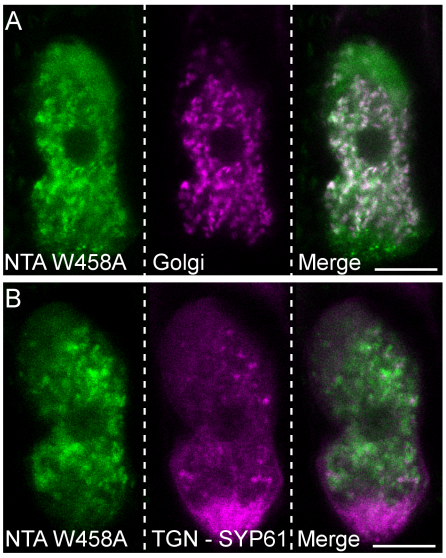

Figure 5.2 - NTA W458A co-localization with Golgi and TGN makers in synergid cells Colocalization of NTA W458A-GFP (green) with: A) Golgi (*LRE:*$_{pro}$*Man49-mCherry*), B) trans-Golgi network (TGN, *MYB98*$_{pro}$*:SYP61:mCherry*) markers (magenta) in the synergid cell of unpollinated ovules. Bars = 10 µm.

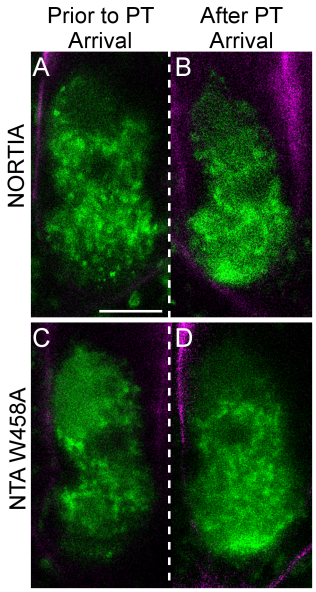

Figure 5.3 – NORTIA and NTA W458A distribution in the synergid at PT arrival NTA-GFP (green) distribution in synergid cells of the same pollinated pistil prior to PT arrival (A) and at PT arrival (B). NTA W458A-GFP (green) distribution in synergid cells of the same pollinated pistil prior to PT arrival (C) and at PT arrival (D). Pollen from the *ACA9*$_{pro}$*:DsRed* PT marker line was used to pollinate emasculated flowers and imaging was done 4-6hrs after pollination. Bar = 10 µm.

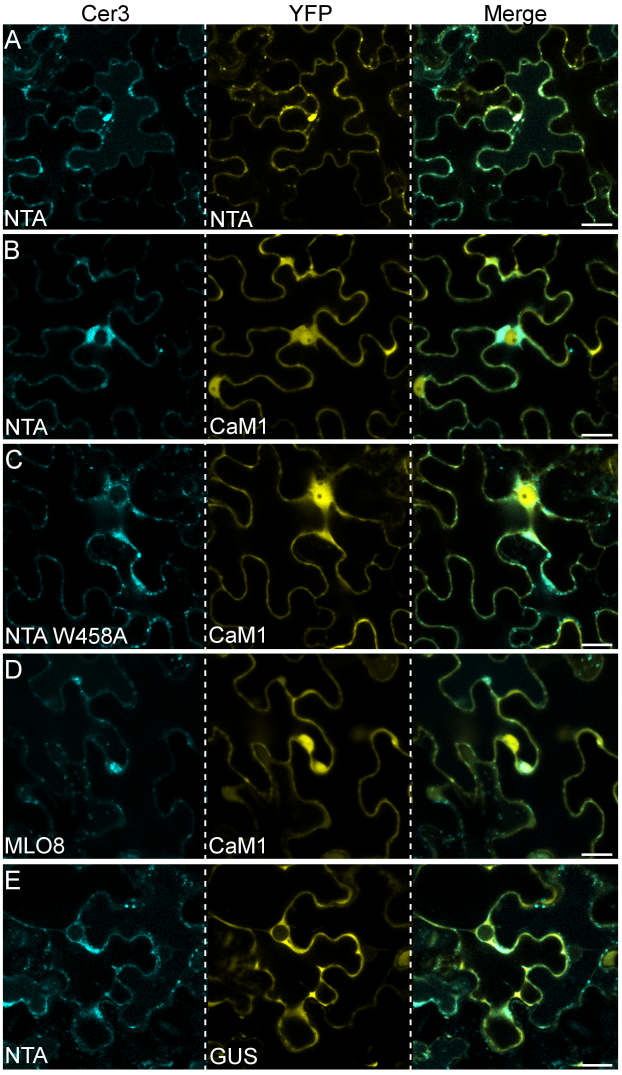

Supplemental Figure 5.1 – Transient expression of MLOs and AtCaM1 in *N. benthamiana* epidermal cells for FRET interaction assay. Epidermal cells with MLO-Cer3 co-localized with NTA-YFP, YFP-AtCaM1, or GUS-YFP for analysis in FRET-based assay (see methods). A) NTA-Cer3 (cyan) + NTA-YFP (yellow). B) NTA-Cer3 (cyan) + YFP-AtCaM1 (yellow). C) NTA W458A-Cer3 (cyan) + YFP-AtCaM1 (yellow). D) MLO8-Cer3 (cyan) + YFP-AtCaM1 (yellow). E) NTA-Cer3 (cyan) + GUS-YFP (yellow). Bars = 20 µm.

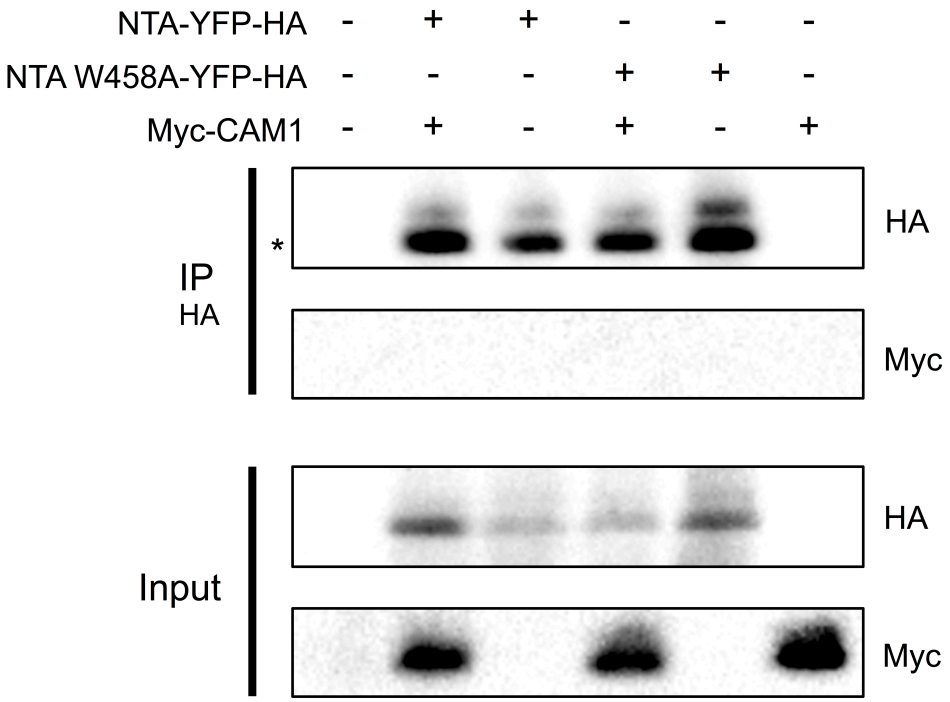

Supplemental Figure 5.2 – Co-IP assay to detect interaction between NTA and AtCaM1. NTA-YFP-HA and NTA W458A-YFP-HA were transiently co-expressed with Myc-CaM1 in tobacco epidermal cells. Extracted protein was incubated with anti-HA magnetic beads, pulled-down on a column and the IP and input samples were analyzed via western blot analysis to detect protein-protein interactions.

Chapter 6: Clade III MLO expression in ovules: regulatory elements in intragenic regions of NTA and the initial characterization of MLO overexpression lines

Daniel S. Jones[1], Arianna J. Dino[1], Thomas C. Davis[2,3], Sharon A. Kessler[2,3]

[1]Department of Microbiology and Plant Biology, The University of Oklahoma, Norman, OK 73069, USA
[2]Department of Botany and Plant Pathology, Purdue University, West Lafayette, IN 47907, USA
[3]Center for Plant Biology, Purdue University, West Lafayette, IN 47907, USA

Part of this chapter was published in *Plant Reproduction*.

Davis, T. C., Jones, D. S., Dino, A. J., Cejda, N. I., Yuan, J., Willoughby, A. C., & Kessler, S. A. (2017). Arabidopsis thaliana MLO Genes Are Expressed in Discrete Domains During Reproductive Development. *Plant Reproduction,* 30 (4), 185-195.

Contributions

Arianna J. Dino cloned NTA_{pro}::NTA_{gDNA}-GUS truncation constructs and generated the stable lines used in Figs. 6.1 and 6.2. Thomas C. Davis cloned the NTA_{pro}::NTA_{cDNA}-GUS fusion used in Fig. 6.3.

Summary

In *Arabidopsis thaliana* the MILDEW RESISTANCE LOCUS O (MLO) protein family, comprised of 15 members, plays roles in diverse cell-cell communication processes such as powdery mildew susceptibility, root thigmomorphogenesis, and pollen tube reception. *NORTIA* (*NTA*) is expressed in the synergid cells of the female gametophyte where it functions in intercellular communication with the pollen tube. Discrepancies between previously published promoter::GUS and promoter::gene-GUS construct expression patterns led us to explore the regulation of *NTA*'s expression. Here we found that sequences within *NTA*'s intragenic regions negatively regulate its expression in the stomata and carpel walls. MLO_{pro}*::MLO-GUS* constructs for all 15 MLOs were then examined focusing specifically on expression in ovules to determine if other MLOs could play a role in reproductive cell-cell communication in this tissue. GUS/GFP MLO10 and MLO8 native promoter constructs were further characterized to determine their expression patterns during ovule development. This revealed differential expression and patterning of these two closely related MLOs in early (MLO10) and late (MLO8) ovule development. Stable overexpression lines of select MLOs were generated and characterized in *A. thaliana* (Col-0 ecotype) to determine their effect on overall plant development.

Results and Discussion

Regulation of NTA's tissue-specific expression requires suppressor elements in the coding sequence

The regulation of *NTA*'s expression in synergid cells was previously shown to require the introns and coding sequence of the gene (Kessler et al., 2010). NTA_{pro}::gNTA-GUS (gNTA refers to NTA's genomic DNA sequence including introns and exons) was detected specifically in the synergid cells of the mature female gametophyte, an expression pattern agreeing with *nta-1*'s female-specific defect during pollen tube (PT) reception (Kessler et al., 2010). Under the same upstream promoter, NTA_{pro}::gNTA-GFP was shown to rescue the *nta-1* mutant phenotype (Kessler et al., 2010), demonstrating the biological relevance of this expression pattern. This is in contrast to an earlier study utilizing promoter-only GUS constructs, which had a pollen specific expression pattern (Chen et al., 2006). Taken together, these data suggest the presence of regulatory elements within *NTA*'s genomic sequence.

To further define the presence of regulatory elements, truncated genomic-GUS fusions expressed under *NTA*'s native promoter were compared to the reported *NTA* full length and promoter-only GUS constructs in mature flowers (Fig. 6.1). As previously demonstrated, NTA_{pro}::gNTA-GUS expression was only detected in the synergids of mature flowers (Fig. 6.1b-e). Removing the 3' end of *NTA* up to the tenth exon (NTA_{pro}::gNTAexon10-GUS) had no detectable effect on this specificity (Fig. 6.1f-i). Further truncation up to the fourth exon (NTA_{pro}::gNTAexon4-GUS) expanded *NTA*'s expression domain to guard cells in the sepals of the mature flower as well as synergids (Fig. 6.1j-m; seen in 5/8 T1 lines analyzed). In contrast to the pollen expression pattern previously reported (Chen et al., 2006), our promoter only constructs (NTA_{pro}::GUS) had an expanded expression domain with GUS detected

within carpel walls, sepal guard cells and in synergid cells (Fig. 6.1n-q; seen in 3/4 T1 lines analyzed). No expression was detected in pollen with any of the truncated NTA constructs used in this study (Fig. 6.1b, f, j, n). While this differs from the previous study utilizing the same *NTA* native promoter reported here (Chen et al., 2006), the consistent detection of our truncated NTA constructs in similar tissues, compared with each other, lends support to our analysis. Additionally, there was similar variability in the expression patterns of independent insertion lines of both NTA_{pro}::gNTAexon4-GUS and NTA_{pro}::GUS. Three out of eight NTA_{pro}::gNTAexon4-GUS lines and one out of four of NTA_{pro}::GUS T1 lines analyzed had expanded expression domains of the same pattern within the mature flower; with GUS detected throughout the pistil, filaments, the pedicel, and synergid cells but in contrast to their other expression pattern, not in sepal guard cells (Fig. 6.2).

These data suggest that either a repressive regulatory element exists within the genomic context of *NTA* (between the fourth and tenth exons) or that *NTA* is post-transcriptionally regulated within these tissues. In order to differentiate between these possibilities, we generated a GUS fusion construct with the *NTA* cDNA expressed under its own promoter (NTA_{pro}::NTAcDNA-GUS) as well as GFP fusion constructs of *NTA* cDNA expressed under promoters of the genes *FERONIA* (*FER*) and *MYB98* (two characterized genes that are expressed in the synergids of *Arabidopsis*) (Kasahara et al., 2005; Escobar-Restrepo et al., 2007). However, out of 14 independent NTA_{pro}::NTAcDNA-GUS T1 lines analyzed, no tissue-level GUS expression was detected (Fig. 6.3b-e) indicating that the *NTA* cDNA sequence may have a negative effect on NTA_{pro} or that this construct is sensitive to silencing by epigenetic mechanisms. In contrast, GFP fusions of NTA cDNA expressed under the promoters of *FER* and *MYB98* (FER_{pro}::NTAcDNA-GFP and $MYB98_{pro}$::NTAcDNA-GFP,

respectively) were both readily detected in synergid cells (Fig. 6.3f-g), indicating that the negative effects of the *NTA* cDNA are specific to the NTA_{pro} construct. Thus, regulation of *NTA* under its native promoter likely requires regulatory elements within *NTA*'s genomic sequence for both promoting and limiting expression to synergid cells.

Expression of MLO10 and MLO8 in developing ovules

Previous analyses of MLO proteins have found redundant roles for phylogenetically related MLOs in both powdery mildew susceptibility (MLO2, 6, 12) and in root thigmomorphogenesis (MLO4, 11) (Consonni et al., 2006; Chen et al., 2009). In contrast, *NTA* is the only *MLO* expressed in the synergid cells and is hypothesized to be the only MLO with a role in PT reception (Jones et al., 2017). *NTA*, *MLO10*, *MLO8, MLO5, and MLO9* are the five MLOs that make up clade III in *A. thaliana*, a clade found in all flowering plants but noticeably absent in lower plants analyzed (Kusch et al., 2016). Thus other clade III MLOs could have different roles, aside from PT reception, in reproductive development and signaling. The two most closely related MLOs to NTA (MLO10 and MLO8) are both expressed in mature ovules (Jones et al., 2017). *MLO10* is expressed in the chalazal end of the ovule near the funiculus (the tissue that supports the ovule within the carpel) and *MLO8* is expressed in the inner integuments around the micropyle (the opening of the ovule where the PT is first received) (Jones et al., 2017). Expression of these *MLO*s in the ovule may represent a yet undescribed role in reproductive development and signaling.

Female gametophytic development relies on cell-cell communication within sporophytic tissues to enable the specification and subsequent development of the female gametophyte (Chevalier et al., 2011; Tucker and Koltunow, 2014). MLO-mediated communication may play a pivotal role during this process. Development initiates within

an ovule primordium with the differentiation of the megaspore mother cell (MMC). The MMC undergoes meiosis to produce four megaspores in a process called megasporogenesis. Three megaspores degenerate while the most chalazal (at the "bottom" of the primordium) is specified as the functional megaspore (FM), which goes through three mitotic divisions giving rise to the cells of the female gametophyte in a process called megagametogenesis. Around the time of megasporogenesis, inner and outer integuments initiate at the base of the ovule primordium and elongate. The integument layers eventually wrap all the way around the nucellus and completely enclose the female gametophyte during its later stages of development (developmental staging of *A. thaliana* ovules as defined in (Robinson-Beers et al., 1992)). To further define expression patterns of *MLO10* and *MLO8* within this developmental process, native promoter GUS/GFP constructs for MLO10 and MLO8 were analyzed throughout ovule development.

$MLO10_{pro}$::MLO10-GUS was detected early in ovule development, stage 10 (MMC differentiation), around the MMC and in the chalazal regions of the ovule primordium (Fig. 6.4A). In stage 11 ovules (following megasporogenesis), expression was also detected around the FM and expression in the chalazal end of the ovule persisted (Fig. 6.4B). Throughout the rest of ovule development, *MLO10* expression appeared limited to the chalazal end of the ovule near the funiculus as noted previously (Fig. 6.4 C-D; (Jones et al., 2017)). Expression of *MLO10* in stage 10 ovules was also detected in $MLO10_{pro}$::MLO10-GFP lines revealing its distribution within cells immediately surrounding the MMC (Fig. 6.5). MLO10's expression pattern does not indicate it would play a role in either PT attraction or reception. However it does suggest that it could function early in reproductive signaling during the transition to gametophytic development, as it is present in sporophytic tissues immediately surrounding the MMC.

$MLO8_{pro}$::MLO8-GUS was expressed during ovule development as early as stage 11 with GUS detected in the nucellus of the ovule toward the micropylar end near the degenerating megaspores and FM (Fig. 6.4F). In early stage 12 ovules, *MLO8* expression was still present in the nucellus near the micropylar end of the of the ovule, but expression was also detected in the inner integuments (Fig. 6.4G). By maturity, MLO8-GUS became limited to the inner integuments of the ovule immediately surrounding the micropyle, the site of PT entry (Fig. 6.4H). This shift of *MLO8* expression from the nucellus of the ovule (around the developing female gametophyte) to the inner integuments was also detected in $MLO8_{pro}$::MLO8-GFP lines (Fig. 6.6). The distribution of MLO8 at the micropyle of the ovule indicates that it could play some role in mediating communication with the PT during PT arrival or reception. To explore its expression pattern immediately following PT reception, $MLO8_{pro}$::MLO8-GFP expressing flowers were hand pollinated with pollen from Col-0 plants expressing the PT marker $ACA9_{pro}$::DsRed (Francis et al., 2007) and imaged 6 hours after pollination (Fig. 6.7). There was a marked decrease in MLO8-GFP outside the micropyle following successful PT reception (Fig. 6.7B). Interestingly, as previously noted (Jones et al., 2017), MLO8-GFP was also occasionally detected (~3-4 ovules per flower) directly outside the filiform apparatus of the synergid cell in mature ovules from flowers 2d post-emasculation (Fig. 6.8). Since no expression was ever detected within the synergid, this could represent residual MLO8 from the degeneration of the nucellus immediately outside the female gametophyte or the export of MLO8 out of inner integument cells into the apoplast of the micropyle. Overall, MLO8 expression data reveal its accumulation throughout ovule development, immediately surrounding the micropyle at maturity (occasionally at the filiform apparatus), and a drastic decrease

following successful PT reception. These data suggest MLO8 could play a role in reproductive signaling either during ovule development, PT arrival/reception, or both.

Stable overexpression of select MLOs in *A. thaliana*

With no verified mutants available for MLO10 or MLO8, characterization of their native function remains difficult. In an attempt to understand what these proteins do within the plant, I looked at the effect of overexpressing MLOs on overall development in *A. thaliana*. A previous study found that overexpression of wildtype barley MLO led to a super-susceptibility phenotype after infection with powdery mildew but had no pleiotropic effects on leaf morphology (Kim et al., 2002). However, in these experiments, the overexpression of MLOs was only explored in transient expression assays and never in stable transgenic lines. I generated stable $35S_{pro}$::MLO-YFP-HA overexpression lines of NTA, MLO10, and MLO8 (closely related Clade III MLOs) and compared them to overexpression lines of MLO1 (Clade I) and the wildtype (Col-0) background to determine general growth and developmental defects. Expression/accumulation of each MLO-YFP construct was verified in rosette leaf epidermal cells and phenotypes from 3 independent insertion lines were analyzed (Fig. 6.9). MLO1 differs from the other three MLOs in that it localizes primarily to the epidermal cell periphery instead of within endomembrane-associated compartments (Figs. 6.9) (Jones and Kessler, 2017). Overall plant development in both $35s_{pro}$::MLO1-YFP-HA and $35s_{pro}$::NTA-YFP-HA did not appear to be different from the WT control (Fig. 6.10) and there was no quantitative effect correlated with protein accumulation among the three $35s_{pro}$::NTA-YFP-HA T1 lines (Fig. 6.11). In contrast, $35s_{pro}$::MLO10-YFP-HA plants were all stunted in growth and had severely reduced fertility (Fig. 6.12). Out of the three $35s_{pro}$::MLO8-YFP-HA lines analyzed, two had extreme pleiotropic effects, and one appeared similar to the WT control (Fig. 6.13). These phenotypes

correlated well with protein accumulation, with the two stunted lines having much higher amounts of MLO8-YFP-HA in comparison to the third WT-like line (Fig. 6.13). Additionally, $35s_{pro}$::MLO8-YFP-HA lines with higher protein accumulation also had reduced fertility, similar to that seen in MLO10.

In order to determine if the fertility defects observed in MLO10 and MLO8 overexpression lines was due to developmental defects in the male gametophyte, and thus unsuccessful pollination, aniline blue staining of PTs in flowers 2d after pollination was used to assess PT entry into the stigma and growth down the transmitting tract. Pollen grains successfully germinated on the stigma of self-pollinated flowers and PTs grew into the style of all flowers analyzed (Fig. 6.14). Aniline blue fluorescently labels callose, a cell wall component predominantly found in the PT (Martin, 1959). Interestingly, flowers of MLO10 and MLO8 lines with high levels of overexpression had ectopic callose accumulation compared to WT flowers (Fig. 6.15). In $35S_{pro}$::MLO8 lines, callose accumulated in the carpel walls of the flower, in the chalazal end of the ovules and in random cells within the pedicel of the flower (Fig. 6.15D-F). $35S_{pro}$::MLO10 plants also accumulated callose in the carpel, but, in contrast to the MLO8 flowers, it was more associated with the transmitting tract at the center of the pistil than in the carpel walls (Fig. 6.15G). MLO10 overexpressers had little to no additional callose in mature ovules but did have random accumulations in the cells of the pedicel similar to MLO8 overexpression lines (Fig. 6.15H-I). It is unclear if the additional accumulations of callose are a direct result of too much MLO protein within these tissues or is a symptom of other pleiotropic effects, as abundance of callose is linked to stress responses and senescence. Ectopic deposition of callose has been more closely associated with *mlo* mutants in the past (Consonni et al., 2006), and more specifically with *mlo*-mediated resistance to powdery mildew infection (Skou, 1982). It

is interesting then to see such increases in callose within MLO overexpression lines; however, more experiments are necessary to determine if a causal relationship exists between overproduction of MLO proteins and callose deposition.

Methods and Materials

Plant growth Conditions

Arabidopsis thaliana Columbia ecotype (Col-0) seeds were surface sterilized by soaking for 10 minutes in a 3% bleach/0.01% Triton solution followed by three washes with sterile water. The seeds were then plated on ½ MS media and stratified in the dark at 4°C for 2 days. Seeds were germinated on MS media containing 20 μg/L of hygromycin for selection of the GUS transgenes. Plates were transferred to a custom built grow room with 16 hr light/8 hr dark at 22°C. 6-day old seedlings were transplanted to 20:20:20 (NPK) supplemented ProMix PDX soil and grown to. Overexpression lines (*$35S_{pro}$::MLO-YFP-HA*) were sown directly on soil, cold-stratified for 2 days at 4°C, and then moved to the same grow room as above. 5d old seedlings were sprayed with BASTA herbicide or 3 subsequent days and resistant plants were maintained through flowering and analyzed.

Generation of GUS fusion constructs

MLO_{pro}::genomic MLO-GUS/GFP constructs for NTA, MLO8, and MLO10 were previously reported (Kessler et al., 2010; Jones et al., 2017). MLO_{pro}::MLO8-GFP-HDEL was generated via LR recombination of the previously described MLO8 genomic construct (Jones et al., 2017) into pMDC204 (Curtis, 2003).

Staining and Microscopy

Tissues were collected from flowering plants and fixed in 90% acetone for 40 minutes at -20 °C. Following fixation, the samples were rinsed 3 times with phosphate buffer (100 mM, pH 7.2) and vacuum infiltrated with GUS staining solution (0.1% Triton X-100, 10 mM EDTA, 2 mM Ferrocyanide, 2 mM Ferricyanide, 100 mM sodium dibasic phosphate, 100 mM sodium monobasic phosphate, and 4 mM 5-bromo-4-chloro-3-indolyl-β-□-glucuronide) for 5 minutes. The tissues were then incubated at 37 °C until GUS stain was visible or up to 5 days. Stained tissues were incubated at room temperature overnight in 70% ethanol and stored at 4°C up to 2 days prior to imaging. Before imaging, the stained tissues were further cleared in Choral Hydrate Solution (8:2:1 (w/v/v) chloral hydrate: distilled water: glycerol). GUS staining patterns were visualized using a Nikon Eclipse NI-U compound microscope equipped with DIC optics and verified in at least three independent expression lines to reduce uncertainty of expression patterns caused by positional effects of the insert. For GFP distribution in ovules, developing and mature ovules were dissected out from young flowers, retained on the septum and mounted on a slide In PIPES Buffer (50mM PIPES, 5mM EGTA and 1mM $MgSO_4$ at pH = 6.8). Epifluorescent microscopy was done on a Nikon Eclipse NI-U compound microscope equipped with an X-Cite 120 LED fluorescent lamp and narrow band eGFP filter cube. CLSM was done on a Leica TCS SP8 CSLM using a HC PL APO 40× water immersion objective (NA = 1.10) with GFP excited with a 488nm argon laser and DsRed excited with a 561nm diode laser in sequential mode. Emission was detected using two HyD detectors set at appropriate wavelength fro GFP and DsRed and signal was gathered in photon counting mode.

Aniline Blue Staining

Pollinated flowers were fixed overnight in 9:1 ethanol:acetic acid at 4°C. Tissue was rehydrated in a gradual ethanol series (70%, 50%, 30% (v/v)) for 5 min each at room temp. Chloral Hydrate Solution was then added and tissues was incubated at 60°C for 5 min. Tissue was then washed in 0.1M phosphate buffer (pH-8) and incubated in 5N NaOH at 60°C for 5 min. Flowers were washed 2× in 0.1M phosphate buffer (pH-8) and then mounted on a slide in 0.1% Methyl Blue. Sampled were imaged on a Nikon Eclipse NI-U compound microscope equipped with an X-Cite 120 LED fluorescent lamp and DAPI filter cube.

Western Blots

Total protein was extracted from whole rosette leaves of *$35S_{pro}$::MLO-YFP-HA* lines. Protein extracted using quick lysis buffer (20mM Tis-HCl pH-8, 150nM NaCl, 1mM EDTA, 1% Triton X-100, 0.1%SDS) supplemented with fresh 5mM DTT, 1x plant protease inhibitor cocktail (see Chapter 5 methods).10µg of total protein was visualized using standard SDS-PAGE methods (12% gel). Western blot detection was performed after protein was transferred to a PDVF membrane (Hybond-P, GE Healthcare/Amersham Biosciences, cat# RPN2020F). MLO-YFP-HA proteins were detected using high affinity anti-HA primary antibody (Roche - 11 867 423 001) and goat anti-rat secondary antibody (Santa Cruz - SC-2032). Secondary antibody conjugated to horseradish peroxidase was visualized using ECL Plus Reagent (GE Healthcare/Amersham - cat# RPN2132) and imaged with a Bio-Rad ChemiDoc XRS imaging system.

Figures

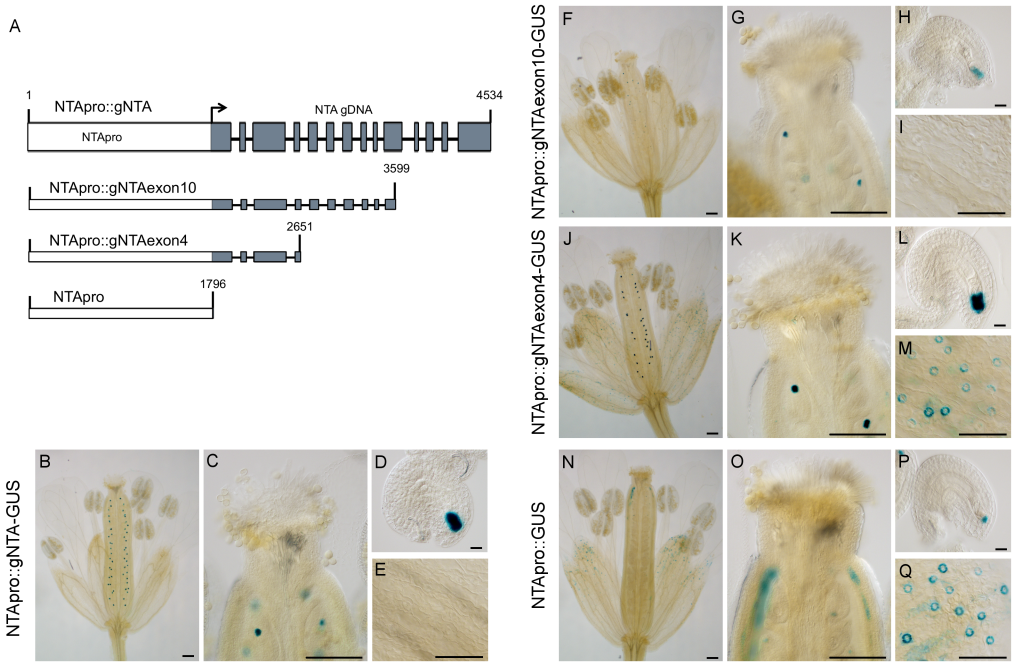

Figure 6.1 – Expression patterns of native promoter NTA genomic GUS constructs in flowers. A) Diagrams of the four NTA native promoter genomic GUS fusion constructs analyzed: full length (*NTA_{pro}::gNTA*), truncated at the tenth exon (*NTA_{pro}::gNTAexon10*), truncated at the fourth exon (*NTA_{pro}::gNTAexon4*), and promoter only (*NTA_{pro}*). GUS distribution of indicated constructs in mature flowers (B, F, J, and N), pollinated stigma (C, G, K, and O), unpollinated ovules (D, H, L, and P) and guard cells of sepals (E, I, M, and Q). Bars = 100μm (flowers - B, F, J, and N), 100μm (stigma - C, G, K, and O), 100μm (guard cells - E, I, M, and Q) and 10μm (ovules - D, H, L, and P)

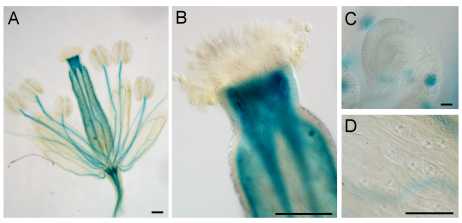

	Frequency in T1 lines
NTApro::GUS	1/4
NTApro::gNTAexon4-GUS	3/8

Figure 6.2 – Alternative NTA-GUS expression pattern in flowers. A-D) A less-common alternative GUS distribution observed with *NTA_{pro}::GUS* and *NTA_{pro}::gNTAexon4-GUS* constructs in the mature flower, pollinated stigma, unpollinated ovules and guard cells of sepals. Table indicates the frequency that this pattern was observed in a T1 analysis of both constructs. Bars = 100μm (A, B and D) and 10μm (C).

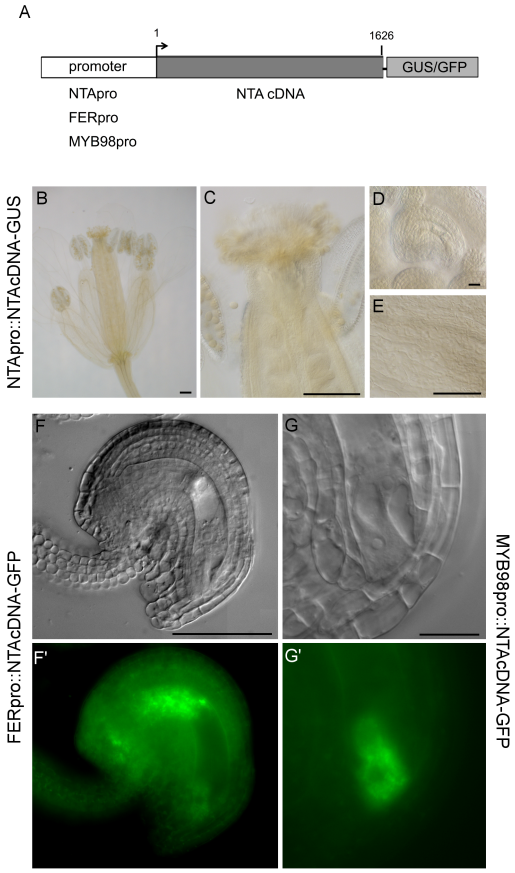

Figure 6.3 – NTA cDNA expression patterns under native and ectopic promoters. A) Diagram of the three NTA cDNA constructs analyzed: NTA-GUS under its native promoter (*NTA$_{pro}$::NTAcDNA-GUS*), NTA-GFP under FERONIA's promoter (*FER$_{pro}$::NTAcDNA-GFP*) and NTA-GFP under MYB98's promoter (*MYB98$_{pro}$::NTAcDNA-GFP*). B-E) *NTA$_{pro}$::NTAcDNA-GUS* distribution in the mature flower, pollinated stigma, unpollinated ovules and guard cells of sepals. F-F') *FER$_{pro}$::NTAcDNA-GFP* in an unpollinated ovule. G-G') *MYB98$_{pro}$::NTAcDNA-GFP* in the synergid cell of an unpollinated ovule. Bars = 100μm (B, C, and E), 50μm (F-F'), 20μm (G-G'), and 10μm (D).

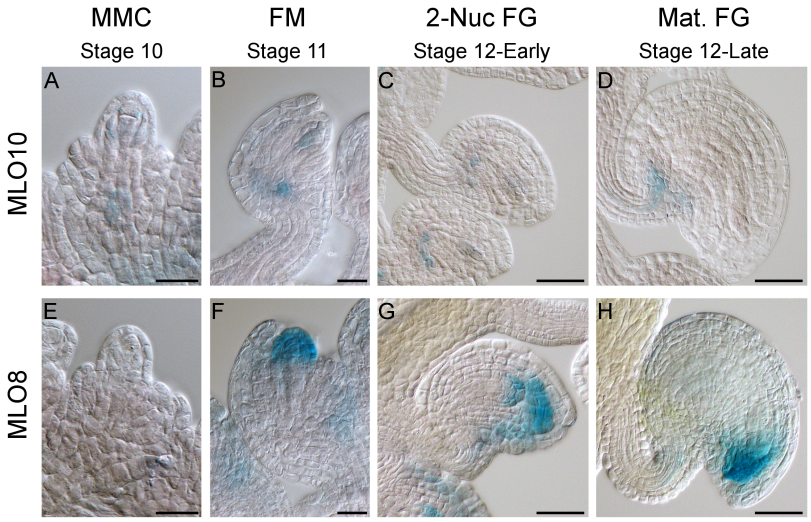

Figure 6.4 – Expression patterns of MLO10-GUS and MLO8-GUS under their native promoters throughout ovule development. A-D) *MLO10*$_{pro}$*::MLO10-GUS* expression in stage 10 (A), stage 11 (B) and stage 12 (C-D) ovules. E-H) *MLO8*$_{pro}$*::MLO8-GUS* expression in stage 10 (E), stage 11 (F) and stage 12 (G-H) ovules. MMC – megaspore mother cell, FM – functional megaspore, 2-Nuc FG – 2-nucleate female gametophyte, Mat FG – mature female gametophyte. Ovule stages based on (Robinson-Beers et al., 1992). Bars = 20μm (C-D, G-H), and 10μm (A-B, E-F).

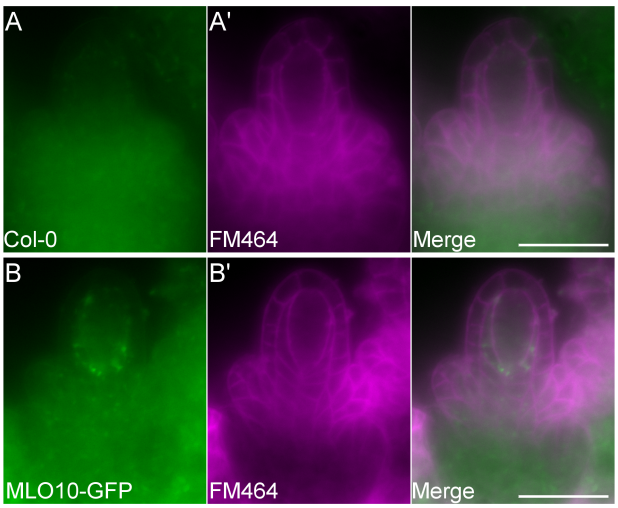

Figure 6.5 – MLO10-GFP expression in tissue surrounding megaspore mother cell. A) Autofluorescence (green) in GFP range from stage 10 Col-0 ovule labeled with FM464 (magenta) (A'). B) *MLO10*$_{pro}$*::MLO10-GFP* (green) expression in stage 10 ovule labeled with FM464 (magenta) (B'). Bars = 20µm.

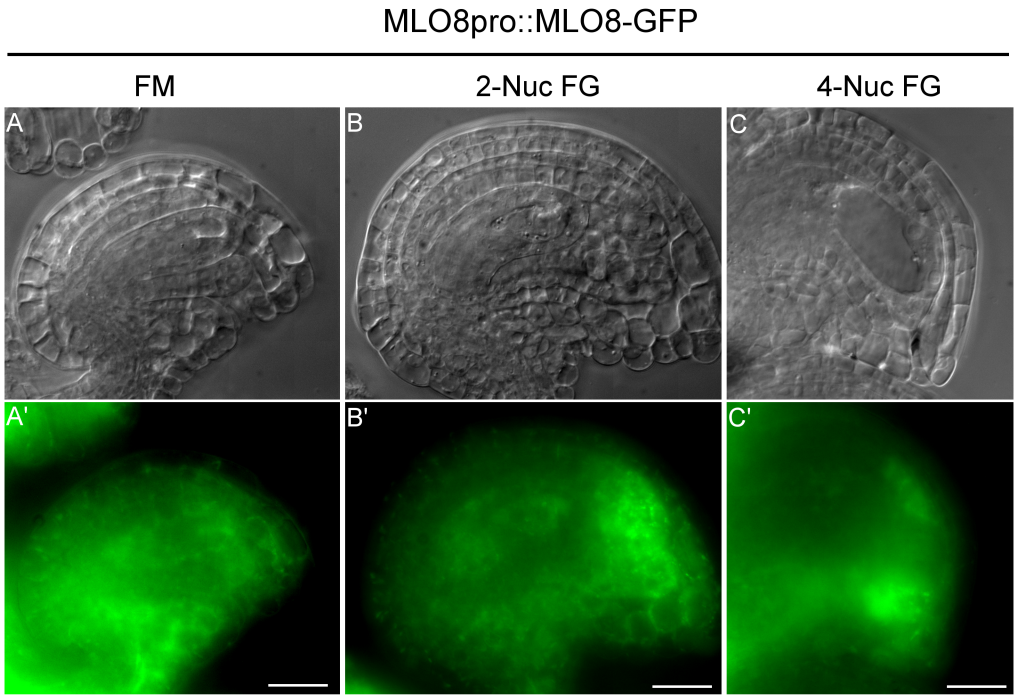

Figure 6.6 – MLO8-GFP expression in developing ovules. A, B, C) Differential Interference Contrast (DIC) of each ovule for staging and context. A',B',C') *MLO8$_{pro}$::MLO8-GFP* expression pattern in each ovule. A-A') stage11, B-B') stage 12 early, C-C') stage 12 mid developing ovules. FM – functional megaspore, 2-Nuc FG – 2-nucleate female gametophyte, 4-Nuc FG – 4-nucleate female gametophyte Bars = 20µm.

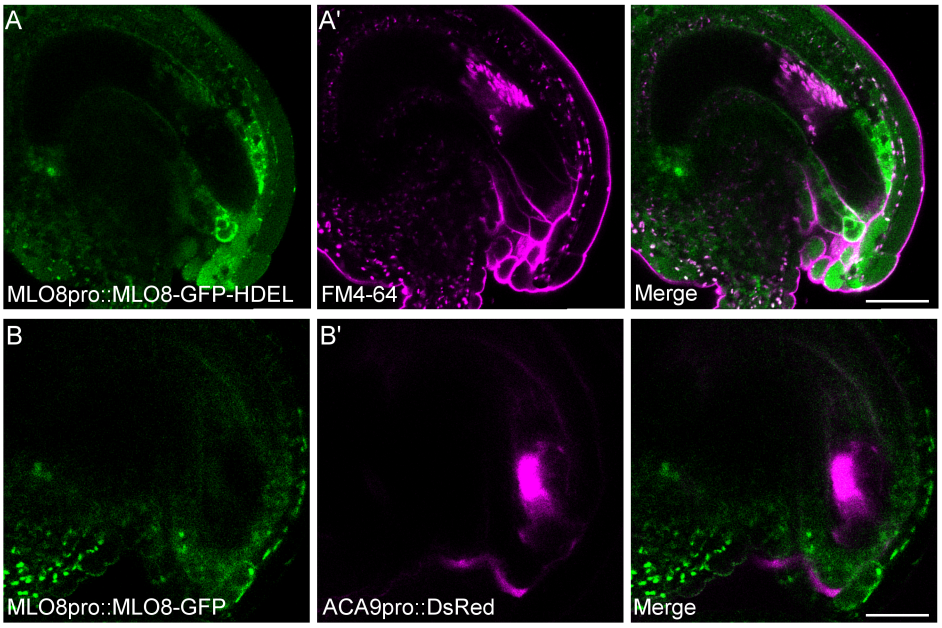

Figure 6.7 – MLO8-GFP expression in following PT reception. A-A') Mature ovule expressing *MLO8$_{pro}$::MLO8-GFP-HDEL* labeled with FM464 (membrane label - magenta) showing the accumulation of MLO8-GFP in the inner integuments of the ovule around the micropyle. B-B') *MLO8$_{pro}$::MLO8-GFP* expression pattern in an ovule after PT reception. *ACA9$_{pro}$::DsRed* PT marker line used to show successful reception of the PT 6 hrs after pollination. MLO8-GFP drastically decreases in inner integuments following PT reception. Bars = 20µm.

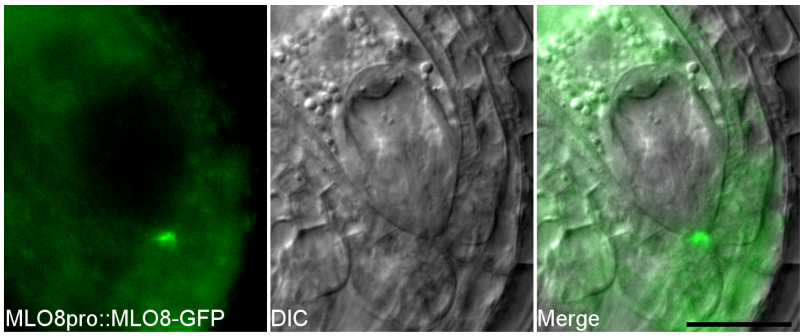

Figure 6.8 – MLO8-GFP accumulation at the filiform apparatus in mature ovules. *MLO8$_{pro}$::MLO8-GFP* detected right outside the synergid cell closely associated with the filiform apparatus in around 3-4 ovules per flower. Bar = 20µm.

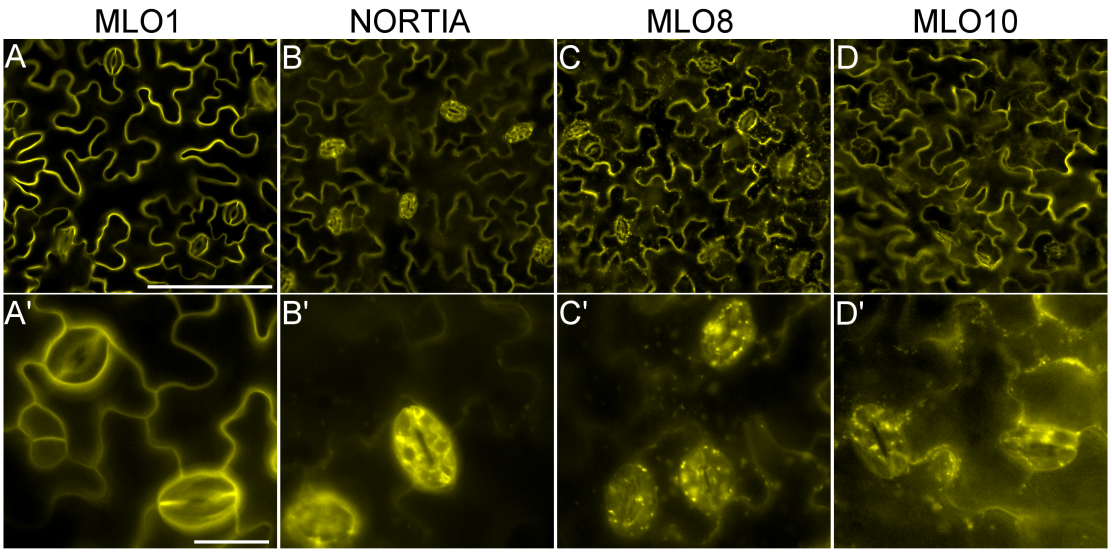

Figure 6.9 – *35S$_{pro}$::MLO-YFP* localization in epidermal cells of *A. thaliana*. A-A') MLO1 localizes primarily to the periphery of epidermal cells. B-D) Clade III MLOs localize within endomembrane-associated compartments of epidermal cells: B-B') NORTIA, C-C') MLO8, D-D') MLO10. Bars = A-D) 100µm; A'-D') 20µm.

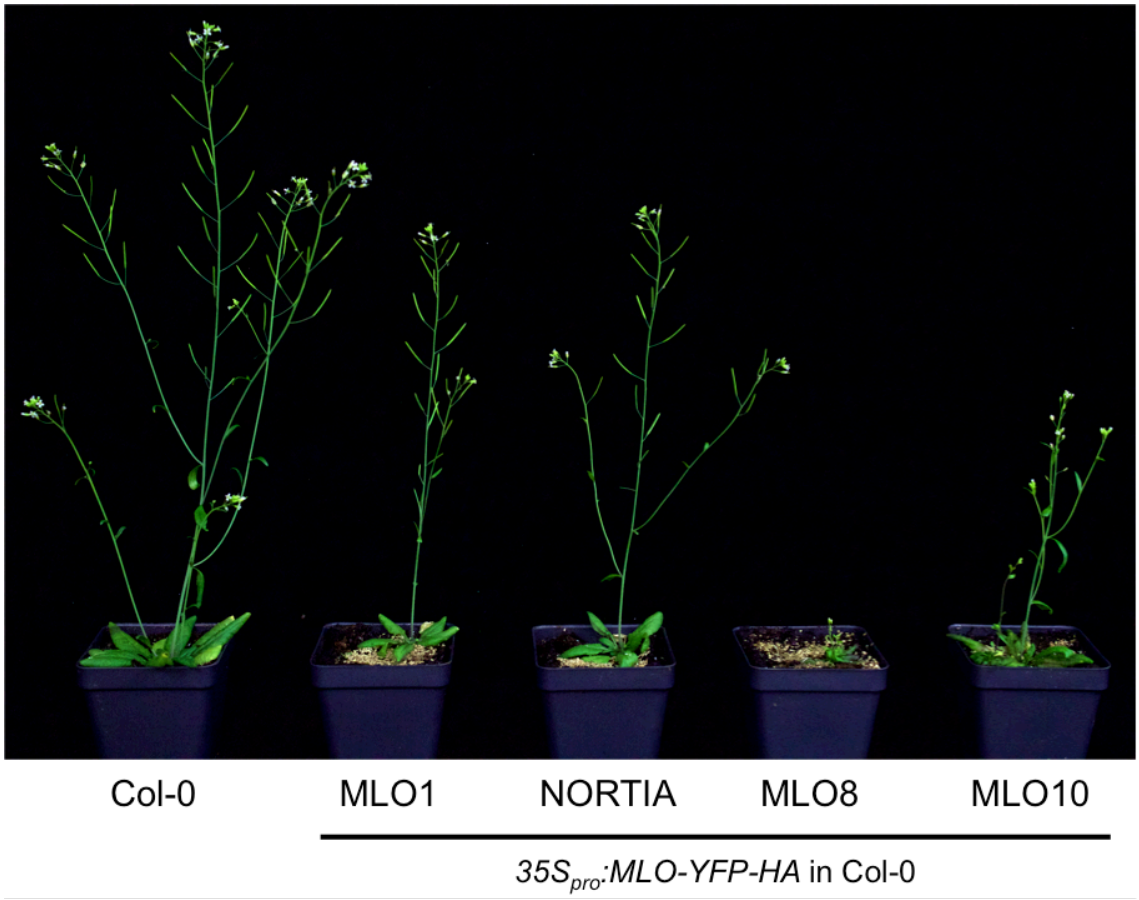

Figure 6.10 – MLO overexpression lines in *A. thaliana*. T1 plants from *35S$_{pro}$::MLO-YFP-HA* lines that best represent overall phenotypes.

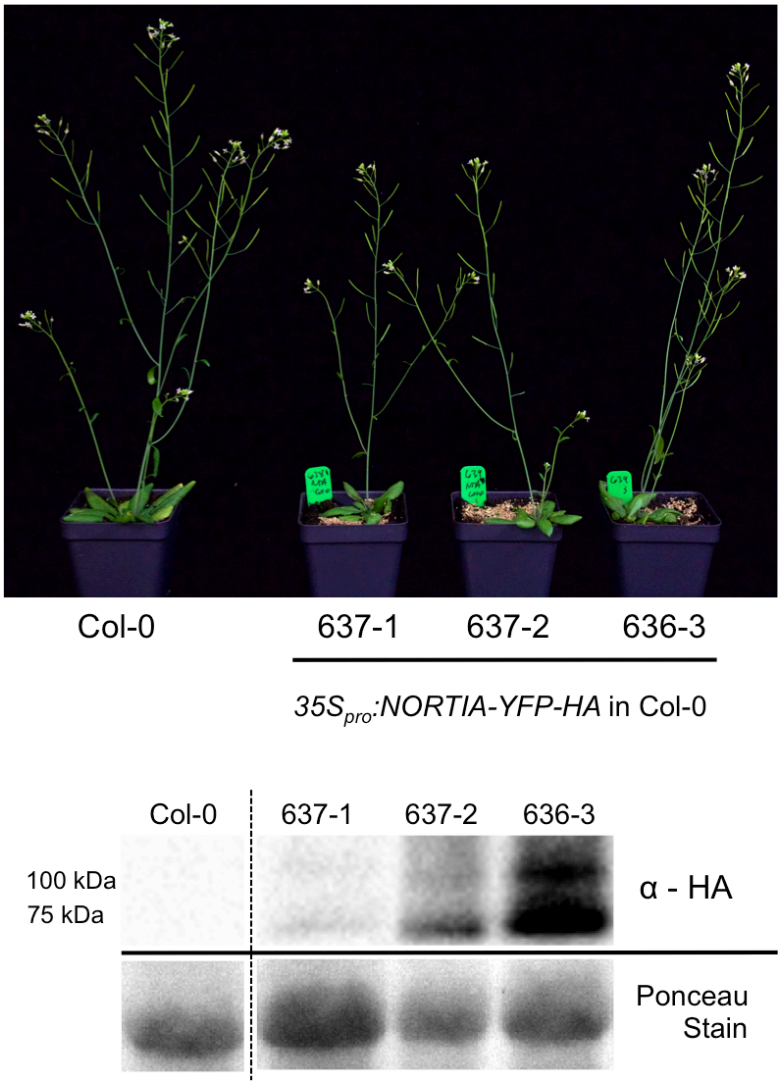

Figure 6.11 – Overexpression of NORTIA in Col-0. 3 independent T1 plants from *35S$_{pro}$::NORTIA-YFP-HA* in the Col-0 background compared to wildtype. (Below) Blot quantifying protein accumulation for each independent line.

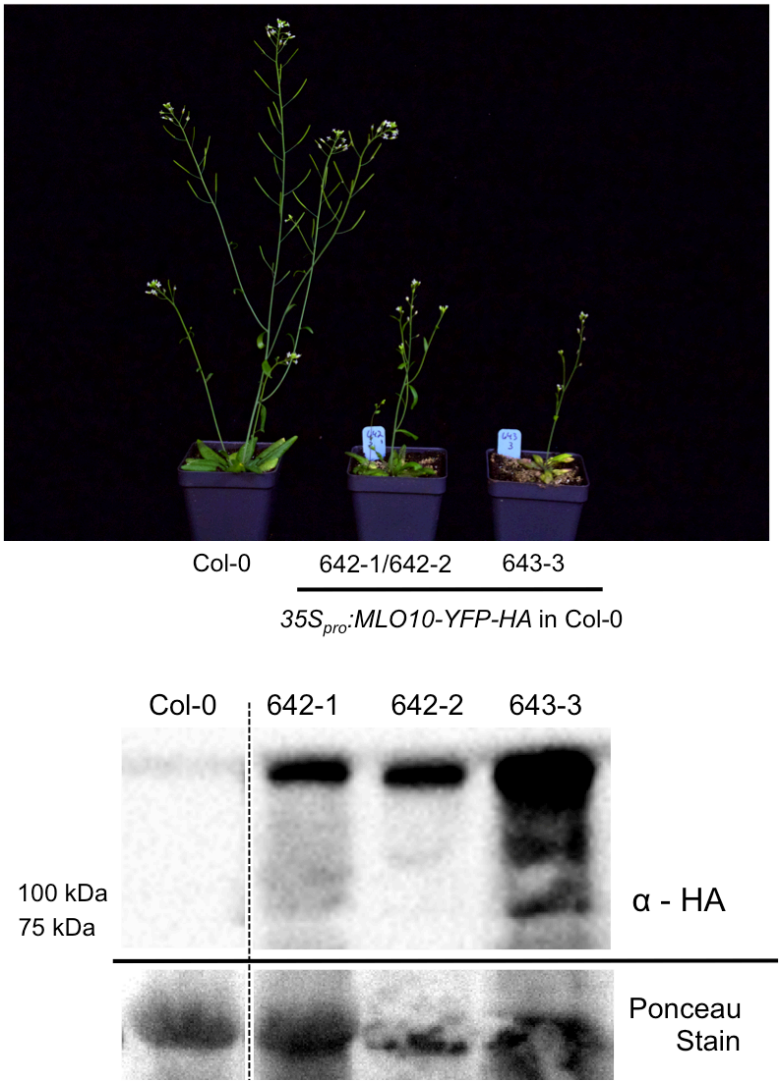

Figure 6.12 – Overexpression of MLO10 in Col-0. 3 independent T1 plants from *35S$_{pro}$::MLO10-YFP-HA* in the Col-0 background compared to wildtype. (Below) Blot quantifying protein accumulation for each independent line.

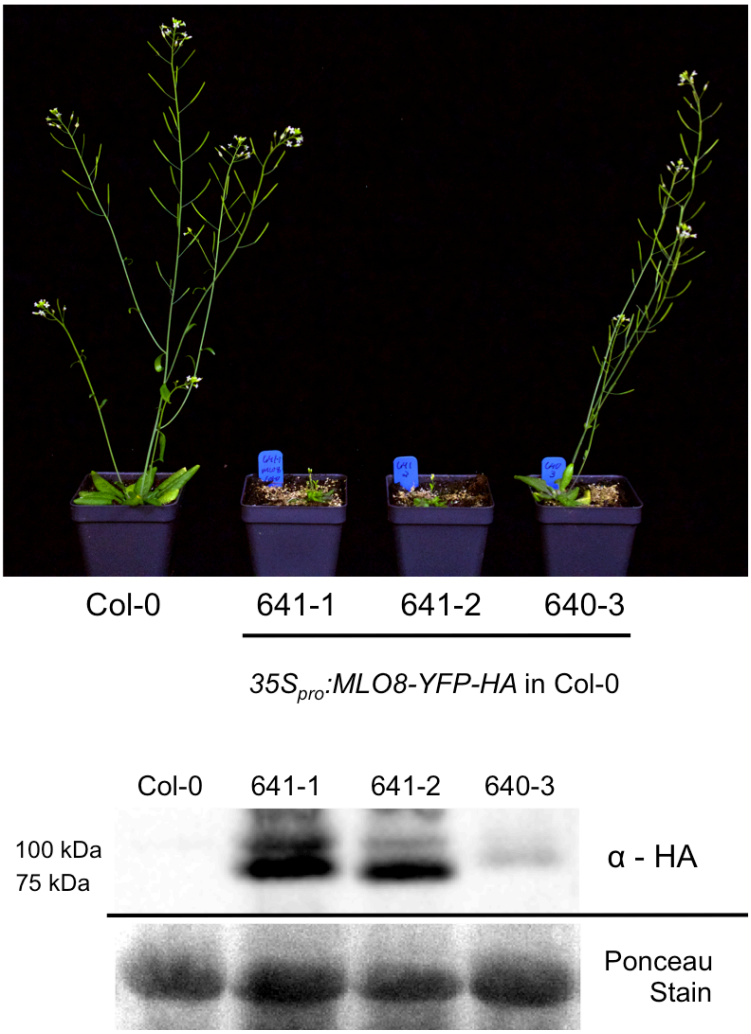

Figure 6.13 – Overexpression of MLO8 in Col-0. 3 independent T1 plants from *35S$_{pro}$::MLO8-YFP-HA* in the Col-0 background compared to wildtype. (Below) Blot quantifying protein accumulation for each independent line.

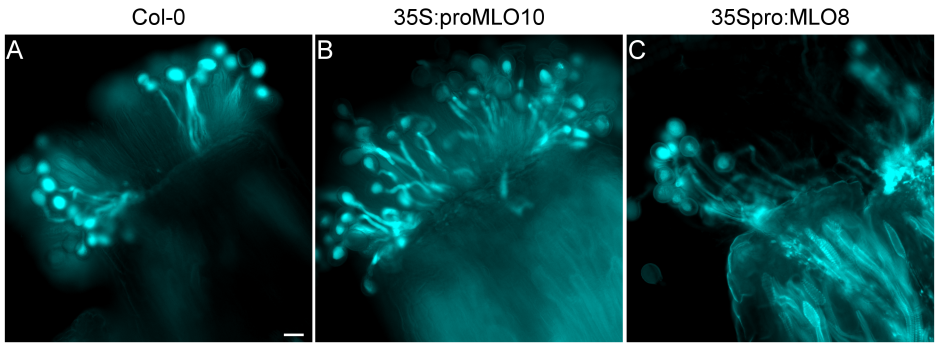

Figure 6.14 – Aniline blue staining reveals successful self-pollination in MLO10 and MLO8 overexpression lines. Aniline blue staining reveals pollen tubes entering papillae cells of stigmas from self-pollinated flowers of: A) Col-0, B) *35S$_{pro}$::MLO10-YFP-HA*, and C) *35S$_{pro}$::MLO8-YFP-HA*. Bar = 20µm.

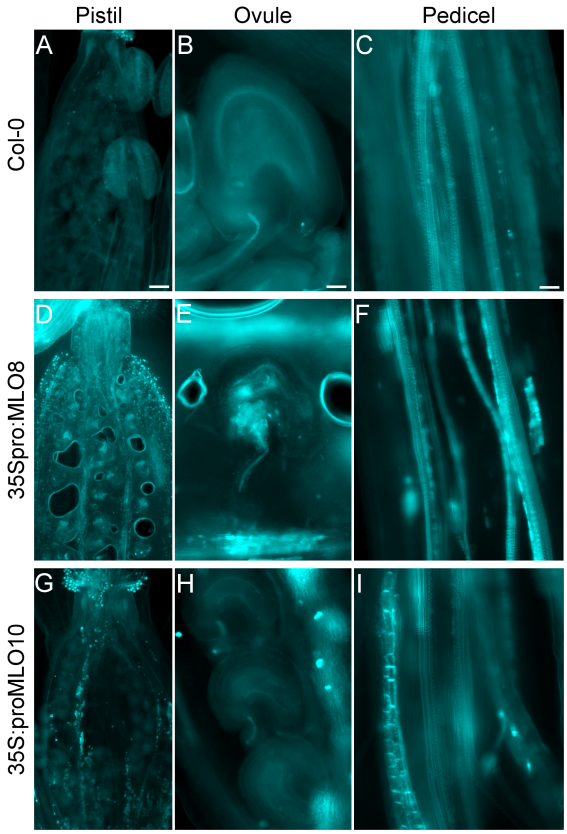

Figure 6.15 – Ectopic callose accumulation in flowers of MLO10 and MLO8 overexpression lines. Aniline blue staining reveals the distribution of callose in whole flowers 2 days after pollination. A-C) Col-0 - whole pistil (A), ovule (B), and flower pedicel (C). D-F) *$35S_{pro}$::MLO8-YFP-HA* - whole pistil (D), ovule (E), and flower pedicel (F). G-I) *$35S_{pro}$::MLO10-YFP-HA* - whole pistil (G), ovule (H), and flower pedicel (I). Bars = A, D, G) 100µm; B, E, H) 20µm; C, F, I) 20µm.

Chapter 7: Conclusions and Future Directions

The MILDEW RESISTANCE LOCUS O (MLO) family of seven-spanning transmembrane proteins plays diverse roles in developmental and environmental signaling within plants. The most well known MLO-linked physiological response is in susceptibility to the fungal pathogen powdery mildew. While the resulting fungal resistance of *mlo* mutants has been fairly well characterized, we still lack an understanding of the native roles of many MLO proteins and have even less of a grasp on their mode of function at the cellular and molecular levels. In this dissertation, I have primarily focused on determining the requirements for MLO-mediated pollen tube (PT) reception by dissecting the role of the MLO protein NORTIA (NTA) in this pathway (Chapters 2 and 5). During this process, I also contributed tools for studying various aspects of cell biology within the specialized synergid cell, important for mediating reproductive communication during PT attraction and reception (Chapter 4). Through the use of a single MLO mutant knockout with a quantitative phenotype (*nta-1*), I was able to compare other MLO proteins in their ability to function in PT reception, determine that additional factors influence characteristics of MLOs in different cell types (such as subcellular distribution), and identify other MLOs related to NTA that could play yet unknown roles in reproductive development or signaling (Chapters 2, 3, and 6). In summary, this dissertation has contributed to our understanding in two primary ways: 1) in the description of the molecular requirements for NTA's function during PT reception and 2) in describing potential roles for other MLO proteins in reproductive communication as well as establishing several conserved characteristics for MLO function.

Concerning NORTIA's role in pollen tube reception

In the structure-function analysis presented in Chapter 2, Golgi-associated subcellular localization and homo-oligomerization were determined to be important for NTA's

function in PT reception. Both of these characteristics were conserved in the full-length MLOs (localization) and domain-swapped constructs (localization and homo-oligomerization) that could substitute for NTA when expressed in the synergid cell. It is still unclear though what the importance of Golgi-localization or homo-oligomerization to NTA's function is during PT reception. Thus many questions remain that could impact our broader understanding of MLO mediated processes.

MLOs that can function in PT reception all localize within Golgi-associated compartments in the synergid cell. This may represent the influence of an interaction partner required for function or may be due to yet undescribed post-translational modifications occurring within this cellular compartment. Peripheral evidence exists for both hypotheses, however; more exists for the former. Differential localization of MLO proteins across cell-types indicates that cellular environments influence their distribution. This is most evident in MLO2, which localized to Golgi-associated compartments in synergid cells and to the cell-periphery of lobes in epidermal cells (see Chapters 2-3). This same effect was observed when removing NTA's predicted signal peptide, truncating its N-terminal domain to be similar to MLO2. This suggests that other proteins (which would differ between cell-types) interact directly with MLOs and influence their recruitment between cellular compartments. However, the predicted signal peptide of NTA may act as a buffer against this recruitment as all of the full-length MLOs tested from Clade III (NTA, MLO10, MLO8) have predicted signal peptides and remain consistently localized across cell-types. As for the latter hypothesis, no experiments exploring the post-translational modification of MLO proteins have yet been reported. The most commonly reported modification occurring within Golgi-associated compartments is O-linked glycosylation. Glycosylation can affect protein folding and function in both secreted and membrane-localized proteins.

The C-terminal intracellular tail of NTA (as well as other MLOs) has many predicted glycosylation sites, including one within the important calmodulin (CaM)-binding domain. Differential glycosylation patterns between MLOs may help to explain how a closely related MLO protein (MLO8) cannot rescue PT reception while a less similar MLO (MLO2) is able to function in this process.

Disruption of the N-terminus of NTA inhibited its ability to efficiently homo-oligomerize and function in PT reception. Homo-oligomerization has now been described in both NTA and barley MLO (Elliott et al., 2005), however; the perceived requirement of oligomerization in PT reception is the first time functional significance has been attributed to this interaction (Chapter 2). It's unclear what the exact function of oligomerization is during PT reception and whether these interactions represent the formation of dimers or higher order protein complexes. Interestingly in barley MLO homo-oligomerization, CaM-binding activity is not required suggesting that CaMs (or CaM-like proteins) likely do not contribute directly to the formation of MLO oligomers (Elliott et al., 2005). Verification of NTA homo-oligomerization within the synergid cell, as well as the identification and description of the dynamics of such interactions, could reveal more about their potential role. As described in Chapter 2, multi-pass transmembrane proteins form oligomeric complexes for the purposes of localization, signal transduction, and pore or channel formation. Understanding any compartmentalization of NTA + NTA interactions or the formation of these interactions in response to a signal or stimulus, such as an arriving PT, would be informative and contribute to developing more targeted hypotheses and experiments to test the role of these complexes.

Concerning MLO-mediated cell-cell communication

MLO-mediated communication is conserved across a wide-variety of essential physiological processes in plants. This is especially true when comparing reproductive and defense signaling as MLOs represent a key similarity between these different pathways (see Chapter 5). Understanding how an MLO functions in one pathway may directly translate to the role of an MLO in another. MLOs all have conserved CaM-binding domains (CaMBDs) in their C-terminal intracellular tails. We now know that the importance of this domain is conserved across both PT reception and MLO-susceptibility. However, a key finding in this study may be in the differences between the CaMBDs of closely related MLOs. Interactions between NTA and AtCaM1 were readily detectable in a FRET-based assay (similar to those used to detect barley MLO + CaM interaction previously), however; no interaction was ever detected between MLO8 and AtCaM1 (Chapter 5). This difference is even more intriguing when looking at C-terminal tail domain swaps, as NTA-MLO8CTerm chimeric proteins only partially rescued *nta-1* at similar levels as the removal of NTA's CaMBD altogether (Chapters 2 and 5). Several different hypotheses can be formed from these data: 1) some MLOs have lost their ability to interact with CaMs; 2) MLOs interact with CaMs differentially; 3) MLOs interact with CaM-like or CaM-domain containing proteins and these interactions differ between even closely related MLOs. Identification of which classes of CaM or CaM-like proteins can interact with NTA vs. MLO8 will provide vital information for designing follow-up experiments to address these hypotheses. Additionally, it will be even more important to identify the CaMs or CaM-like proteins that have relevant physiological roles in the respective MLO-mediated processes (see Chapter 5).

Lastly, determining the native function of other MLO proteins is a vital step towards fully understanding their varied roles in cell-cell communication. MLO10 and MLO8 are

the two most closely related MLOs to NTA and are expressed in key reproductive tissues during development suggesting they could also function in similar pathways as NTA (Chapter 6). When each is ectopically expressed in the synergids of *nta-1*, MLO10 can function in PT reception while MLO8 could not (Chapter 2). MLO10 is natively expressed in the chalazal end of ovules at maturity so its role in signaling during PT attraction or reception appears unlikely. MLO8 on the other hand, accumulates in inner integument layers around the micropyle of the ovule and is occasionally detected at the filiform apparatus outside of the synergid cell. If MLO8 is involved in mediating communication with the PT, this could explain its inability to rescue *nta* when expressed in *nta-1* synergids. This suggests however, that MLO8 plays a direct role in "synergid" PT attraction/reception pathways in a non-cell autonomous manner (from outside the synergid in the apoplast of the micropyle). A recent analysis on the PT reception component LORELEI (LRE) found that, although it is only natively expressed in synergid cells at this stage, the *lre* mutant phenotype could be rescued from the male side when *lre* mutant flowers were pollinated with LRE-YFP expressing pollen (Liu et al., 2016). LRE is a GPI-anchored protein and is thought to function within the apoplast of the micropyle, the site of interaction between the synergid and PT. Much more work is needed to understand MLO8 function, but it is clear that it is expressed and localized within the appropriate tissues and could play some part in this pathway. As no mutants for MLO10 or MLO8 exist, generating knockout lines will be key to determining roles for either in reproductive signaling.

Broader implications of MLO research

Mutations in *MLO* genes have generated fungal-pathogen resistant accessions in various crop and ornamental plant species (Buschges et al., 1997; Linde et al., 2006; Dean et al., 2012). The overwhelming use of *mlo* mutant accessions (i.e. the majority

of barley grown in the United States) exemplifies just how much MLO-mediated resistance has proven to be economically important (Acevedo-Garcia et al., 2014). As the *MLO*s manipulated in this fashion are susceptibility genes, many crucial *mlo* mutations involved in conferring resistance belong to MLO proteins with poorly understood native functions. Additionally, recent studies have suggested that *mlo*-resistance comes with unwanted trade-offs, such as increased susceptibility to other unrelated pathogens (McGrann et al., 2014). This has made understanding *mlo*-resistance extremely important, as determining the exact mode of this resistance could provide insight into how to overcome these trade-offs. Key to this will be in determining the native functions of other MLO proteins and in the identification of proteins with conserved roles in the MLO pathways. This dissertation has focused on a single *MLO*, *NORTIA*, which represents the only model species (*A. thaliana*) *MLO* with a quantitative phenotype from a single knockout mutation. Characterization of NTA, along with related MLO proteins, in the context of PT reception has provided insight into the molecular requirements for MLO function in this pathway. Interestingly MLO2, an *A. thaliana* susceptibility MLO, could replace NTA and function during PT reception. This suggests that greater conservation may exist between MLO-mediated PT reception and susceptibility pathways. Aside from any conservation between these two pathways, the functional data pertaining to NTA's role in PT reception provides an excellent baseline for follow-up analyses on other MLO proteins.

References

Acevedo-Garcia J, Kusch S, Panstruga R (2014) Magical mystery tour: MLO proteins in plant immunity and beyond. New Phytol **204:** 273-281

An Q, Ehlers K, Kogel KH, van Bel AJ, Huckelhoven R (2006) Multivesicular compartments proliferate in susceptible and resistant MLA12-barley leaves in response to infection by the biotrophic powdery mildew fungus. New Phytol **172:** 563-576

An Q, Huckelhoven R, Kogel KH, van Bel AJ (2006) Multivesicular bodies participate in a cell wall-associated defence response in barley leaves attacked by the pathogenic powdery mildew fungus. Cell Microbiol **8:** 1009-1019

Arazi T, Baum G, Snedden WA, Shelp BJ, Fromm H (1995) Molecular and Biochemical Analysis of Calmodulin Interactions with the Calmodulin-Binding Domain of Plant Glutamate Decarboxylase. Plant Physiol **108:** 551-561

Beale KM, Johnson MA (2013) Speed dating, rejection, and finding the perfect mate: advice from flowering plants. Curr Opin Plant Biol **16:** 590-597

Bent A (2006) Arabidopsis thaliana Floral Dip Transformation Method. *In* K Wang, ed, Methods in Molecular Biology, Vol 343. Humana Press Inc., Totowa, NJ

Bhat RA, Miklis M, Schmelzer E, Schulze-Lefert P, Panstruga R (2005) Recruitment and interaction dynamics of plant penetration resistance components in a plasma membrane microdomain. Proc Natl Acad Sci U S A **102:** 3135-3140

Bidzinski P, Noir S, Shahi S, Reinstaedler A, GRATKOWSKA D, Panstruga R (2014) Physiological characterization and genetic modifiers of aberrant root thigmomorphogenesis in mutants of Arabidopsis thaliana MILDEW LOCUS O genes. Plant, cell & environment **37:** 2738-2753

Bircheneder S, Dresselhaus T (2016) Why cellular communication during plant reproduction is particularly mediated by CRP signalling. Journal of experimental botany **67:** 4849-4861

Braam J, Davis RW (1990) Rain-, wind-, and touch-induced expression of calmodulin and calmodulin-related genes in Arabidopsis. Cell **60:** 357-364

Buschges R, Hollricher K, Panstruga R, Simons G, Wolter M, Frijters A, van Daelen R, van der Lee T, Diergaarde P, Groenendijk J, Topsch S, Vos P, Salamini F, Schulze-Lefert P (1997) The barley Mlo gene: a novel control element of plant pathogen resistance. Cell **88:** 695-705

Capron A, Gourgues M, Neiva LS, Faure J-E, Berger F, Pagnussat G, Krishnan A, Alvarez-Mejia C, Vielle-Calzada J-P, Lee Y-R (2008) Maternal control of male-gamete delivery in Arabidopsis involves a putative GPI-anchored protein encoded by the LORELEI gene. The Plant Cell **20:** 3038-3049

Chaiwanon J, Wang W, Zhu JY, Oh E, Wang ZY (2016) Information Integration and Communication in Plant Growth Regulation. Cell **164:** 1257-1268

Chen J, Gutjahr C, Bleckmann A, Dresselhaus T (2015) Calcium signaling during reproduction and biotrophic fungal interactions in plants. Molecular plant **8:** 595-611

Chen Z, Hartmann HA, Wu MJ, Friedman EJ, Chen JG, Pulley M, Schulze-Lefert P, Panstruga R, Jones AM (2006) Expression analysis of the AtMLO gene family encoding plant-specific seven-transmembrane domain proteins. Plant Mol Biol **60:** 583-597

Chen Z, Noir S, Kwaaitaal M, Hartmann HA, Wu MJ, Mudgil Y, Sukumar P, Muday G, Panstruga R, Jones AM (2009) Two seven-transmembrane domain MILDEW RESISTANCE LOCUS O proteins cofunction in Arabidopsis root thigmomorphogenesis. Plant Cell **21:** 1972-1991

Chevalier É, Loubert-Hudon A, Zimmerman EL, Matton DP (2011) Cell–cell communication and signalling pathways within the ovule: from its inception to fertilization. New Phytologist **192:** 13-28

Consonni C, Humphry ME, Hartmann HA, Livaja M, Durner J, Westphal L, Vogel J, Lipka V, Kemmerling B, Schulze-Lefert P, Somerville SC, Panstruga R (2006) Conserved requirement for a plant host cell protein in powdery mildew pathogenesis. Nat Genet **38:** 716-720

Curtis MD (2003) A Gateway Cloning Vector Set for High-Throughput Functional Analysis of Genes in Planta. Plant Physiology **133:** 462-469

Dean R, Van Kan JA, Pretorius ZA, Hammond-Kosack KE, Di Pietro A, Spanu PD, Rudd JJ, Dickman M, Kahmann R, Ellis J (2012) The Top 10 fungal pathogens in molecular plant pathology. Molecular plant pathology **13:** 414-430

Denninger P, Bleckmann A, Lausser A, Vogler F, Ott T, Ehrhardt DW, Frommer WB, Sprunck S, Dresselhaus T, Grossmann G (2014) Male-female communication triggers calcium signatures during fertilization in Arabidopsis. Nat Commun **5:** 4645

Dettmer J, Hong-Hermesdorf A, Stierhof Y-D, Schumacher K (2006) Vacuolar H+-ATPase activity is required for endocytic and secretory trafficking in Arabidopsis. The Plant Cell **18:** 715-730

Devoto A, Hartmann HA, Piffanelli P, Elliott C, Simmons C, Taramino G, Goh CS, Cohen FE, Emerson BC, Schulze-Lefert P, Panstruga R (2003) Molecular phylogeny and evolution of the plant-specific seven-transmembrane MLO family. J Mol Evol **56:** 77-88

Ding Y, Robinson DG, Jiang L (2014) Unconventional protein secretion (UPS) pathways in plants. Curr Opin Cell Biol **29:** 107-115

Dodd AN, Kudla J, Sanders D (2010) The language of calcium signaling. Annual review of plant biology **61:** 593-620

Drakakaki G, Dandekar A (2013) Protein secretion: how many secretory routes does a plant cell have? Plant Sci **203-204:** 74-78

Dresselhaus T, Márton ML (2009) Micropylar pollen tube guidance and burst: adapted from defense mechanisms? Current opinion in plant biology **12:** 773-780

Drews GN, Yadegari R (2002) Development and function of the angiosperm female gametophyte. Annual Review of Genetics **36:** 99-124

Duan Q, Kita D, Johnson EA, Aggarwal M, Gates L, Wu HM, Cheung AY (2014) Reactive oxygen species mediate pollen tube rupture to release sperm for fertilization in Arabidopsis. Nat Commun **5:** 3129

Elliott C, Muller J, Miklis M, Bhat RA, Schulze-Lefert P, Panstruga R (2005) Conserved extracellular cysteine residues and cytoplasmic loop-loop interplay are required for functionality of the heptahelical MLO protein. Biochem J **385:** 243-254

Endo S, Betsuyaku S, Fukuda H (2014) Endogenous peptide ligand–receptor systems for diverse signaling networks in plants. Current opinion in plant biology **21:** 140-146

Escobar-Restrepo JM, Huck N, Kessler S, Gagliardini V, Gheyselinck J, Yang WC, Grossniklaus U (2007) The FERONIA receptor-like kinase mediates male-female interactions during pollen tube reception. Science **317:** 656-660

Foresti O, Denecke J (2008) Intermediate organelles of the plant secretory pathway: identity and function. Traffic **9:** 1599-1612

Francis KE, Lam SY, Harrison BD, Bey AL, Berchowitz LE, Copenhaver GP (2007) Pollen tetrad-based visual assay for meiotic recombination in Arabidopsis. Proceedings of the national academy of sciences **104:** 3913-3918

Freymark G, Diehl T, Miklis M, Romeis T, Panstruga R (2007) Antagonistic control of powdery mildew host cell entry by barley calcium-dependent protein kinases (CDPKs). Molecular plant-microbe interactions **20:** 1213-1221

Ge LL, Tian HQ, Russell SD (2007) Calcium function and distribution during fertilization in angiosperms. American Journal of Botany **94:** 1046-1060

Geldner N, Anders N, Wolters H, Keicher J, Kornberger W, Muller P, Delbarre A, Ueda T, Nakano A, Jürgens G (2003) The Arabidopsis GNOM ARF-GEF mediates endosomal recycling, auxin transport, and auxin-dependent plant growth. Cell **112:** 219-230

Geldner N, Dénervaud-Tendon V, Hyman DL, Mayer U, Stierhof YD, Chory J (2009) Rapid, combinatorial analysis of membrane compartments in intact plants with a multicolor marker set. The Plant Journal **59:** 169-178

Gibson DG, Young L, Chuang R-Y, Venter JC, Hutchison CA, Smith HO (2009) Enzymatic assembly of DNA molecules up to several hundred kilobases. Nature methods **6:** 343-345

Gilroy S, Suzuki N, Miller G, Choi W-G, Toyota M, Devireddy AR, Mittler R (2014) A tidal wave of signals: calcium and ROS at the forefront of rapid systemic signaling. Trends in Plant Science **19:** 623-630

Goder V, Spiess M (2001) Topogenesis of membrane proteins: determinants and dynamics.pdf. FEBS Letters **504:** 87-93

Gookin TE, Assmann SM (2014) Significant reduction of BiFC non-specific assembly facilitates in planta assessment of heterotrimeric G-protein interactors. Plant J **80:** 553-567

Graham LE, Cook ME, Busse JS (2000) The origin of plants: body plan changes contributing to a major evolutionary radiation. Proc Natl Acad Sci U S A **97:** 4535-4540

Gunning BES, Pate JS (1969) "Transfer Cells" Plant Cells with Wall Ingrowths, Specialized in Relation to Short Distance Transport of Solutes – Their Occurrence, Structure, and Development. Protoplasma **68:** 107-133

Hafidh S, Fíla J, Honys D (2016) Male gametophyte development and function in angiosperms: a general concept. Plant Reproduction **29:** 31-51

Hamamura Y, Nishimaki M, Takeuchi H, Geitmann A, Kurihara D, Higashiyama T (2014) Live imaging of calcium spikes during double fertilization in Arabidopsis. Nat Commun **5:** 4722

Hamilton C (1997) A binary-BAC system for plant transformation with high-molecular-weight DNA. Gene **200:** 107-116

Harper JF, Sussman MR, Schaller GE, Putnam-Evans C, Charbonneau H, Harmon AC (1991) A calcium-dependent protein kinase with a regulatory domain similar to calmodulin. Science **252:** 951-955

Haruta M, Sussman MR (2017) Chapter Ten-Ligand Receptor-Mediated Regulation of Growth in Plants. Current Topics in Developmental Biology **123:** 331-363

Higashiyama T (2002) The synergid cell: attractor and acceptor of the pollen tube for double fertilization. Journal of plant research **115:** 0149-0160

Higashiyama T, Kuroiwa H, Kawano S, Kuroiwa T (1998) Guidance in vitro of the pollen tube to the naked embryo sac of torenia fournieri. Plant Cell **10:** 2019-2032

Higashiyama T, Takeuchi H (2015) The mechanism and key molecules involved in pollen tube guidance. Annu Rev Plant Biol **66:** 393-413

Hirakawa Y, Torii KU, Uchida N (2017) Mechanisms and strategies shaping plant peptide hormones. Plant and Cell Physiology**:** pcx069

Hofmeister W (1862) On the germination, development and fructification of the higher Cryptogamia and on the fructification of the Conifera. Ray Society, London

Huang B-Q, Russell SD (1992) Female Germ Unit: Organization, Isolation, and Function. **140:** 233-293

Huck N, Moore JM, Federer M, Grossniklaus U (2003) The Arabidopsis mutant feronia disrupts the female gametophytic control of pollen tube reception. Development **130:** 2149-2159

Hückelhoven R, Panstruga R (2011) Cell biology of the plant–powdery mildew interaction. Current opinion in plant biology **14:** 738-746

Iwano M, Ngo QA, Entani T, Shiba H, Nagai T, Miyawaki A, Isogai A, Grossniklaus U, Takayama S (2012) Cytoplasmic Ca2+ changes dynamically during the interaction of the pollen tube with synergid cells. Development **139:** 4202-4209

Jensen WA (1965) The Ultrastructure and Histochemistry of the Synergids of Cotton. American Journal of Botany **52:** 238-256

Jones AM, Xuan Y, Xu M, Wang R-S, Ho C-H, Lalonde S, You CH, Sardi MI, Parsa SA, Smith-Valle E (2014) Border control—a membrane-linked interactome of Arabidopsis. Science **344:** 711-716

Jones DS, Kessler SA (2017) Cell Type-Dependent Localization of MLO Proteins. Plant Signaling & Behavior

Jones DS, Yuan J, Smith BE, Willoughby AC, Kumimoto EL, Kessler SA (2017) MILDEW RESISTANCE LOCUS O Function in Pollen Tube Reception Is Linked to Its Oligomerization and Subcellular Distribution. Plant Physiology **175:** 172-185

Karpova TS, Baumann CT, He L, Wu X, Grammer A, Lipsky P, Hager GL, McNally JG (2003) Fluorescence resonance energy transfer from cyan to yellow fluorescent protein detected by acceptor photobleaching using confocal microscopy and a single laser. Journal of Microscopy-Oxford **209:** 56-70

Kasahara RD, Portereiko MF, Sandaklie-Nikolova L, Rabiger DS, Drews GN (2005) MYB98 is required for pollen tube guidance and synergid cell differentiation in Arabidopsis. Plant Cell **17:** 2981-2992

Kessler SA, Grossniklaus U (2011) She's the boss: signaling in pollen tube reception. Curr Opin Plant Biol **14:** 622-627

Kessler SA, Lindner H, Jones DS, Grossniklaus U (2015) Functional analysis of related CrRLK1L receptor-like kinases in pollen tube reception. EMBO Rep **16:** 107-115

Kessler SA, Shimosato-Asano H, Keinath NF, Wuest SE, Ingram G, Panstruga R, Grossniklaus U (2010) Conserved molecular components for pollen tube reception and fungal invasion. Science **330:** 968-971

Kim MC, Lee SH, Kim JK, Chun HJ, Choi MS, Chung WS, Moon BC, Kang CH, Park CY, Yoo JH (2002) MLO, a modulator of plant defense and cell death, is a novel calmodulin-binding protein isolation and characterization of a rice Mlo homologue. Journal of Biological Chemistry **277:** 19304-19314

Kim MC, Panstruga R, Elliott C, Muller J, Devoto A, Yoon HW, Park HC, Cho MJ, Schulze-Lefert P (2002) Calmodulin interacts with MLO protein to regulate defence against mildew in barley. Nature **416:** 447-451

Kusch S, Pesch L, Panstruga R (2016) Comprehensive Phylogenetic Analysis Sheds Light on the Diversity and Origin of the MLO Family of Integral Membrane Proteins. Genome Biol Evol **8:** 878-895

Kwon C, Bednarek P, Schulze-Lefert P (2008) Secretory pathways in plant immune responses. Plant Physiol **147:** 1575-1583

Lee SH, Seo HY, Kim JC, Do Heo W, Chung WS, Lee KJ, Kim MC, Cheong YH, Choi JY, Lim CO (1997) Differential activation of NAD kinase by plant calmodulin isoforms THE CRITICAL ROLE OF DOMAIN I. Journal of Biological Chemistry **272:** 9252-9259

Leshem Y, Johnson C, Sundaresan V (2013) Pollen tube entry into the synergid cell of Arabidopsis is observed at a site distinct from the filiform apparatus. Plant reproduction **26:** 93-99

Li C, Yeh FL, Cheung AY, Duan Q, Kita D, Liu MC, Maman J, Luu EJ, Wu BW, Gates L, Jalal M, Kwong A, Carpenter H, Wu HM (2015) Glycosylphosphatidylinositol-anchored proteins as chaperones and co-receptors for FERONIA receptor kinase signaling in Arabidopsis. Elife **4**

Linde M, Hattendorf A, Kaufmann H, Debener T (2006) Powdery mildew resistance in roses: QTL mapping in different environments using selective genotyping. Theoretical and applied genetics **113:** 1081-1092

Lindner H, Kessler SA, Müller LM, Shimosato-Asano H, Boisson-Dernier A, Grossniklaus U (2015) TURAN and EVAN mediate pollen tube reception in Arabidopsis synergids through protein glycosylation. PLoS Biol **13:** e1002139

Liu X, Castro C, Wang Y, Noble J, Ponvert N, Bundy M, Hoel C, Shpak E, Palanivelu R (2016) The Role of LORELEI in Pollen Tube Reception at the Interface of the Synergid Cell and Pollen Tube Requires the Modified Eight-Cysteine Motif and the Receptor-Like Kinase FERONIA. Plant Cell **28:** 1035-1052

Luschnig C, Vert G (2014) The dynamics of plant plasma membrane proteins: PINs and beyond. Development **141:** 2924-2938

Mansfield SG, Briarty LG, Erni S (1991) Early embryogenesis in Arabidopsis thaliana. I. The mature embryo sac. Canadian Journal of Botany **69:** 447-460

Markwardt ML, Kremers GJ, Kraft CA, Ray K, Cranfill PJ, Wilson KA, Day RN, Wachter RM, Davidson MW, Rizzo MA (2011) An improved cerulean fluorescent protein with enhanced brightness and reduced reversible photoswitching. PLoS One **6:** e17896

Martin FW (1959) Staining and observing pollen tubes in the style by means of fluorescence. Stain technology **34:** 125-128

Maurel D, Comps-Agrar L, Brock C, Rives M-L, Bourrier E, Ayoub MA, Bazin H, Tinel N, Durroux T, Prézeau L (2008) Cell-surface protein-protein interaction analysis with time-resolved FRET and snap-tag technologies: application to GPCR oligomerization. Nature methods **5:** 561-567

McGrann GR, Stavrinides A, Russell J, Corbitt MM, Booth A, Chartrain L, Thomas WT, Brown JK (2014) A trade off between mlo resistance to powdery mildew and increased susceptibility of barley to a newly important disease, Ramularia leaf spot. Journal of experimental botany **65:** 1025-1037

Muller LM, Lindner H, Pires ND, Gagliardini V, Grossniklaus U (2016) A subunit of the oligosaccharyltransferase complex is required for interspecific gametophyte recognition in Arabidopsis. Nat Commun **7:** 10826

Musil LS, Goodenough DA (1993) Multisubunit assembly of an integral plasma membrane channel protein, gap junction connexin43, occurs after exit from the ER. Cell **74:** 1065-1077

Myers C, Romanowsky SM, Barron YD, Garg S, Azuse CL, Curran A, Davis RM, Hatton J, Harmon AC, Harper JF (2009) Calcium-dependent protein kinases regulate polarized tip growth in pollen tubes. The Plant Journal **59:** 528-539

Myers ZA, Kumimoto RW, Siriwardana CL, Gayler KK, Risinger JR, Pezzetta D, Holt Iii BF (2016) NUCLEAR FACTOR Y, Subunit C (NF-YC) Transcription Factors Are Positive Regulators of Photomorphogenesis in Arabidopsis thaliana. PLoS Genet **12:** e1006333

Nagai T, Ibata K, Park ES, Kubota M, Mikoshiba K, Miyawaki A (2002) A variant of yellow fluorescent protein with fast and efficient maturation for cell-biological applications. Nat Biotechnol **20:** 87-90

Nakagawa Y, Katagiri T, Shinozaki K, Qi Z, Tatsumi H, Furuichi T, Kishigami A, Sokabe M, Kojima I, Sato S (2007) Arabidopsis plasma membrane protein crucial for Ca2+ influx and touch sensing in roots. Proceedings of the National Academy of Sciences **104:** 3639-3644

Naramoto S (2017) Polar transport in plants mediated by membrane transporters: focus on mechanisms of polar auxin transport. Current Opinion in Plant Biology **40:** 8-14

Nelson BK, Cai X, Nebenfuhr A (2007) A multicolored set of in vivo organelle markers for co-localization studies in Arabidopsis and other plants. Plant J **51:** 1126-1136

Ngo QA, Vogler H, Lituiev DS, Nestorova A, Grossniklaus U (2014) A calcium dialog mediated by the FERONIA signal transduction pathway controls plant sperm delivery. Dev Cell **29:** 491-500

Nielsen ME, Feechan A, Bohlenius H, Ueda T, Thordal-Christensen H (2012) Arabidopsis ARF-GTP exchange factor, GNOM, mediates transport required for innate immunity and focal accumulation of syntaxin PEN1. Proc Natl Acad Sci U S A **109:** 11443-11448

Okuda S, Tsutsui H, Shiina K, Sprunck S, Takeuchi H, Yui R, Kasahara RD, Hamamura Y, Mizukami A, Susaki D, Kawano N, Sakakibara T, Namiki S, Itoh K, Otsuka K, Matsuzaki M, Nozaki H, Kuroiwa T, Nakano A, Kanaoka MM, Dresselhaus T, Sasaki N, Higashiyama T (2009) Defensin-like polypeptide LUREs are pollen tube attractants secreted from synergid cells. Nature **458:** 357-361

Otero S, Helariutta Y, Benitez-Alfonso Y (2016) Symplastic communication in organ formation and tissue patterning. Curr Opin Plant Biol **29:** 21-28

Petersen TN, Brunak S, von Heijne G, Nielsen H (2011) SignalP 4.0: discriminating signal peptides from transmembrane regions. Nat Methods **8:** 785-786

Popescu SC, Popescu GV, Bachan S, Zhang Z, Seay M, Gerstein M, Snyder M, Dinesh-Kumar S (2007) Differential binding of calmodulin-related proteins to their targets revealed through high-density Arabidopsis protein microarrays. Proceedings of the National Academy of Sciences **104:** 4730-4735

Qu L-J, Li L, Lan Z, Dresselhaus T (2015) Peptide signalling during the pollen tube journey and double fertilization. Journal of experimental botany **66:** 5139-5150

Rea AC, Nasrallah JB (2004) Self-incompatibility systems: barriers to self-fertilization in flowering plants. International Journal of Developmental Biology **52:** 627-636

Reyes FC, Buono R, Otegui MS (2011) Plant endosomal trafficking pathways. Current opinion in plant biology **14:** 666-673

Robinson-Beers K, Pruitt RE, Gasser CS (1992) Ovule development in wild-type Arabidopsis and two female-sterile mutants. The Plant Cell **4:** 1237-1249

Rotman N, Rozier F, Boavida L, Dumas C, Berger F, Faure J-E (2003) Female control of male gamete delivery during fertilization in Arabidopsis thaliana. Current Biology **13:** 432-436

Russell SD (1992) Double Fertilization. International Review of Cytology **140:** 357-388

Russell SD, Jones DS (2015) The male germline of angiosperms: repertoire of an inconspicuous but important cell lineage. Frontiers in Plant Science **6**

Rutherford S, Moore I (2002) The Arabidopsis Rab GTPase family: another enigma variation. Current opinion in plant biology **5:** 518-528

Safavian D, Goring DR (2013) Secretory activity is rapidly induced in stigmatic papillae by compatible pollen, but inhibited for self-incompatible pollen in the Brassicaceae. PLoS One **8:** e84286

Samuel MA, Chong YT, Haasen KE, Aldea-Brydges MG, Stone SL, Goring DR (2009) Cellular pathways regulating responses to compatible and self-incompatible pollen in Brassica and Arabidopsis stigmas intersect at Exo70A1, a putative component of the exocyst complex. The Plant Cell **21:** 2655-2671

Sanderfoot AA, Kovaleva V, Bassham DC, Raikhel NV (2001) Interactions between syntaxins identify at least five SNARE complexes within the Golgi/prevacuolar system of the Arabidopsis cell. Molecular Biology of the Cell **12:** 3733-3743

Schindelin J, Arganda-Carreras I, Frise E, Kaynig V, Longair M, Pietzsch T, Preibisch S, Rueden C, Saalfeld S, Schmid B, Tinevez JY, White DJ, Hartenstein V, Eliceiri K, Tomancak P, Cardona A (2012) Fiji: an open-source platform for biological-image analysis. Nat Methods **9:** 676-682

Schulz P, Herde M, Romeis T (2013) Calcium-dependent protein kinases: hubs in plant stress signaling and development. Plant physiology **163:** 523-530

Signorell A (2015) DescTools: Tools for descriptive statistics. R package version 0.99 **15**

Skou J-P (1982) Callose Formation Responsible for the Powdery Mildew Resistance in Barley with Genes in the ml-o Locus. Journal of Phytopathology **104:** 90-95

Stahl Y, Faulkner C (2016) Receptor Complex Mediated Regulation of Symplastic Traffic. Trends Plant Sci **21:** 450-459

Sumner M, Caeseele LV (1989) The ultrastructure and cytochemistry of the egg apparatus of Brassica campestris. Canadian journal of botany **67:** 177-190

Takeuchi H, Higashiyama T (2012) A species-specific cluster of defensin-like genes encodes diffusible pollen tube attractants in Arabidopsis. PLoS Biology **10:** e1001449

Tamura K, Stecher G, Peterson D, Filipski A, Kumar S (2013) MEGA6: molecular evolutionary genetics analysis version 6.0. Molecular biology and evolution **30:** 2725-2729

Team RC (2014) R: A language and environment for statistical computing. R Foundation for Statistical Computing, Vienna, Austria. 2013. *In*. ISBN 3-900051-07-0

Tian G-W, Mohanty A, Chary SN, Li S, Paap B, Drakakaki G, Kopec CD, Li J, Ehrhardt D, Jackson D (2004) High-throughput fluorescent tagging of full-length Arabidopsis gene products in planta. Plant physiology **135:** 25-38

Tsukamoto T, Qin Y, Huang Y, Dunatunga D, Palanivelu R (2010) A role for LORELEI, a putative glycosylphosphatidylinositol-anchored protein, in Arabidopsis thaliana double fertilization and early seed development. The Plant Journal **62:** 571-588

Tucker MR, Koltunow AM (2014) Traffic monitors at the cell periphery: the role of cell walls during early female reproductive cell differentiation in plants. Current opinion in plant biology **17:** 137-145

Véry A-A, Sentenac H (2002) Cation channels in the Arabidopsis plasma membrane. Trends in plant science **7:** 168-175

Viotti C, Bubeck J, Stierhof Y-D, Krebs M, Langhans M, van den Berg W, van Dongen W, Richter S, Geldner N, Takano J (2010) Endocytic and secretory

traffic in Arabidopsis merge in the trans-Golgi network/early endosome, an independent and highly dynamic organelle. The Plant Cell **22:** 1344-1357

Wang J, Ding Y, Wang J, Hillmer S, Miao Y, Lo SW, Wang X, Robinson DG, Jiang L (2010) EXPO, an exocyst-positive organelle distinct from multivesicular endosomes and autophagosomes, mediates cytosol to cell wall exocytosis in Arabidopsis and tobacco cells. The Plant Cell **22:** 4009-4030

Weisz OA, Swift AM, Machamer CE (1993) Oligomerization of a membrane protein correlates with its retention in the Golgi complex. The Journal of Cell Biology **122:** 1185-1196

Wickham H, Francois R (2015) dplyr: A grammar of data manipulation. R package version 0.4 **1:** 20

Yamada M, Miyawaki A, Saito K, NakaJima T, Yamamoto-Hino M, Ryo Y, Furuichi T, Mikoshiba K (1995) The calmodulin-binding domain in the mouse type1 inositol 1,4,5- trisphosphate receptor. Biochemical Journal **300:** 83-88

Yang T, Poovaiah B (2003) Calcium/calmodulin-mediated signal network in plants. Trends in plant science **8:** 505-512

Yi M, Valent B (2013) Communication between filamentous pathogens and plants at the biotrophic interface. Annu Rev Phytopathol **51:** 587-611

Zhao L-N, Shen L-K, Zhang W-Z, Zhang W, Wang Y, Wu W-H (2013) Ca2+-dependent protein kinase11 and 24 modulate the activity of the inward rectifying K+ channels in Arabidopsis pollen tubes. The Plant Cell **25:** 649-661

Zielinski RE (1998) Calmodulin and calmodulin-binding proteins in plants. Annual review of plant biology **49:** 697-725

Zipfel C, Oldroyd GE (2017) Plant signalling in symbiosis and immunity. Nature **543:** 328-336

Appendix A: List of Constructs

Plasmid Number	Construct	Insert (if used)	Vector Backbone
pDSJ1	pMLO1::MLO1-GFP exp vector	pDSJ10 (pMLO1::MLO1 in pDONR207)	pMDC107
pDSJ2	pMLO8::MLO8-GFP exp vector	pDSJ11 (pMLO8::MLO8 in pDONR207)	pMDC107
pDSJ3	pMLO10::MLO10-GFP exp vector	pDSJ12 (pMLO10::MLO10 in pDONR207)	pMDC107
pDSJ4	pMLO6::MLO6-GUS exp vector	pDSJ13 (pMLO6::MLO6 in pDONR207)	pMDC163
pDSJ5	pMLO6::MLO6-GFP exp vector	pDSJ13 (pMLO6::MLO6 in pDONR207)	pMDC107
pDSJ10	pMLO1::MLO1 pDONR207	-	pDONR207
pDSJ11	pMLO8::MLO8 pDONR207	-	pDONR207
pDSJ12	pMLO10::MLO10 pDONR207	-	pDONR207
pDSJ13	pMLO6::MLO6 pDONR207	-	pDONR207
pDSJ14	pMLO1::MLO1-GUS exp vector	pDSJ10	pMDC163
pDSJ15	pMLO8::MLO8-GUS exp vector	pDSJ11	pMDC163
pDSJ16	pMLO10::MLO10-GUS exp vector	pDSJ12	pMDC163
pDSJ18	35S::MLO2-GFP	pELK16	pMDC83
pDSJ19	35S::MLO8-GFP	pELK20	pMDC83
pDSJ20	35S::MLO10-GFP	pELK26	pMDC83
pDSJ23	35S::MLO2sp-MLO7TM1C1-GFP	pDSJ31	pMDC83
pDSJ24	35S::MLO8N1EL1-MLO7C1-GFP	pDSJ32	pMDC83
pDSJ27	pMyb98::MLO2sp-MLO7TM1C1-GFP	pDSJ31	pMDC83 (with pMyb98 promoter)
pDSJ28	pMyb98::MLO8N1EL1-MLO7C1-GFP	pDSJ32	pMDC83 (with pMyb98 promoter)
pDSJ29	MLO7sp-MLO8 in pDONR207 entry vector	-	pDONR207
pDSJ31	MLO2sp-MLO7TM1C1 in pDONR207 entry vector	-	pDONR207
pDSJ32	MLO8N1EL1-MLO7C1 in pDONR207 entry vector	-	pDONR207
pDSJ33	pMLO2::MLO2 pDONR207	-	pDONR207
pDSJ34	MLO1 cDNA in pDONR207	-	pDONR207
pDSJ35	pMyb98::MLO1-GFP	pDSJ34	pMDC83 (with pMyb98 promoter)
pDSJ36	35S::MLO1-GFP	pDSJ34	pMDC83
pDSJ37	pMLO2::MLO2-GFP	pDSJ33	pMDC107
pDSJ38	pMLO2::MLO2 GUS	pDSJ33	pMDC163
pDSJ39	pMyb98::MLO7sp-MLO8-GFP	pDSJ29	pMDC83 (with pMyb98 promoter)
pDSJ41	MLO7sp-MLO2TM1C1 in pDONR207 entry vector	-	pDONR207
pDSJ42	MLO7N1EL1-MLO8C1 in pDONR207 entry vector	-	pDONR207
pDSJ43	MLO7-MLO8EL1-MLO7 in pDONR207 entry vector	-	pDONR207
pDSJ44	MLO8-MLO7EL1-MLO8 in pDONR207 entry vector	-	pDONR207
pDSJ45	35S::MLO7sp-MLO2TM1C1-GFP	pDSJ41	pMDC83
pDSJ46	pMyb98::MLO7sp-MLO2TM1C1-GFP	pDSJ41	pMDC83 (with pMyb98 promoter)
pDSJ47	35S::MLO7N1EL1-MLO8C1-GFP	pDSJ42	pMDC83
pDSJ48	pMyb98::MLO7N1EL1-MLO8C1-GFP	pDSJ42	pMDC83 (with pMyb98 promoter)
pDSJ49	35S::MLO7-MLO8EL1-MLO7-GFP	pDSJ43	pMDC83
pDSJ50	pMyb98::MLO7-MLO8EL1-MLO7-GFP	pDSJ43	pMDC83 (with pMyb98 promoter)
pDSJ51	35S::MLO8-MLO7EL1-MLO8-GFP	pDSJ44	pMDC83
pDSJ52	pMyb98::MLO8-MLO7EL1-MLO8-GFP	pDSJ44	pMDC83 (with pMyb98 promoter)
pDSJ53	MLO7 no sp in pDONR207 entry vector	-	pDONR207
pDSJ55	MLO8sp-MLO7 redo in pDONR207 entry vector	-	pDONR207
pDSJ56	MLO7TM5-MLO8C2 in pDONR207 entry vector	-	pDONR207
pDSJ57	MLO8TM5-MLO7C2 in pDONR207 entry vector	-	pDONR207
pDSJ58	pMyb98::MLO7 no sp-GFP	pDSJ53	pMDC83 (with pMyb98 promoter)
pDSJ59	35S::MLO7 no sp-GFP	pDSJ53	pMDC83
pDSJ60	pMyb98::MLO8sp-MLO7-GFP	pDSJ55	pMDC83 (with pMyb98 promoter)
pDSJ61	35S::MLO8sp-MLO7-GFP	pDSJ55	pMDC83
pDSJ62	pMyb98::MLO7TM5-MLO8C2-GFP	pDSJ56	pMDC83 (with pMyb98 promoter)
pDSJ63	35S::MLO7TM5-MLO8C2-GFP	pDSJ56	pMDC83
pDSJ64	MLO7TM7-MLO8C3 in pDONR207 entry vector	-	pDONR207
pDSJ65	MLO8TM7-MLO7C3 in pDONR207 entry vector	-	pDONR207
pDSJ66	pMyb98::MLO8TM5-MLO7C2-GFP	pDSJ57	pMDC83 (with pMyb98 promoter)
pDSJ67	35S::MLO8TM5-MLO7C2-GFP	pDSJ57	pMDC83
pDSJ68	pMyb98::MLO7TM7-MLO8C3-GFP	pDSJ64	pMDC83 (with pMyb98 promoter)
pDSJ69	35S::MLO7TM7-MLO8C3-GFP	pDSJ64	pMDC83
pDSJ70	pMyb98::MLO8TM7-MLO7C3-GFP	pDSJ65	pMDC83 (with pMyb98 promoter)
pDSJ71	35S::MLO8TM7-MLO7C3-GFP	pDSJ65	pMDC83
pDSJ79	pMyb98 GG promoter module - traditional	-	pGGA000
pDSJ80	pMyb98 GG promoter module - GG rxn	GG rxn	pGGA000
pDSJ81	pUBI10::ERsig-mCherry	GG rxn	pGGZ001
pDSJ82	MLO7 GG CDS module	GG rxn	pGGC000
pDSJ83	MLO8 GG CDS module	GG rxn	pGGC000
pDSJ84	35S::MLO7-mCherry	GG rxn with pDSJ82	pGGZ001
pDSJ85	35S::MLO8-mCherry	GG rxn with pDSJ83	pGGZ001
pDSJ86	CrispR B module	GG rxn	pGGB000
pDSJ87	CrispR D module	GG rxn	pGGD000
pDSJ88	MLO8 CrispR target 8.1	gibson assembly	M4 UC
pDSJ89	MLO8 CrispR target 8.2	gibson assembly	M4 UC
pDSJ90	MLO8 CrispR target 8.3	gibson assembly	M4 UC
pDSJ91	MLO8 CrispR target 10.1	gibson assembly	M4 UC
pDSJ92	MLO8 CrispR target 10.2	gibson assembly	M4 UC
pDSJ93	MLO8 CrispR target 10.3	gibson assembly	M4 UC
pDSJ94	MLO8NTM1-NTAIL1-MLO8TM2C4 in pDONR207 entry vector	-	pDONR207
pDSJ95	NTANTM1-MLO8IL1-NTATM2C4 in pDONR207 entry vector	-	pDONR207
pDSJ96	MLO8NTM3-NTAIL2-MLO8TM4C5 in pDONR207 entry vector	-	pDONR207
pDSJ97	NTANTM3-MLO8IL2-NTATM4C5 in pDONR207 entry vector	-	pDONR207
pDSJ98	MLO8 R475H	-	pDONR207
pDSJ99	NTA H459R	-	pDONR207
pDSJ100	C-Dummy module	GG rxn	pGGC000
pDSJ105	ARA7 GG CDS module	GG rxn	pGGC000
pDSJ106	Exo70E2 GG CDS module	GG rxn	pGGC000
pDSJ107	Syp61 GG CDS module	GG rxn	pGGC000
pDSJ108	VHA-a1 GG CDS module	GG rxn	pGGC000
pDSJ109	pMyb98::NTANTM1-MLO8IL1-NTATM2C4-GFP	pDSJ95	pMDC83 (with pMyb98 promoter)
pDSJ110	pMyb98::MLO8NTM3-NTAIL2-MLO8TM4C5-GFP	pDSJ96	pMDC83 (with pMyb98 promoter)
pDSJ111	pMyb98::MLO8 R475H-GFP	pDSJ98	pMDC83 (with pMyb98 promoter)
pDSJ112	pMyb98::NTA H459R-GFP	pDSJ99	pMDC83 (with pMyb98 promoter)
pDSJ116	pMyb98::MLO8NTM1-NTAIL1-MLO8TM2C4-GFP	pDSJ94	pMDC83 (with pMyb98 promoter)
pDSJ117	pMyb98::NTANTM3-MLO8IL2-NTATM4C5-GFP	pDSJ97	pMDC83 (with pMyb98 promoter)
pDSJ118	35S::NTA-Cer3	pSAK172	p845
pDSJ119	35s::NTA-YFP	pSAK172	p184
pDSJ125	35S::NTA-Cer3-YFP	PCR - Gibson assembly	pDSJ118

Plasmid Number	Construct	Insert (if used)	Vector Backbone
pDSJ128	pMyb98::ARA7-mCherry	PCR - Gibson assembly	pEarlyGate 301
pDSJ129	pMyb98::Exo70E2-mCherry	PCR - Gibson assembly	pEarlyGate 301
pDSJ130	pMyb98::Syp61-mCherry	PCR - Gibson assembly	pEarlyGate 301
pDSJ131	pMyb98::VHA-a1-mCherry	PCR - Gibson assembly	pEarlyGate 301
pDSJ132	35S::MLO8-Cer3	pELK20	p845
pDSJ133	35S::MLO8-YFP	pELK20	p184
pDSJ134	35S::MLO8N1EL1-MLO7C1-Cer3	pDSJ32	p845
pDSJ135	35S::MLO8N1EL1-MLO7C1-YFP	pDSJ32	p184
pDSJ136	35S::MLO7 W458A - Cer3	pPD5	p845
pDSJ137	35S::CaM7-YFP	pPD15	p184
pDSJ139	35S::MLO7TM7-MLO8C3-Cer3	pDSJ64	p845
pDSJ140	35S::MLO7TM7-MLO8C3-YFP	pDSJ64	p184
pDSJ141	35S::MLO8TM7-MLO7C3-Cer3	pDSJ65	p845
pDSJ142	35S::MLO8TM7-MLO7C3-YFP	pDSJ65	p184
pDSJ143	35S::MLO7N1EL1-MLO8C1-Cer3	pDSJ42	p845
pDSJ144	35S::MLO7N1EL1-MLO8C1-YFP	pDSJ42	p184
pDSJ145	MLO8 C-Terminus in pDONR207 entry vector (with stop for Y2H)	-	pDONR207
pDSJ146	CaM1 in pDONR207 entry vector (with stop for Y2H)	-	pDONR207
pDSJ147	CaM2 in pDONR207 entry vector (with stop for Y2H)	-	pDONR207
pDSJ148	CaM3 in pDONR207 entry vector (with stop for Y2H)	-	pDONR207
pDSJ149	CaM4 in pDONR207 entry vector (with stop for Y2H)	-	pDONR207
pDSJ150	CaM5 in pDONR207 entry vector (with stop for Y2H)	-	pDONR207
pDSJ151	CaM6 in pDONR207 entry vector (with stop for Y2H)	-	pDONR207
pDSJ152	pMLO1::MLO1-GFP-HDEL exp vector	pDSJ10	pMDC204
pDSJ153	pMLO2::MLO2-GFP-HDEL exp vector	pDSJ33	pMDC204
pDSJ154	pMLO7::MLO7-GFP-HDEL exp vector	pSAK 168-B4	pMDC204
pDSJ155	pMLO8::MLO8-GFP-HDEL exp vector	pDSJ11	pMDC204
pDSJ156	pMLO10::MLO10-GFP-HDEL exp vector	pDSJ12	pMDC204
pDSJ157	pEC::MLO8.1 Crispr vector	-	pHEE401E
pDSJ158	pEC::MLO8.2 Crispr vector	-	pHEE401E
pDSJ159	pEC::MLO10.1 Crispr vector	-	pHEE401E
pDSJ160	pEC::MLO10.2 Crispr vector	-	pHEE401E
pDSJ161	pEC::NTA Crispr vector	-	pHEE401E
pDSJ162	35S::YFP-CaM1	pDSJ146	pEarlyGate 104
pDSJ163	35S::YFP-CaM3	pDSJ148	pEarlyGate 104
pDSJ164	pEC::PNPA.1 Crispr vector	-	pHEE401E
pDSJ165	pEC::PNPA.2 Crispr vector	-	pHEE401E
pDSJ166	pEC::UNK.1 Crispr vector	-	pHEE401E
pDSJ170	35s::MLO1-YFP	pDSJ34	p184
pDSJ171	35s::MLO10-YFP	pELK26	p184
pDSJ172	NTAN-MLO1	-	pDONR207
pDSJ173	MLO1N-NTA	-	pDONR207
pDSJ174	NTANIL1-MLO1	-	pDONR207
pDSJ175	MLO1NIL1-NTA	-	pDONR207
pDSJ176	NTANEL1-MLO1	-	pDONR207
pDSJ177	MLO1NEL1-NTA	-	pDONR207
pDSJ178	NTANIL2-MLO1	-	pDONR207
pDSJ179	MLO1NIL2-NTA	-	pDONR207
pDSJ180	NTA-MLO1TM5C	-	pDONR207
pDSJ181	MLO1-NTATM5C	-	pDONR207
pDSJ182	NTA-MLO1CTerm	-	pDONR207
pDSJ183	MLO1-NTACTerm	-	pDONR207
pDSJ184	NTATM3	-	pDONR207
pDSJ185	NTATM5	-	pDONR207
pDSJ186	NTA--TM3	-	pDONR207
pDSJ187	NTA--TM6	-	pDONR207
pDSJ188	NTA--TM7	-	pDONR207
pDSJ189	NTAN-MLO1	pDSJ172	pMDC83 (with pMyb98 promoter)
pDSJ190	MLO1N-NTA	pDSJ173	pMDC83 (with pMyb98 promoter)
pDSJ191	MLO1NIL1-NTA	pDSJ175	pMDC83 (with pMyb98 promoter)
pDSJ192	MLO1NEL1-NTA	pDSJ177	pMDC83 (with pMyb98 promoter)
pDSJ193	NTA-MLO1CTerm	pDSJ182	pMDC83 (with pMyb98 promoter)
pDSJ194	NTATM3	pDSJ184	pMDC83 (with pMyb98 promoter)
pDSJ195	NTATM5	pDSJ185	pMDC83 (with pMyb98 promoter)
pDSJ196	NTA--TM3	pDSJ186	pMDC83 (with pMyb98 promoter)
pDSJ197	NTA--TM6	pDSJ187	pMDC83 (with pMyb98 promoter)
pDSJ198	NTA--TM7	pDSJ188	pMDC83 (with pMyb98 promoter)
pDSJ199	NTAN-MLO1	pDSJ172	p184
pDSJ200	MLO1N-NTA	pDSJ173	p184
pDSJ201	MLO1NIL1-NTA	pDSJ175	p184
pDSJ202	MLO1NEL1-NTA	pDSJ177	p184
pDSJ203	NTA-MLO1CTerm	pDSJ182	p184
pDSJ204	NTATM3	pDSJ184	p184
pDSJ205	NTATM5	pDSJ185	p184
pDSJ206	NTA--TM3	pDSJ186	p184
pDSJ207	NTA--TM6	pDSJ187	p184
pDSJ208	NTA--TM7	pDSJ188	p184
pDSJ210	p35S::ccdB-Cer3-YFP Destination Vector	pDONR ccdB	pDSJ125
pDSJ212	p35S::NFYB2-mCer3-YFP	Gibson assembly	
pDSJ213	NTA C-term Tail entry vector (with stop for Y2H)	-	pDONR207
pDSJ215	NTA C-term W458A Tail entry vector (with stop for Y2H)	-	pDONR207
pDSJ217	MLO8 C-term Tail entry vector (with stop for Y2H)	-	pDONR207
pDSJ219	NTA C-term Tail in Y2H bait construct	pDSJ213	pDEST32
pDSJ221	NTA C-term W458A Tail in Y2H bait construct	pDSJ215	pDEST32
pDSJ223	MLO8 C-term Tail in Y2H bait construct	pDSJ217	pDEST32
pDSJ225	CaM1 in Y2H prey construct	pDSJ146	pDEST22
pDSJ226	Myc-CaM1	pDSJ146	pEarlyGate 203
pDSJ227	Myc-CaM3	pDSJ148	pEarlyGate 203
pDSJ228	Myc-CaM4	pDSJ149	pEarlyGate 203
pDSJ229	HA-NTA Cterm	pDSJ213	pEarlyGate 201
pDSJ230	HA-NTA W458A	pDSJ215	pEarlyGate 201
pDSJ231	HA-MLO8 Cterm	pDSJ217	pEarlyGate 201